# A PULSED MAGNET FOR HIGH-FIELD MAGNETIZATION MEASUREMENTS

by

Bryan Neufeldt

A thesis submitted to the Faculty of Graduate Studies and Research in partial fulfillment of the requirements for the degree of Master of Science.

Department of Physics

McGill University

Montreal, Canada

February, 1989

**ABSTRACT**

The design and construction of a capacitor-discharge pulsed magnet is described. The magnet is capable of generating peak fields up to 22 T in a multi-turn solenoid coil with a 3/4" (19 mm) bore. The coil design, calculation of peak field, and an analysis of the eddy currents in the metal surrounding the coil are discussed in detail. The pulsed magnet includes a magnetometer and a data acquisition system which measure the coil field and sample magnetization. A series of magnetization curves have been obtained for a sample of $Nd_2Fe_{14}B$.

**RESUME**

La thèse décrit la conception et la construction d'un aimant à impulsion à décharge par condensateur. L'aimant peut fournir des champs magnétiques atteignant 22 T dans une bobine solénoïdale à enroulement multiple ayant un diamètre interne de 3/4" (19 mm). La conception de la bobine, le calcul des champs magnétiques maximaux et l'examen des courants parasites dans le métal entourant la bobine font l'objet d'une discussion détaillée. L'aimant à impulsions contient un magnétometre et un système de collection de données qui permettent de mesurer le champ magnétique de la bobine, ainsi que la magnétisation de l'échantillon. On a obtenu une série de courbes de magnétisation pour un échantillon de $Nd_2Fe_{14}B$.

**ACKNOWLEDGEMENTS**

I would like to thank my supervisor, Prof. John Strom-Olsen, for suggesting a project which was well-suited to my interests and for allowing me to approach the problems in my own way. I am very grateful to Dr. Dominic Ryan who was willing to help me at every stage of my work. Finally, I would like to thank Frank Van Gils who solved many of the technical problems I encountered.

CONTENTS

# 1 INTRODUCTION

## 1.1 MOTIVATION

Recent actitvity in the area of high field permanent magnets has centered around the development of materials based on an alloy of neodymium, iron, and boron ($Nd_2Fe_{14}B$). The extraordinary magnetic properties of this intermetallic compound are the stimuli for concentrated research efforts aimed at developing a new generation of permanent magnets. In most respects NdFeB magnets are far superior to high performance Sm-Co magnets presently used, and it is believed that they will also eventually replace low-cost Alnico and ferrite magnets in many applications. Further information on NdFeB may be found in the references [1,2].

Several parameters are used to describe the quality of a permanent magnet, the most important of which is its maximum energy product $(BH)_{max}$. This is an intrinsic property of a magnetic material and its value is essentially a measure of the magnet's capability of storing energy in a static magnetic field. Since energy storage is the primary use of a permanent magnet, as in, for example, an electric motor, $(BH)_{max}$ is the best single indicator of the quality of a permanent magnet material. Two other requirements for a good permanent magnet are high remanent magnetization, $\mu_0 M_r$, defined as the magnetization remaining in the magnet material after an applied field is removed, and high

coercivity, $\mu_0 H_c$, which is the applied field necessary to reduce the magnetization to zero after the material has been magnetized.

For a permanent magnet material all three of the parameters mentioned above, $(BH)_{max}$, $\mu_0 M_r$, and $\mu_0 H_c$, are determined from its magnetization curve. This is the plot of a sample's magnetization M vs. the applied field B. For NdFeB, magnetization curves with applied fields up to 20 T are necessary in order to fully investigate this material's magnetic properties. This has been the motivation for designing and constructing a pulsed magnet and magnetometer capable of inexpensively generating fields between 20 and 30 T, and of measuring the magnetization of a sample in such a field.

## 1.2 PRINCIPLES OF OPERATION

There are three basic techniques for generating fields above 2 T, i.e. above those which are produced by conventional iron-cored electromagnets. Continuous fields up to 15 T are most easily acheived with superconducting solenoids. Above this it is necessary to use high powered resistive solenoids, some of which produce 19 T continuous fields. This is only accomplished, however, with large power-producing facilities. Hybrid systems, combining resistive and superconducting solenoids, also exist and are capable of producing 35 T continuous fields [3].

The generation of even higher fields is possible using pulsed field magnets. This relatively inexpensive technique involves discharging stored energy into a solenoid coil to produce pulses lasting typically 0.1 to 100 msec. Kapitza in 1924 was the first to produce high fields with a pulsed magnet. He used lead-acid cells and later an ac generator as the means of storing energy [4,5]. Systems using capacitor storage were built by Wall [6] and others [7-9], although it was not until 1956 that they were used to produce very high fields. Foner and Kolm [10], and subsequently Furth, Levine and Waniek [11], describe techniques for producing fields between 75 and 120 T. There are many general references [12-18] which describe the detailed operation of pulsed magnet systems.

The basic principle of the capacitor-discharge pulsed magnet is most easily understood by considering the following simplified circuit model:

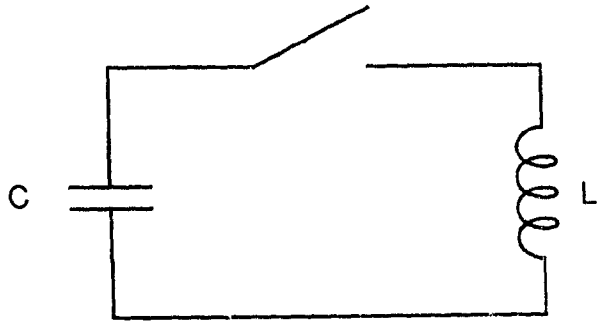


The capacitor is charged to a nominal voltage $V_c$, then discharged through the switch into a solenoid coil with an inductance L and a resistance R. Ignoring the coil resistance, an estimate of the peak field can be made by equating the energy stored in the capacitor with the energy stored in an ideal solenoid, $\frac{1}{2\mu_0}B^2v$, where $v$ is the volume of the bore. Then

$$\frac{1}{2}CV^2 = \frac{1}{2\mu_0}B^2v.$$

Typical values of the circuit parameters are C = 2 mF, V = 5 kV and $v = 30\ cm^3$, giving an estimated peak field of 45 T.

This is roughly twice what can be expected in a practical circuit with the same parameters, and the difference is mainly due to corrections to the ideal solenoid energy expression to account for the finite dimensions of the coil. Also, the transfer of energy does not occur without losses; Joule heating, and to a lesser extent eddy currents in

the metal mantle surrounding the coil, reduce the maximum field by 15 to 20%.

The instantaneous field in the coil may be determined by measuring the current passing through the coil and multiplying this by a predetermined factor B/I which is, neglecting the eddy current effects, dependent on the geometry of the coil.

The sample magnetization may be measured by an astatic pair of pick-up coils positioned in the center of the solenoid (see Fig. 3.1). With no sample, and assuming a uniform field within the solenoid, each coil will produce an equal and opposite voltage which is proportional to the time derivative of the field. When the sample is placed within one of the coils, that coil produces an additional voltage proportional to the rate of change of flux due to the sample magnetization. Since the two coils are connected in opposition, the voltage due to the applied field cancels out and only the signal due to the sample remains. The constant of proportionality between the voltage and magnetization may be calculated but is most easily found by using a sample whose magnetization dependence on magnetic field is known (e.g. a paramagnetic sample of known susceptibility). Integration of the signal yields M as a function of time, which may be plotted as a function of B, if B itself as a function of time is known. In this way the first and fourth quadrants of the magnetization curve may be obtained. Since the field in a pulsed

magnet is usually unidirectional, the other two quadrants can only be found by turning the sample end over end and repeating the measurement. In the system that is to be described, the voltages corresponding to the field and the rate of change of magnetization are stored as a function of time on a digitizing oscilloscope and transferred to a personal computer (PC) for processing.

# 2 DESIGN AND CONSTRUCTION OF THE PULSED MAGNET

## 2.1 BASIC CIRCUIT

The pulsed magnet circuit consists of a bank of five 6 kV capacitors (Maxwell #33553), each nominally 400 μF, connected in parallel to a solenoid coil through either a set of silicon controlled rectifiers (SCRs) or an ignitron. The coil is surrounded by a stainless steel mantle which restrains the Lorentz forces acting on the conductors in the winding.

The timing and current parameters of the circuit are calculated by first considering the following model where the coil is represented by an inductance L and a resistance R in series:

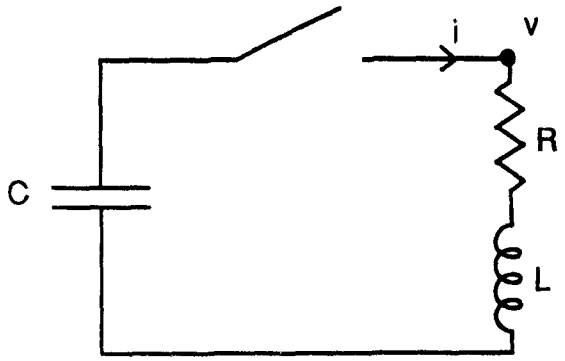


Neglecting to first order the coil resistance, the differential current equation is

$$\frac{d^2i}{dt^2} + \left(\frac{1}{LC}\right) i = 0 \qquad (2.1)$$

yielding

$$i(t) = \frac{V_c}{\omega L}\sin\omega t \tag{2.2}$$

$$v(t) = V_c\cos\omega t \tag{2.3}$$

where $\omega = \frac{1}{\sqrt{LC}}$ and $V_c$ is the initial capacitor voltage. In the actual circuit a series of three diodes (Inernational Rectifiers #C03-1001) are connected between the leads of the coil so that v(t) is clamped at the end of the first quarter cycle of the oscillation, where its value becomes negative. This prevents a large negative voltage from being applied to the capacitors, which would severely shorten their lifetime. Each diode is rated at 3.5 kV and the three in series are voltage-balanced by a snubber network identical to that used for the SCRs (see Fig. 2.21).

The field in the solenoid coil is approximately proportional to the current i(t) so that, besides $V_c$ and C, the shape of the field pulse is determined by the resistance and inductance of the coil. Therefore the steps involved in designing the coil are first to accurately calculate the circuit current in terms of unknown R and L, and then to calculate the field-current relationship of the coil which is dependent, to first order, on the solenoid dimensions and the characteristics of the winding.

## 2.2 CALCULATION OF CURRENT

The following circuit model includes an equivalent diode representing the diodes in the actual circuit:

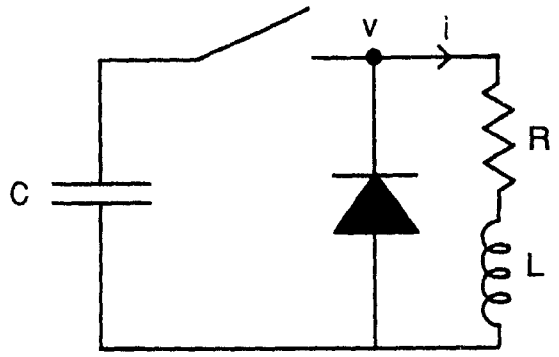


The current and voltage expressions (2.2) and (2.3), derived for R = 0, are valid for this circuit up to the time $t_d$. This is the time at which the diodes become conducting. For three diodes in series the equivalent cut-in voltage is $V_\gamma = 1.5$ V and $t_d$ is found from

$$V_c \cos\omega t_d = -V_\gamma \tag{2.4}$$

At normal operating voltages

$$\frac{V_\gamma}{V_c} \simeq 0$$

so that

$$t_d \simeq \frac{\pi}{2\omega} = \frac{\pi}{2}\sqrt{LC} \tag{2.5}$$

With R = 0 this coincides with the rise time of the current pulse, $t_p$, defined as the time to peak:

$$i(t=t_p) = i_{max} = \frac{V_c}{\omega L} = V_c\sqrt{\frac{C}{L}} \tag{2.6}$$

and

$$t_p = \frac{\pi}{2}\sqrt{LC} \tag{2.7}$$

The maximum instantaneous current is an important parameter because it is proportional to the maximum field, $B_{max}$, produced in the coil. An accurate calculation of $i_{max}$ is therefore necessary, but this cannot be made unless the coil resistance is included in the calculations. Assuming that the coil has a constant resistance R, the differential current equation becomes

$$\frac{d^2i}{dt^2} + \left(\frac{R}{L}\right)\frac{di}{dt} + \left(\frac{1}{LC}\right)i = 0 \tag{2.8}$$

and

$$i(t) = \frac{V_c}{\omega L} e^{\frac{-R}{2L}t} \sin\omega t \ , \qquad t \le t_d \tag{2.9}$$

$$v(t) = V_c e^{\frac{-R}{2L}t} \cos\omega t + \frac{R}{2}i \ , \qquad t \le t_d \tag{2.10}$$

where

$$\omega = \left[\frac{1}{LC} - \left(\frac{R}{2L}\right)^2\right]^{1/2} \tag{2.11}$$

The peak current is

$$i_{max} = i(t=t_p) = V_c\sqrt{\frac{C}{L}}\, e^{\frac{-R}{2L}t_p} \tag{2.12}$$

and the timing parameters are now solutions to the following equations:

$$\tan\omega t_p = \frac{2\omega L}{R}$$

$$\tan\omega t_d = \frac{-2\omega L}{R}\left[1 + 0\left(\frac{V_\gamma}{V_c}\right)\right] \simeq \frac{-2\omega L}{R} \qquad (2.13)$$

This is shown in Fig. 2.1.

After $t = t_d$ current circulates through the diode and coil only, decaying exponentially as energy dissipates in the coil wire. This second part of the waveform is therefore described by

$$i(t') = Ae^{\frac{-R}{L}t'} \qquad (2.14)$$

where $t' = t - t_d$ and $A \equiv i_d = i_{max}$ (see Fig. 2.2).

The calculations so far have ignored the fact that energy dissipated in the coil causes it to heat, thereby changing its resistance. The coil is wound with copper because of its low resistivity, but copper has a temperature coefficient of resistance which is high enough that the change in resistance cannot be neglected. The energy dissipated in the coil is

$$E(t) = \int_0^t R(t)i^2(t)dt \qquad (2.15)$$

Since E is itself a function of coil resistance, an exact expression for current requires the self-consistent solution of an integral equation.

However, the problem of determining $i_{max}$ may be simplified by assuming that the change in resistance during the rise of the pulse is small enough that an average value $\bar{R}$ can be used [19]. Then the previous expressions, which assume a constant resistance, can be retained.

The exact expression for the energy dissipated in the coil up to the time of the pulse peak is

$$E_p = \int_0^{t_p} R(t) i^2(t) dt \tag{2.16}$$

where $t_p$ as well as i(t) depend on R(t). After replacing R(t) with $\bar{R}$, the expression for $E_p$ becomes

$$E_p = \int_0^{t_p} \bar{R} \left(\frac{V_c}{\omega L}\right)^2 e^{\frac{-\bar{R}}{L}t} \sin^2(\omega t) dt$$

$$= \frac{V_c^2}{2L\omega^2} \left[ \left(1 - e^{\frac{-\bar{R}}{L}t_p}\right) + \frac{1 + \left(\cos 2\omega t_p - \frac{2\omega L}{\bar{R}} \sin 2\omega t_p\right) e^{\frac{-\bar{R}}{L}t_p}}{\left(1 + \frac{4L^2\omega^2}{\bar{R}^2}\right)} \right] \tag{2.17}$$

It is convenient at this point to introduce the damping ratio r which indicates the degree to which the coil is non-ideal:

$$r = \frac{1}{2} \sqrt{\frac{\bar{C}}{L}} \bar{R} \tag{2.18}$$

so that

$$\omega = \frac{1}{\sqrt{LC}} \sqrt{1 - r^2} \tag{2.19}$$

and

$$\omega t_p = \tan^{-1}\left[\frac{1}{r}\sqrt{1-r^2}\right] \tag{2.20}$$

As $r \to 0$, the circuit becomes an LC circuit and the current waveform up to $t = t_p$ is oscillatory. If $0 < r < 1$, the oscillation is damped, and for $r > 1$, the system is overdamped.

Now, $E_p$ can be rewritten

$$E_p = \frac{1}{2}CV_c^2 x \tag{2.21}$$

where

$$x = 1-(1+4r^2)\exp\left[\frac{-2\tan^{-1}\left(\frac{1}{r}\sqrt{1-r^2}\right)}{\left(\frac{1}{r}\sqrt{1-r^2}\right)}\right] \tag{2.22}$$

The parameter x is the fraction of the total pulse energy which is transferred to the coil winding up to the time of the pulse peak. It depends only on r (see Figs. 2.3 and 2.4).

Knowing the specific heat and the resistance of the coil wire as a function of the temperature, $R_p$ can be determined for a given $E_p$:

$$mC_p = \frac{dE}{dt} \tag{2.23}$$

and

$$R(T) = R_0\left[1+\alpha(T-T_0)\right] \tag{2.24}$$

$$R(T) = R_0\left[1 + \alpha(T-T_0)\right] \tag{2.24}$$

so that

$$\frac{dR}{dt} = \alpha R_0 \tag{2.25}$$

where m is the mass of the coil wire and $R_0$ is the coil resistance at the initial coil temperature $T_0$. To reduce R, the coil is cooled to liquid nitrogen temperature, making $T_0 = 77$ K. For copper the temperature coefficient of resistance is $\alpha = 0.032$ and the specific heat is given in Fig. 2.5.

In the present system, the time to peak is approximately 10 msec so that little of the heat dissipated in the coil will have had time to flow out of the coil. It is therefore reasonable to assume that the heat transfer is adiabatic during the start of the pulse and

$$\frac{dR}{dE} = \frac{\alpha R_0}{mC_p} \tag{2.26}$$

$$\frac{R_p}{R_0} = \int_0^{E_p} \frac{\alpha}{mC_p} dE = f(E_p/m) \tag{2.27}$$

This is integrated numerically and plotted in Fig. 2.6.

To solve for $R_p$ it is necessary to make an estimate of $E_p$ based on an initial guess of $\bar{R}$. The resulting value of $R_p$ is used to calculate a new value of $\bar{R}$ such that

$$\bar{R} = \frac{R_0 + R_p}{2} \tag{2.28}$$

In this way an iterative solution for $\bar{R}$ is found and $i_{max}$ can be calculated:

$$i_{max} = V_c\sqrt{\frac{\bar{C}}{L}}\, e^{\frac{-\bar{R}}{2L}t_p}$$

$$= V_c\sqrt{\frac{\bar{C}}{L}}\, \exp\left[\frac{-\tan^{-1}\left(\frac{1}{r}\sqrt{1-r^2}\right)}{\left(\frac{1}{r}\sqrt{1-r^2}\right)}\right] \qquad (2.29)$$

where

$$\omega = \left[\frac{1}{LC} - \left(\frac{\bar{R}}{2L}\right)^2\right]^{1/2} \qquad (2.30)$$

and

$$t_p = \frac{1}{\omega}\tan^{-1}\left(\frac{2\omega L}{\bar{R}}\right) = \frac{1}{\omega}\tan^{-1}\left[\frac{1}{r}\sqrt{1-r^2}\right] \qquad (2.31)$$

Typical physical parameters of the system are

$$C = 2 \text{ mF}$$
$$L = 20 \text{ mH}$$
$$R_0 = 0.5\ \Omega$$
$$m = 1.25 \text{ kg}$$
$$V_c = 5 \text{ kV}$$

Using as the initial estimate $\bar{R} = R_0$, the peak current is calculated as $i_{max} = 1353$ A. This is 86% of the value predicted by $V_c\sqrt{\frac{\bar{C}}{L}}$, i.e. with no resistance. The peak current values can be calculated for successive

shots if it is assumed that no heat flows out of the coil winding. The results of this calculation for various capacitor voltages are shown in Fig. 2.7. A similar calculation which allows for some cooling of the coil is discussed in Sec. 5.2.

Fig. 2.1. Circuit Timing Parameters

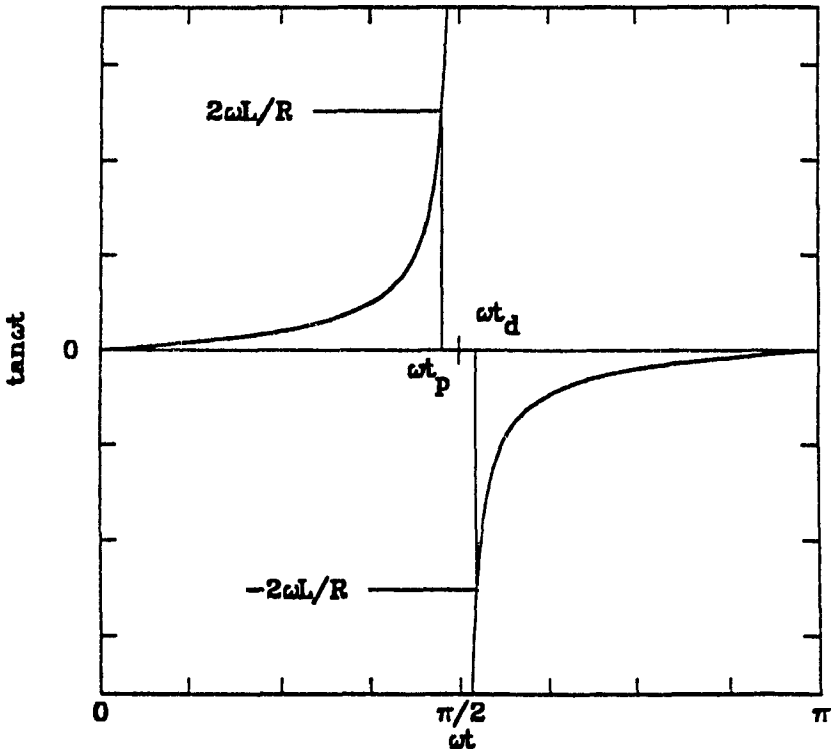


Fig. 2.2. Current Pulse

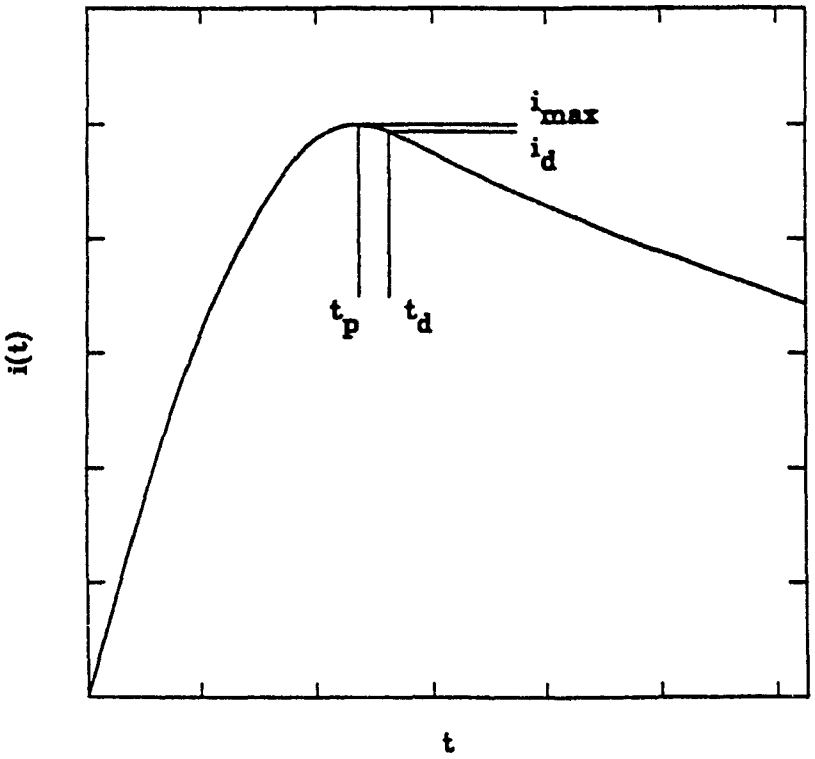

Fig. 2.3. Fraction of Energy Dissipated at Peak

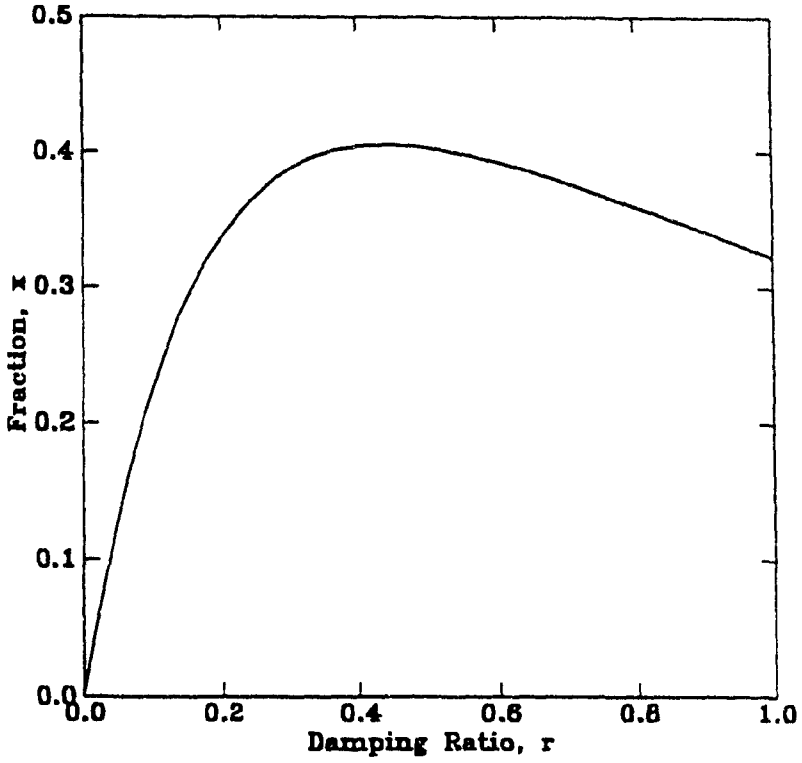


Fig. 2.4. Fraction of Energy Dissipated at Peak

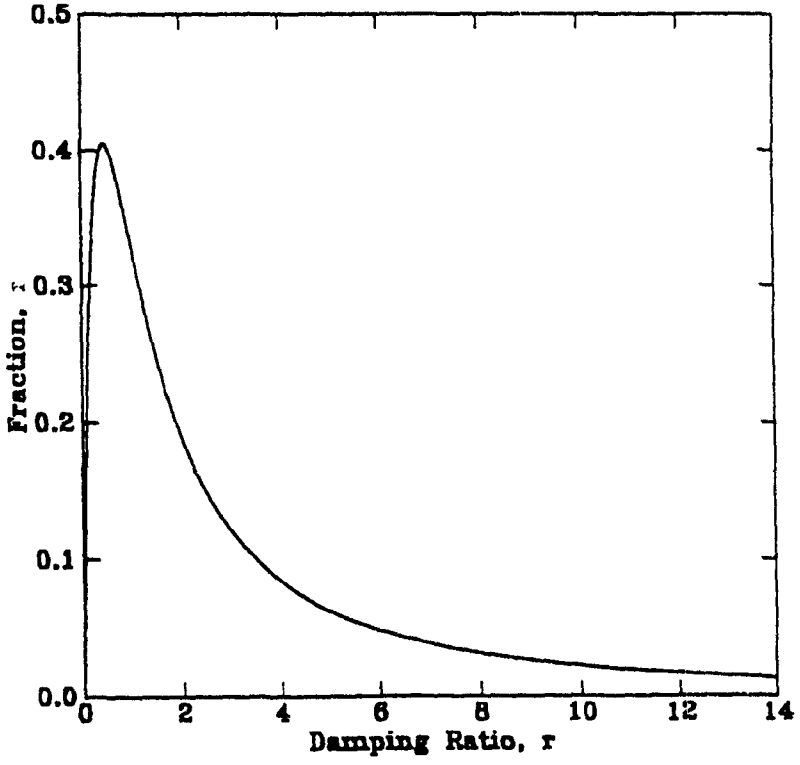

Fig. 2.5. Specific Heat of Copper

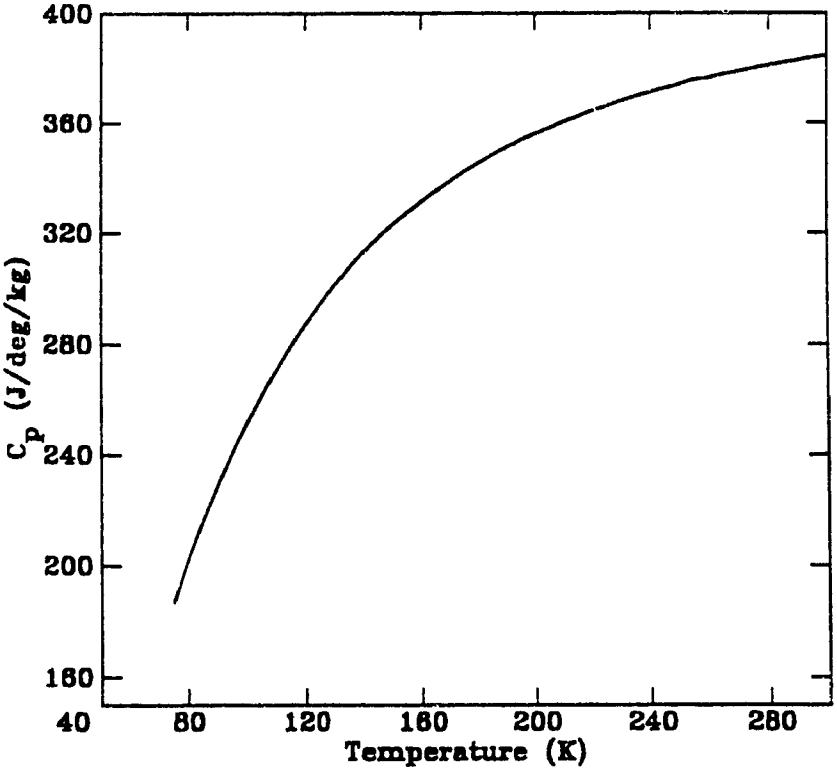


Fig. 2.6. Coil Resistance vs. Energy Transferred to Coil

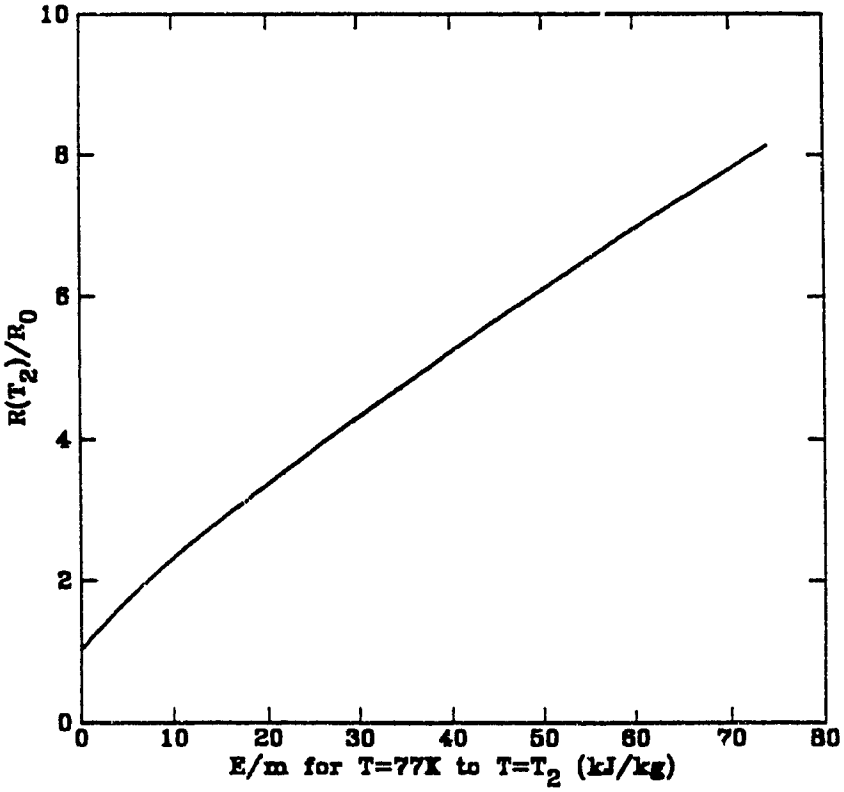

Fig. 2.7. Peak Current vs. Coil Resistance

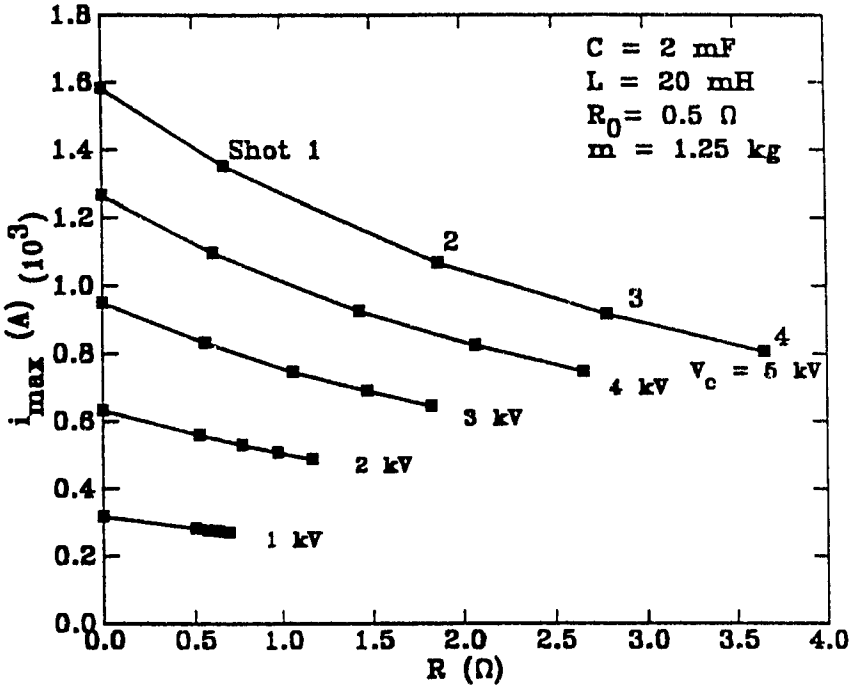

The effects of eddy currents in the coil mantle may be estimated by treating the coil and mantle as a transformer, the coil being the primary and the mantle being a single turn secondary with resistance $R_m$ and self inductance $L_m$:

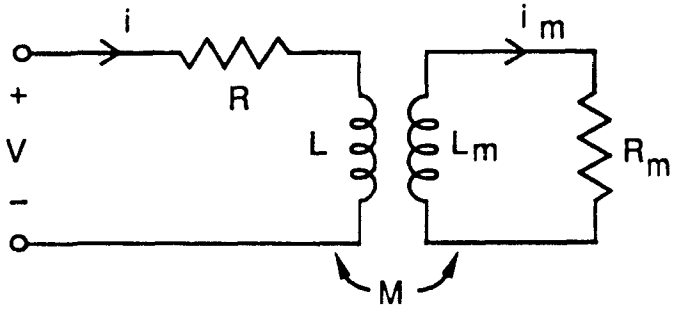


The mutual inductance between the coil and mantle is represented by the coupling coefficient k according to the relation

$$M^2 = LL_m k^2 \tag{2.32}$$

and k has a value between 0 and 1. The transformer equations are:

$$V = RI + j\omega LI - j\omega MI_m \tag{2.33}$$

$$0 = R_m I_m + j\omega L_m I_m - j\omega MI \tag{2.34}$$

Solving these equations for Z = V/I yields the impedance seen from the coil leads. This is

$$Z = R\left[1 + \frac{\omega^2\left(\frac{L}{R}\right)\left(\frac{R_m}{L_m}\right)k^2}{\omega^2 + \left(\frac{R_m}{L_m}\right)^2}\right] + j\omega L\left[\frac{\omega^2(1-k^2) + \left(\frac{R_m}{L_m}\right)^2}{\omega^2 + \left(\frac{R_m}{L_m}\right)^2}\right] \tag{2.35}$$

Typical values of R and L are

$$R = 0.5\ \Omega \quad \text{(at 77 K)}$$

$$L = 20\ \text{mH}$$

so that $R/L \simeq 25\ \text{sec}^{-1}$. The ratio $R_m/L_m$ is not easy to calculate but an order-of-magnitude estimate can be made based on the equations

$$R_m = \rho\frac{2\pi r}{tl} \tag{2.36}$$

$$L_m = \mu_0\frac{\pi r^2}{l} \tag{2.37}$$

and an idealized mantle consisting of a stainless steel cylinder with an average radius $r = 4$ cm, wall thickness $t = 2$ cm, and length $l = 10$ cm. At liquid nitrogen temperature the resistivity $\rho$ of stainless steel is $\sim 40\ \mu\Omega\cdot$cm. Therefore

$$R_m \sim 10^{-4}\ \Omega \quad \text{(at 77 K)}$$

$$L_m \sim 10^{-7}\ \text{H}$$

so that $R_m/L_m \sim 10^3\ \text{sec}^{-1}$.

Using these values, a low frequency approximation of the impedance equation can be made. For $\omega < 600\ \text{sec}^{-1}$

$$Z = R\left[1 + \omega^2\left(\frac{L}{R}\right)\left(\frac{L_m}{R_m}\right)k^2\right] + j\omega L \tag{2.38}$$

If a frequency dependent resistance $R'(\omega)$ is defined such that

$$R'(\omega) \equiv \omega^2 L \left(\frac{L_m}{R_m}\right) k^2 \tag{2.39}$$

then the approximation may be written:

$$Z = R + R'(\omega) + j\omega L \tag{2.40}$$

Thus the eddy current effects can be accounted for in the current calculation, at low frequencies, by including in the circuit a small effective resistance $R'(\omega)$.

$R'(\omega)$ was found experimentally by measuring the phase angle of the impedance over a range of frequencies using a lock-in amplifier. The measurement was made with the coil and mantle in liquid nitrogen. The coil (coil #2 in Table 2.1) has a resistance and inductance

$$R = 0.49\ \Omega \quad \text{(at 77 K)}$$

$$L = 21.8\ \text{mH}$$

The inductance was measured, at room temperature, for the coil without the mantle using an impedance meter.

Figure 2.8 shows the results of the phase angle measurement. The low frequency part of the curve, where the eddy current effects are negligible, is linear with a slope 0.25. This is consistent with the above values for R and L:

$$\frac{\tan\phi}{f} = \frac{2\pi L}{R} = 0.28 \text{ sec} \tag{2.41}$$

The phase angle derived from Eqn. (2.35) is

$$\tan\phi = \frac{\omega L}{R}\left\{\frac{1 + \omega^2\left(\frac{L_m}{R_m}\right)^2(1-k^2)}{1 + \omega^2\left[\left(\frac{L_m}{R_m}\right)^2 + k^2\left(\frac{L}{R}\right)\left(\frac{L_m}{R_m}\right)\right]}\right\} \tag{2.42}$$

and a plot of $\tan\phi$ vs. $\omega$, shown in Fig. 2.8, best fits the data if

$$\frac{R_m}{L_m} = 2000 \text{ sec}^{-1} \quad \text{and} \quad k = 0.7$$

Therefore the effective resistance is

$$R'(\omega) = (5.3 \times 10^{-6})\omega^2 \quad \Omega \tag{2.43}$$

The impedance magnitude, $|Z|$, was also measured and the results are plotted in Fig. 2.9 with a prediction of $|Z|$ based on Eqn. (2.35).

Now that the effective coil resistance is known, its significance in the circuit can be examined. The expression for $R'(\omega)$ in differential form is

$$R'(\omega) = -L\left(\frac{L_m}{R_m}\right)k^2\frac{d^2i}{dt^2} \tag{2.44}$$

and to include this in the circuit analysis, Eqn. (2.8) must be replaced

with a third order differential equation:

$$-\left(\frac{L_m}{R_m}\right)k^2 \frac{d^3i}{dt^3} + \frac{d^2i}{dt^2} + \left(\frac{R}{L}\right)\frac{di}{dt} + \left(\frac{1}{LC}\right)i = 0 \qquad (2.45)$$

However, since $R' \simeq 0.25R$ for $\omega = \frac{1}{\sqrt{LC}} = 157 \text{ sec}^{-1}$ ,R' may be combined with R and

$$R \rightarrow R + R' \simeq 1.25R \qquad (2.46)$$

in the original second order current equation. For the present system, the effect of R', and therefore of eddy currents, is to reduce the peak current by about 3%.

Fig. 2.8. Phase Angle of Coil and Mantle

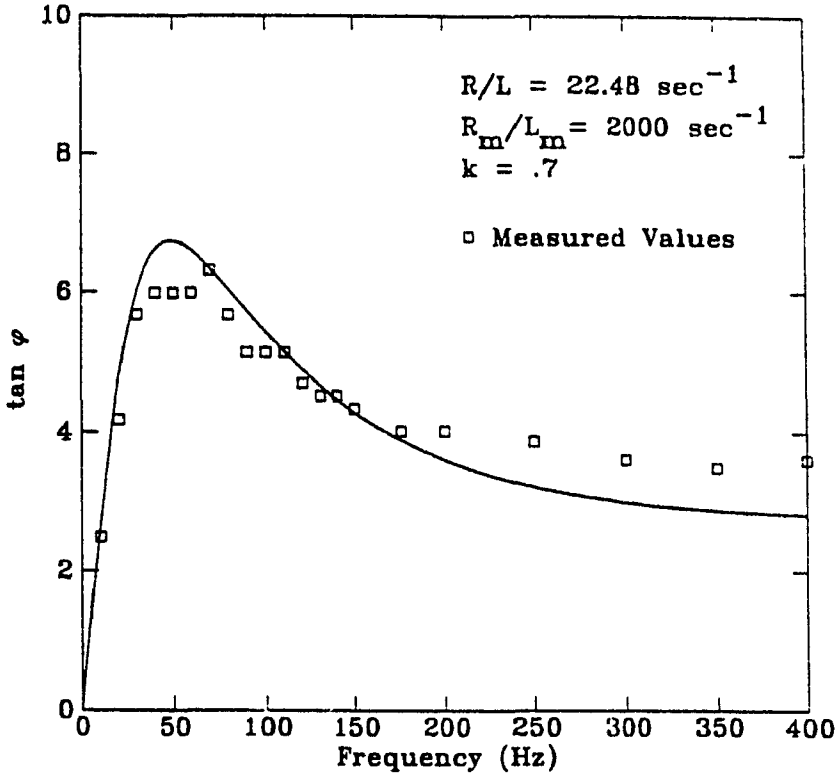


Fig. 2.9. Impedance Magnitude of Coil and Mantle

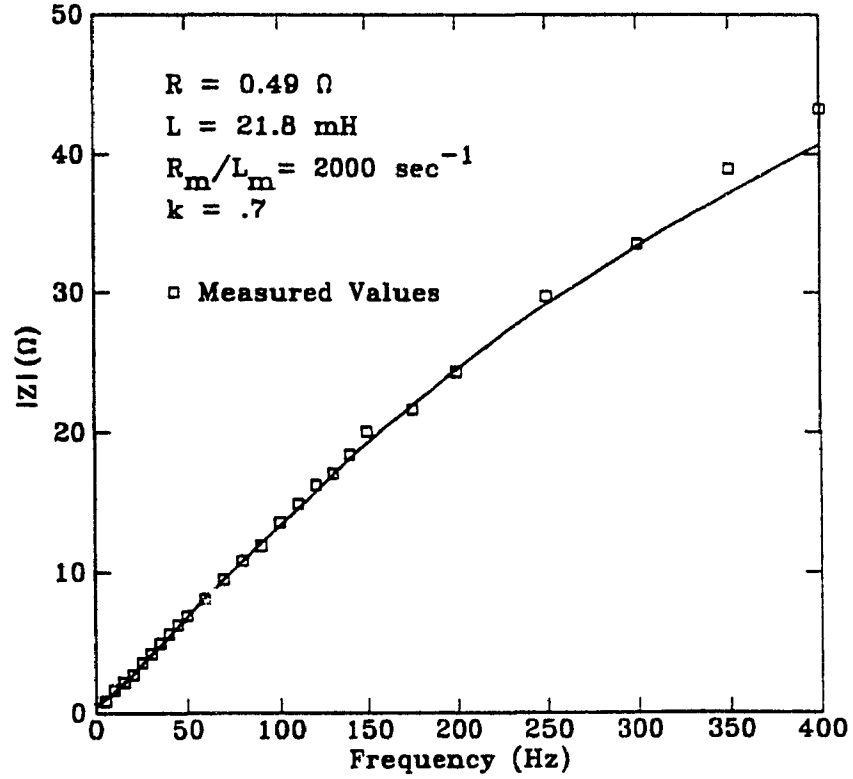

## 2.3 CALCULATION OF FIELD

The following calculation determines the field generated in the coil of the pulsed magnet. The calculation is based on a solenoid coil having a rectangular cross section and a uniform current density. At any point in the coil the field is found by applying the Biot-Savart Law and integrating over the winding volume:

$$d\vec{H}(\vec{R}) = \frac{Jdsd\vec{l} \times (\vec{R}-\vec{R}')}{4\pi|\vec{R}-\vec{R}'|^3} \tag{2.47}$$

The primed coordinates refer to an elemental volume in the winding which is, in cylindrical coordinates,

$$dv = dsdl = dr'dz'r'd\phi' \tag{2.48}$$

It will be assumed that the current density in the winding has a constant average value given by

$$J = \frac{NI}{(\text{X-sectional area})} = \frac{NI}{(\alpha-1)a_1 2\beta a_1} \tag{2.49}$$

where N is the number of turns and the cross-sectional area is written in terms of the inner radius $a_1$ and normalized solenoid dimensions $\alpha$ and $\beta$ (see Fig. 2.10).

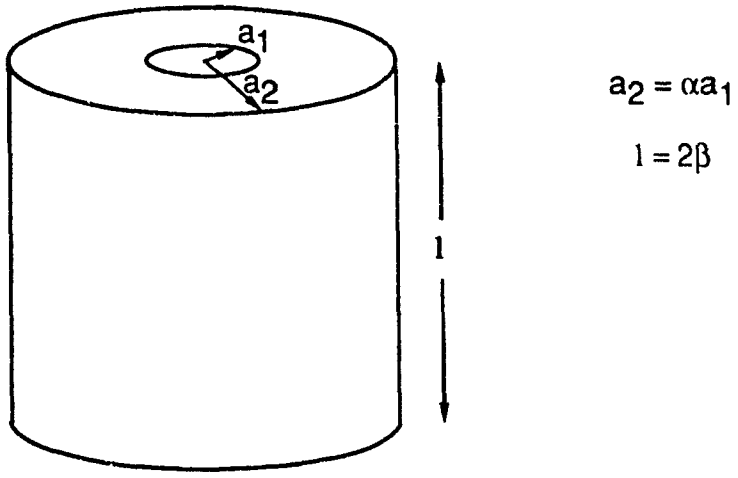


Fig. 2.10. Solenoid Coil Notation

Calculating the field along the z-axis is relatively easy because of axial symmetry:

$$\vec{H}(r=0,z) = \hat{z}H_z(r=0,z)$$

$$= \hat{z}\frac{J}{2}\int_{r'=a_1}^{r'=\alpha a_1}\int_{z'=-\beta a_1}^{z'=\beta a_1}\frac{r'^2\,dz'\,dr'}{\left[r'^2+(z-z')^2\right]^{3/2}} \tag{2.50}$$

$$H_z(r=0,z) = \frac{Ja_1}{2}\left\{-\left(z/a_1-\beta\right)\ln\left[\frac{\alpha+\sqrt{\alpha^2+(z/a_1-\beta)^2}}{1+\sqrt{1+(z/a_1-\beta)^2}}\right]\right.$$

$$\left. +\left(z/a_1+\beta\right)\ln\left[\frac{\alpha+\sqrt{\alpha^2+(z/a_1+\beta)^2}}{1+\sqrt{1+(z/a_1+\beta)^2}}\right]\right\} \tag{2.51}$$

The maximum field is at the center of the solenoid. This is

$$H_z(r=0,z=0) = H_0 = Ja_1\beta \ln\left[\frac{\alpha+\sqrt{\alpha^2+\beta^2}}{1+\sqrt{1+\beta^2}}\right] \tag{2.52}$$

For points which are off the center axis, the field also includes a radial component. The expressions are

$$H_z(r,z) = \frac{J}{4\pi}\int_v \frac{(r'-r\cos\phi')r'd\phi'dr'dz'}{\left[r^2+r'^2-2rr'\cos\phi'+(z-z')^2\right]3/2} \tag{2.53}$$

$$H_r(r,z) = \frac{J}{4\pi}\int_v \frac{(z-z')\cos\phi'r'd\phi'dr'dz'}{\left[r^2+r'^2-2rr'\cos\phi'+(z-z')^2\right]3/2} \tag{2.54}$$

The integrations are complicated and cannot be done analytically. For points close to the origin, however, it is possible to approximate $H_r(r,z)$ by making expansions which only involve the expression for the z-axis field [20].

The field inside the solenoid is the gradient of a magnetic scalar potential $\Phi_m$ such that [21]

$$\vec{H} = -\nabla\Phi_m \tag{2.55}$$

and

$$\nabla^2\Phi_m = 0 \tag{2.56}$$

In spherical coordinates, and recognizing azimuthal symmetry, the solution to the Laplacian can be written [22]

$$\Phi_m(r,\theta) = \sum_{l=0}^{\infty} A_l r^l P_l(\cos\theta) \tag{2.57}$$

and the field is

$$\vec{H}(r,\theta) = -\nabla\Phi_m(r,\theta) = H_r\hat{r} + H_\theta\hat{\theta} \tag{2.58}$$

where $H_r = -\frac{\partial\Phi_m}{\partial r}$ and $H_\theta = -\frac{1}{r}\frac{\partial\Phi_m}{\partial\theta}$.

The z-axis field can now be expressed in terms of the spherical variables:

$$H_z(r,\theta) = \cos\theta H_r - \sin\theta H_\theta \tag{2.59}$$

and this reduces to the expression

$$H_z(r,\theta) = -\sum_{l=1}^{\infty} lA_l r^{l-1} P_{l-1}(\cos\theta) \tag{2.60}$$

A similar calculation yields the cylindrical radial component in terms of spherical variables:

$$H_r^{(cyl)}(r,\theta) = \sin\theta H_r + \cos\theta H_\theta$$

$$= \sum_{l=1}^{\infty} A_l r^{l-1} \sin\theta P'_{l-1}(\cos\theta) \tag{2.61}$$

By setting $\theta = 0$ and $r \to z$, Eqn. (2.60) gives the field along the axis in cylindrical coordinates:

$$H_z(z,r=0) = \sum_{l=1}^{\infty} lA_l z^{l-1} \tag{2.62}$$

The unknown coefficients $A_l$ can now be determined by comparing this expression with a Taylor-series expansion of $H_z$ using the exact formula, Eqn. (2.51):

$$H_z(z,r=0) = H_0 + \sum_{l=1}^{\infty} H_l z^l \tag{2.63}$$

where

$$H_l = \frac{1}{l!} \frac{\partial^l H_z}{\partial z^l}\bigg|_{\substack{z=0 \\ r=0}} \tag{2.64}$$

and $H_0$ is the field at the origin. Therefore

$$-lA_l = H_{l-1} \tag{2.65}$$

and the field expansions for any point near the origin are

$$H_z(r,\theta) = H_0 + \sum_{l=1}^{\infty} H_l r^l P_l(\cos\theta) \tag{2.66}$$

$$H_r^{(cyl)}(r,\theta) = -\sum_{l=1}^{\infty} \frac{1}{(l+1)} H_l r^l \sin\theta P'_l(\cos\theta) \tag{2.67}$$

These expressions give the field component within the radius of convergence $a_l$. But their importance lies in their being used to define a parameter indicating the degree of homogeneity of the coil field. Since $H_z(z,r=0)$ is an even function of z, only the coefficients $H_l$ with even l are nonzero. Therefore the first order approximations are

$$H_z(r,\theta) = H_0 + \frac{1}{2}H_2 r^2\left(3\cos^2\theta - 1\right) \tag{2.68}$$

$$H_r^{(cyl)}(r,\theta) = - H_2 r^2 \sin\theta\cos\theta \tag{2.69}$$

where

$$H_2 = \frac{J}{2\beta a_1}\left[\frac{1}{(1+\beta^2)^{3/2}} - \frac{\alpha^3}{(\alpha^2+\beta^2)^{3/2}}\right] \tag{2.70}$$

The maximum difference of either field component from the magnitude of the field at the origin is

$$H_0 - H_2 r^2 \tag{2.71}$$

It is reasonable then to use the dimensionless parameter

$$\frac{H_2}{H_0} a_1^2 \tag{2.72}$$

to indicate field homogeneity (see Fig. 2.18).

The maximum field at the center of the solenoid, $H_{0\ max}$, can be expressed as the maximum field of an ideal solenoid (i.e. one which is infinitely long) multiplied by a correction factor due to finite dimensions of the coil:

$$\begin{aligned} H_{0\ max} &= \frac{N}{l}\, i_{max} H_{corr}(\alpha,\beta) \\ &= \frac{N}{2\beta a_1}\, i_{max} H_{corr}(\alpha,\beta) \end{aligned} \tag{2.73}$$

where

$$H_{corr} = \frac{\beta}{\alpha-1} \ln\left[\frac{\alpha+\sqrt{\alpha^2+\beta^2}}{1+\sqrt{1+\beta^2}}\right] \tag{2.74}$$

Similarly, the inductance is that of an ideal solenoid multiplied by the correction factor $L_{corr}(\alpha,\beta)$:

$$\begin{aligned} L &= \mu_0 N^2 \left(\frac{A}{l}\right) L_{corr}(\alpha,\beta) \\ &= \mu_0 N^2 \left(\frac{\pi a_1}{2\beta}\right) L_{corr}(\alpha,\beta) \end{aligned} \tag{2.75}$$

A good approximation for $L_{corr}$ is [23]

$$L_{corr}(\alpha,\beta) = \frac{1}{4}(1+\alpha)^2\left[1 + .9\left(\frac{1+\alpha}{4\beta}\right) + .64\left(\frac{\alpha-1}{\alpha+1}\right) + .84\left(\frac{\alpha-1}{2\beta}\right)\right]^{-1} \tag{2.76}$$

For normal coil dimensions, $H_{corr}$ is between 0.9 and 1.0 while $L_{corr}$ varies from 1 to 3 (see Figs. 2.11 and 2.12).

Combining the expressions for $H_{0\ max}$ and L with the first order approximation for $i_{max}$, Eqn. (2.6), the field is, neglecting the coil resistance,

$$H_{0\ max} = \sqrt{\frac{2E_0}{\mu_0(volume)}}\left(\frac{H_{corr}}{\sqrt{L_{corr}}}\right) \tag{2.77}$$

This formula shows clearly the significance of the initial stored energy of the system, $E_0 = \frac{1}{2}CV_c^2$ and of the interior volume of the coil,

$$\text{volume} = (\pi a_1^2)(2\beta a_1) \tag{2.78}$$

It is interesting to note that the maximum field is independent of the number of turns in the coil. This parameter does, however, appear in the inductance formula which can be rewritten as

$$L = \left[\frac{(\alpha-1)a_1 2\beta a_1 \lambda}{\delta A}\right]^2 \frac{\mu_0 \pi a_1}{2\beta} L_{corr}(\alpha,\beta) \tag{2.79}$$

where $\delta A$ is the wire cross-sectional area and $\lambda$ is the space factor defined as

$$\lambda \equiv \frac{\text{volume of conductor}}{\text{volume of coil}} \tag{2.80}$$

For round wire $\lambda = \frac{\pi}{2\sqrt{3}} = 0.91$, but, after constructing a coil, a more realistic value was found to be $\lambda \sim 0.7$.

The resistance of the coil is

$$R = \rho N \frac{\pi(\alpha+1)a_1}{\delta A} = \rho\lambda \frac{2\pi(\alpha^2-1)\beta a_1^3}{\delta A^2} \tag{2.81}$$

At liquid nitrogen temperature $\rho = 0.2 \times 10^{-8}$ $\Omega\cdot m$.

Fig. 2.11. Field Correction Factor

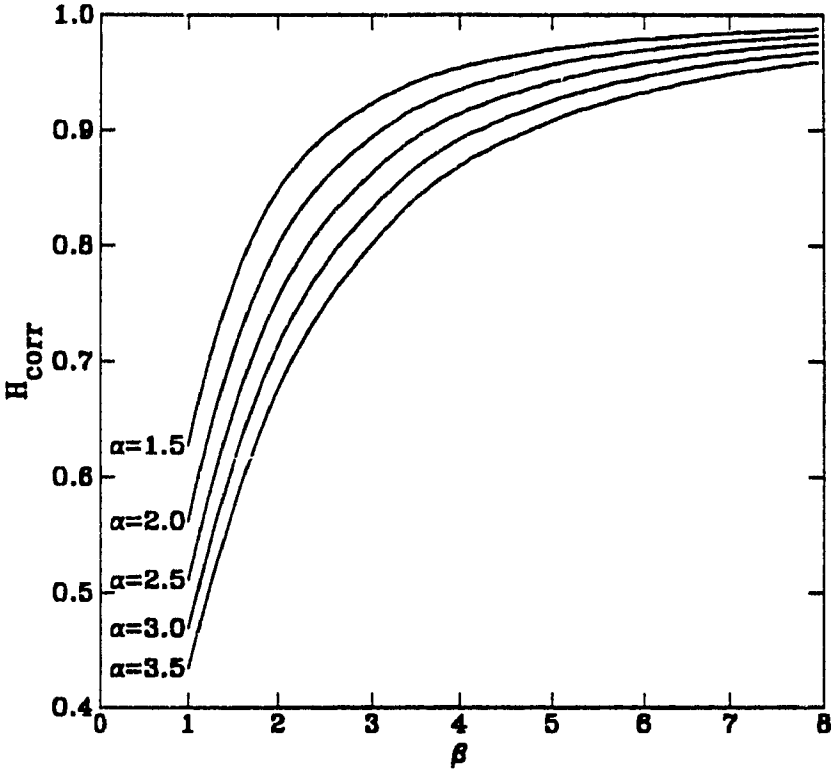


Fig. 2.12. Inductance Correction Factor

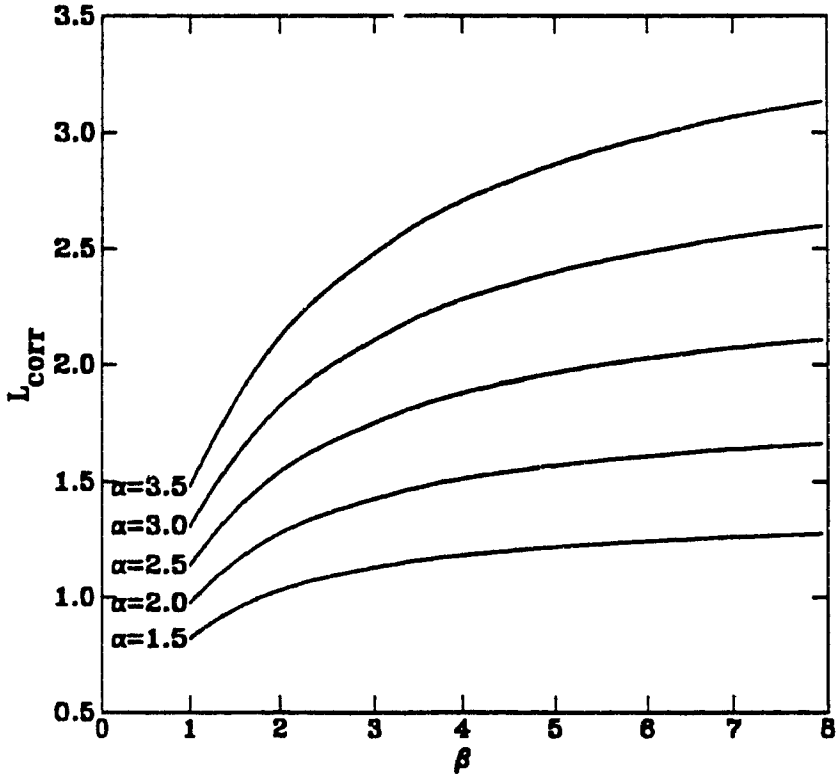

The above calculation of the coil field as a function of coil current is based on an isolated coil. As already discussed, eddy currents in the mantle surrounding the coil generate a field component in the coil which affects the coil current as well as the total field. The decrease in current due to this field component reduces $B_{max}$ by a few percent, and this is discussed in Sec. 2.2. Of greater importance, however, is the reduction in the total coil field for a given coil current, since this affects the linearity of the field-current relationship, Eqn. (2.73), and therefore the B/I calibration.

At the start of the pulse the field generated by the eddy currents, $B_{eddy}$, is opposed to that generated by the coil winding, $B_{coil}$, and the relation between the two is found by combining the energy equation

$$\frac{1}{2\mu_0}B^2 = \frac{1}{2}LI^2 \tag{2.82}$$

with the second transformer Eqn. (2.34):

$$I_m = \frac{j\omega k\sqrt{L_m L}}{R_m + j\omega L_m} I \tag{2.83}$$

This gives the relationship

$$B_{eddy} = \frac{-\omega^2 k - j\omega k\left(\frac{R_m}{L_m}\right)}{\omega^2 + \left(\frac{R_m}{L_m}\right)^2} B_{coil} = -j\omega k\left(\frac{L_m}{R_m}\right) B_{coil} \tag{2.84}$$

or

$$B_{eddy} = -k\left(\frac{L_m}{R_m}\right)\frac{dB_{coil}}{dt} \tag{2.85}$$

For $t \leq t_d$, the equation for $B_{coil}$ may be approximated by

$$B_{coil} = B_{max}e^{\frac{-R}{2L}t}\sin\omega t \tag{2.86}$$

so that

$$B_{eddy} = -k\left(\frac{L_m}{R_m}\right)B_{max}e^{\frac{-R}{2L}t}\left[\omega\cos\omega t - \frac{R}{2L}\sin\omega t\right] \tag{2.87}$$

and

$$B_{total} = B_{coil} + B_{eddy}$$

$$= B_{max}e^{\frac{-R}{2L}t}\left[\sin\omega t - k\left(\frac{L_m}{R_m}\right)\left(\omega\cos\omega t - \frac{R}{2L}\sin\omega t\right)\right] \tag{2.88}$$

Similarly for $t \geq t_d$

$$B_{eddy} = k\left(\frac{L_m}{R_m}\right)\left(\frac{R}{L}\right)B_d e^{\frac{-R}{L}(t-t_d)} \tag{2.89}$$

and

$$B_{total} = B_d e^{\frac{-R}{L}(t-t_d)}\left[1 + k\left(\frac{L_m}{R_m}\right)\left(\frac{R}{L}\right)\right] \tag{2.90}$$

where $B_d \equiv B(t=t_d)$. Using the typical values $R = 0.5\ \Omega$, $L = 20$ mH, and $\omega = 157\ \text{sec}^{-1}$ with the experimental parameters found in Sec. 2.2,

$\left(\frac{R_m}{L_m}\right) = 2000\ \text{sec}^{-1}$ and $k = 0.7$, the field equations are:

$$B(t) = \begin{cases} B_{max} e^{\frac{-R}{2L}t}\left[1.004\sin\omega t - .0550\cos\omega t\right] & \text{for } t \le t_d \qquad (2.91) \\ B_d e^{\frac{-R}{L}(t-t_d)}\left[1 + .0088\right] & \text{for } t \ge t_d \qquad (2.92) \end{cases}$$

From these equations it can be seen that the effect of the eddy currents on the pulse shape is most significant at the beginning of the pulse (see Fig. 2.13). The initial value is negative with a magnitude which is 5.5% of $B_{max}$. Actually it is impossible for a field to exist in the coil immediately after the switching time. The nonzero initial value is obtained only because the high frequency transients have been neglected in the calculation. It is also important to note that the contribution of $B_{eddy}$ to the total field is zero at the time of peak field, and therefore the dc B/I calibration is accurate at this point.

Fig. 2.13. Eddy Current Effects on Coil Field

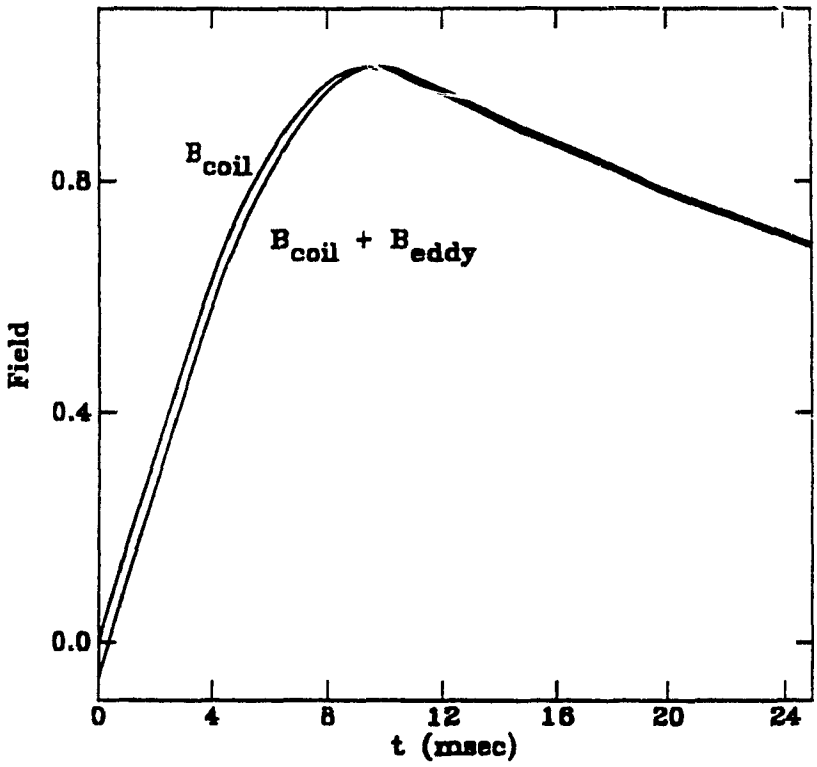

## 2.4 COIL DESIGN AND CONSTRUCTION

The goal in designing the coil is to produce the maximum field possible with the energy available, $\frac{1}{2}CV_c^2$. But this is necessarily limited by other considerations such as the desire for a uniform field. It is also important to design a slow pulse rise time, since this avoids large eddy currents and spreads out the length of the peak of the sample magnetization signal. If SCRs are used in the circuit, a fast rise time could result in a rate of change of current large enough to exceed the maximum rating of the SCRs. In the following the design for a solenoid coil with rectangular cross section, uniform current density, and round copper wire conductors is optimized. There are variations of this design which improve the performance and reliability of the coil but they are more difficult to build or require material which is not readily available. These will be discussed at the end of the section.

For the optimization procedure, it is convenient to define a geometrical factor $B'(\alpha,\beta)$ such that

$$B'(\alpha,\beta) \equiv \frac{H_{corr}}{\sqrt{\beta L_{corr}}} \tag{2.93}$$

Then the equation for the maximum field, (2.77), which ignores the coil resistance, can be rewritten

$$B_{max} = \mu_0 H_{0\ max} = \sqrt{\frac{\mu_0 E_0}{\pi a_1^3}}\, B'(\alpha,\beta) \tag{2.94}$$

Figures 2.15 and 2.17 show the dependence of $B_{max}$ on $\alpha$ and $\beta$, and on $a_1$.

In the expression for inductance, (2.79), the geometry dependent variables $\alpha$ and $\beta$ may be grouped together in a similar way so that

$$L = \frac{2\pi\lambda^2\mu_0 a_1^5}{\delta A^2} L'(\alpha,\beta) \tag{2.95}$$

where

$$L'(\alpha,\beta) \equiv (\alpha-1)^2\beta L_{corr} \tag{2.96}$$

This is shown in Fig. 2.16.

Altogether there are four independent parameters which specify the coil design: $a_1$, $\delta A$, $\alpha$ and $\beta$ (see Fig. 2.10). The design procedure begins with choosing $a_1$ as small as possible, then maximizing B' by choosing $\alpha$ and $\beta$. The desired field homogeneity must be considered here also, since $\frac{H_2}{H_0}a_1^2$ is strongly dependent on $\beta$ (see Fig. 2.18). Then there remains only the choice of wire size, which, apart from changing the resistance, does not affect the field but determines the value of inductance.

The coil inductance is important because it is the only variable besides C which significantly affects the pulse rise time:

$$t_p = \frac{\pi}{2}\sqrt{LC} \tag{2.97}$$

For reasons already mentioned it is advantageous to make $t_p$, and therefore L, as large as possible.

Decreasing $\delta A$ to raise the value of L has the adverse effect of raising the coil resistance, which has so far not been taken into account in the coil design. The expression for $i_{max}$ which includes the first order effects of resistance is

$$i_{max} \simeq V_c \sqrt{\frac{C}{L}}\, e^{\frac{-\pi}{2} r_0} \tag{2.98}$$

where

$$r_0 \equiv \frac{1}{2} \sqrt{\frac{C}{L}}\, R_0 \tag{2.99}$$

and $R_0$ is the initial resistance. Therefore

$$B_{max} \rightarrow \sqrt{\frac{\mu_0 \overline{E_0}}{\pi a_1^3}}\, e^{\frac{-\pi}{2} r_0}\, B'(\alpha,\beta) \tag{2.100}$$

If $\delta A$ is small enough that the term containing R becomes large, $B_{max}$ will have to be recomputed using the better approximation for $i_{max}$. It may then be necessary to change other parameters, $a_1$ or $\alpha$, in order to maximize $B_{max}$ for a given inductance, and meet the field homogeneity criteria.

Since the choice of $a_i$ and $\delta A$ depends on the sizes that are commercially available, they should be chosen first. This will determine the value of L' which then specifies a particular set of possible values

of $\alpha$ and $\beta$. With these $B_{max}$ and $\frac{H_2}{H_0}a_1$ are easily optimized. Repeating this procedure for other choices of $a_1$ and $\delta A$ will eventually lead to optimum values of the four coil parameters.

Fig. 2.14. Dependence of L on $a_1$ and $\delta A$

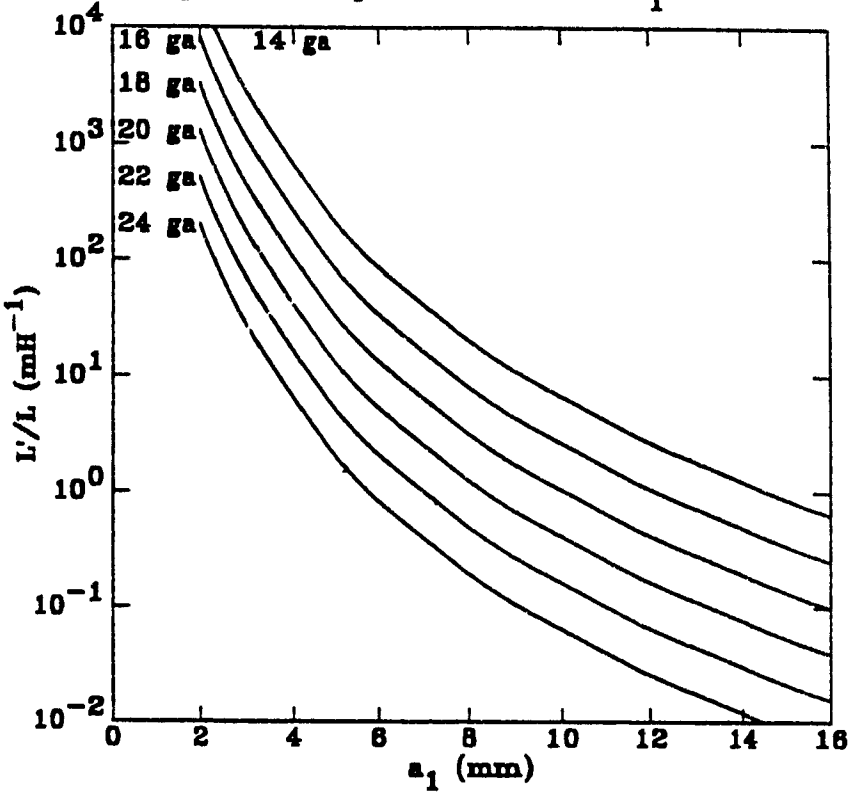


Fig. 2.15. Dependence of $B_{max}$ on $a_1$ and $r_0$

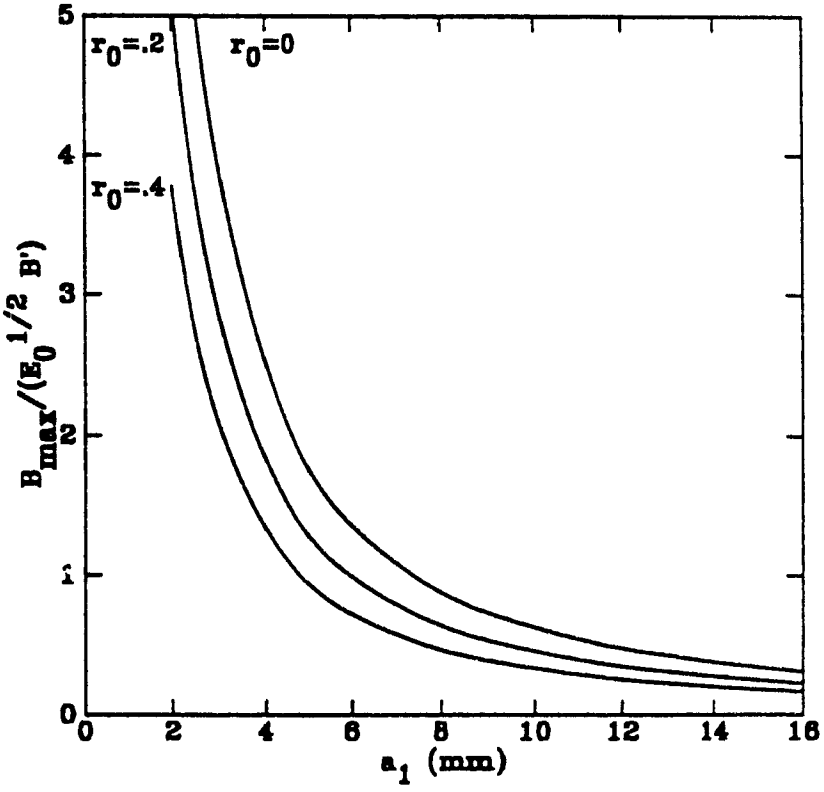

Fig. 2.16. Inductance Geometrical Factor, L'

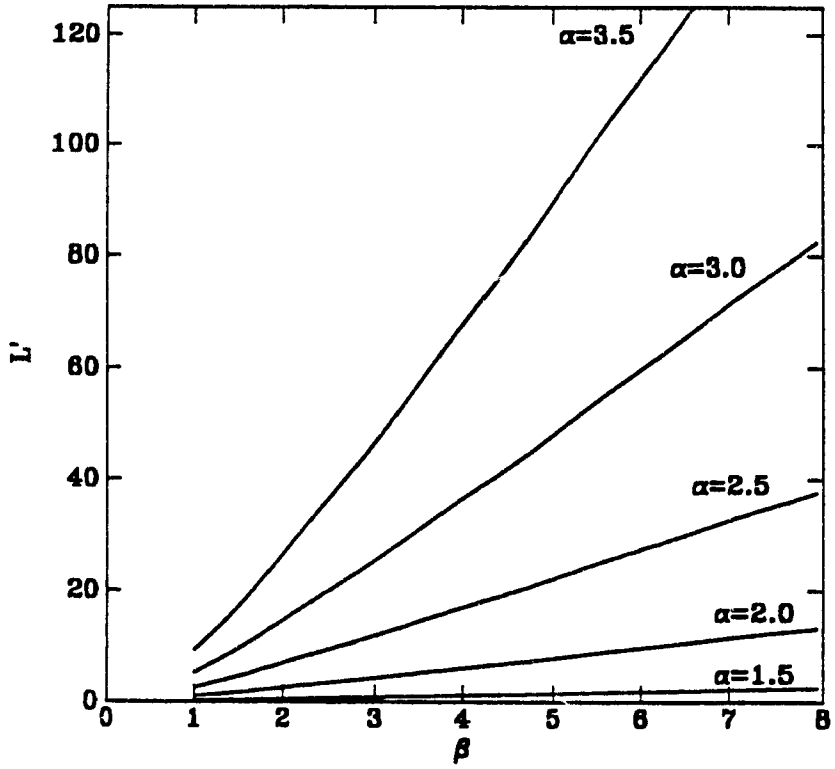


Fig. 2.17. Field Geometrical Factor, B'

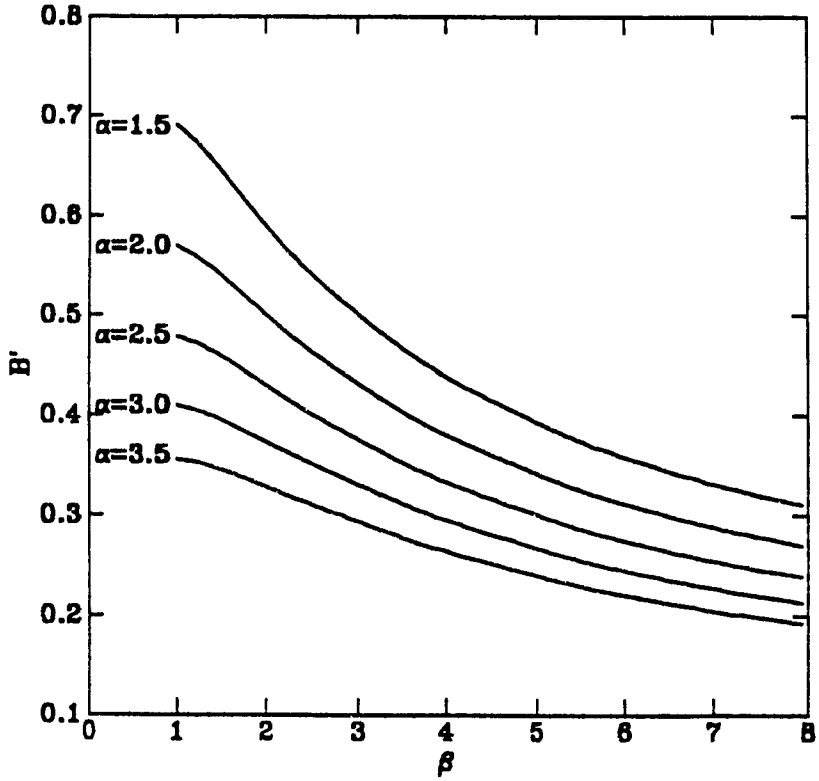

**Fig. 2.18. Field Homogeneity**

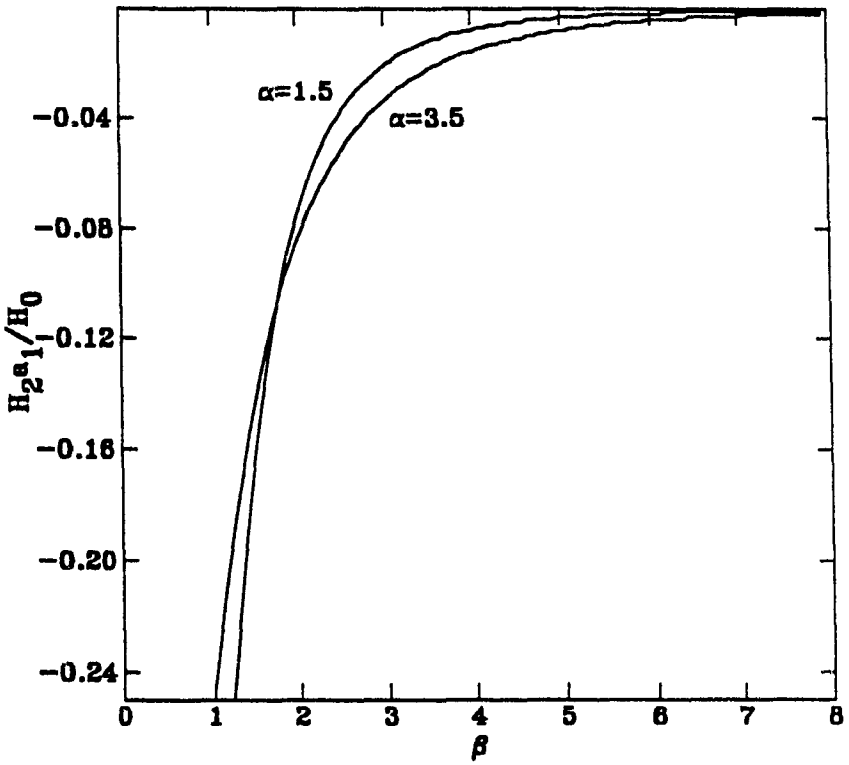

A final consideration in the coil design is the Lorentz force acting on the conductors. These forces cause movement of the conductors in the winding and, for fields above 20 T, the resulting stress in the conductors may exceed the tensile strength of copper.

An estimate of the maximum stress encountered can be made by assuming that the individual turns in the winding do not interact and by calculating the forces on a single conductor loop [24]. The radial force acting on an element of the loop, (see Fig. 2.19), is

$$dF_r = iBrd\phi \tag{2.101}$$

where B is the axial field. By summing the components of the forces in the radial direction the tangential force $F_t$ is found,

$$dF_r = 2F_t\left(\frac{1}{2}d\phi\right) \tag{2.102}$$

and the tensile stress $\sigma$ in the conductor is

$$\sigma = \frac{F_t}{\delta A} = iBr\left(\frac{1}{\delta A}\right) \tag{2.103}$$

The conductors on the midplane have the highest stress since this is where the axial field is the greatest. But to find the maximum of the product Br the dependence of the field on the radius at the midplane must be known. It is reasonable to assume that within the winding the field varies linearly with r, having a value of $B_{max}$ at the bore wall and

reaching zero at the outside edge [25]. Then

$$B(r) = B_{max}\left[\frac{\alpha-(r/a_1)}{\alpha-1}\right] \qquad a_1 \leq r \leq \alpha a_1 \tag{2.104}$$

and the maximum stress is at a radius equal to $\frac{1}{2}\alpha a_1$ so that

$$\sigma_{max} = i_{max}B_{max}\frac{\alpha^2 a_1}{4(\alpha-1)\delta A} \tag{2.105}$$

$$= \left[\frac{1}{2\mu_0}B^2_{max}\right]\frac{\alpha^2}{2(\alpha-1)^2\lambda H_{corr}} \tag{2.106}$$

The ultimate tensile strength of hard copper is 40 kg/mm$^2$ [26]. For typical multi-turn solenoids this is reached at about 20 T.

The above stress calculation shows that the part of the solenoid where $r < \frac{1}{2}\alpha a_1$ is a region of increasing stress with radius so that the turns tend to separate, and the assumption that the turns are isolated is a good one. In the region where $r > \frac{1}{2}\alpha a_1$, the turns press against each other, each one restraining the force from its neighbour on the inside [27]. The calculation of $\sigma_{max}$, therefore, is an upper limit and it is safe to use this value in estimating the maximum pressure on the inside of the mantle surrounding the coil.

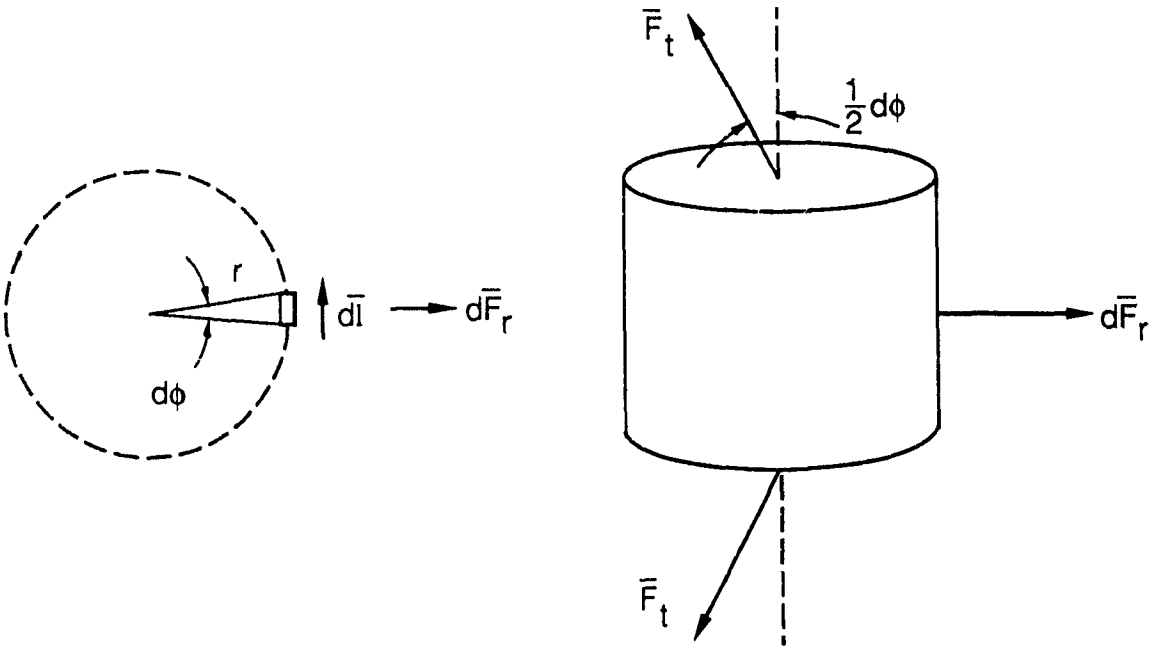


Fig. 2 19. Element of Conductor Loop

Axial forces on the conductors are also present, especially at the ends of the solenoid where the radial field component is maximum. The effect of these forces is the tendency for the turns to slip over each other. Although there is no radial field component on the solenoid midplane, the axial forces here are the greatest because they are cumulative. The resulting stress is generally less than 25% of the tangential stress [28] and so is not significant, but this depends on the restraining forces of the epoxy and the friction between adjacent turns.

Discussions on alternative or more exact methods of calculating stress may be found elsewhere [29-31].

A coil was designed to produce a peak field of at least 20 T, and, for timing considerations, to have an inductance of approximately 20 mH. Based on these requirements, and a convenient 3/4" bore diameter, the following design paramters were chosen using the optimization procedure:

$$a_1 = 9.5 \text{ mm} \quad (3/4\text{" dia.})$$

$$\delta A = 0.823 \text{ mm}^2 \quad (18 \text{ gauge})$$

$$\alpha = 3.0$$

$$\beta = 5.0$$

The maximum field, assuming R = 0, is calculated as 25.8 T with 0.7% uniformity within a sphere of radius $a_1$. The stress calculations show that the maximum tensile stress experienced by the conductors is 47 kg/mm$^2$ at this field, which is comparable with the ultimate tensile strength of copper. Using the values $R_0 = 0.43\ \Omega$ and m = 1.25 kg (see Table 2.1) the maximum field is estimated as

$$B_{max} = 24.0 \text{ T}$$

The relatively large inductance of the coil, 17.5 mH, corresponding to a rise time of 9 msec, was designed in an attempt to reduce eddy currents in the mantle. The slow rise time also broadens the sample response peak making the analysis of the signal easier.

Two coils based on this design were constructed. The first coil was wound onto a former consisting of a 3/4" dia. x .010" wall stainless

steel tube with stainless steel endplates. Each layer of wire was coated with epoxy as it was wound. The finished coil was inserted into a stainless steel mantle with a 7/8" thick wall and 3/8" endplates.

Two important and related problems encountered in the operation of the coil, which must be considered in the coil construction, are the possibility of arcing and movement of the turns in the winding. To prevent arcing between the winding and any of the surrounding stainless steel, double sheets of mylar .008" thick were placed around the former before winding and around the outside of the coil before inserting it into the mantle. Also double sheets of .001" mylar were placed between most of the layers in the winding to isolate the turns at the ends of the solenoid where the voltage difference between layers is quite large, and possibility of slip-over is high due to axial forces. Between individual turns in a layer the insulation of the magnet wire is sufficient.

In a properly built coil, electrical breakdown will only occur after prolonged use and then only because of the gradual displacement of the inner turns in the winding [13,14]. The purpose of the epoxy is to restrain this movement as much as possible. Tra-Bond 2151 was used both because of its strength at liquid nitrogen temperature and because of its thermal conductivity. The radial forces on the winding are also restrained by the surrounding mantle. For fields reaching 40 T the mantle may undergo substantial deformation [13].

Table 2.1 lists the dimensions of the finished coil with the predicted and measured parameters. The predicted parameters were recalculated using the actual space factor and the measured resistance. The linear field-current relationship was then established so that during operation, the current can be used to measure the field. The calibration was made by momentarily passing 15 A direct current through the coil and measuring the field along the coil axis with a Hall-probe (see Fig. 2.20). Of course, this calibration does not take into account the effects of eddy currents in the mantle, which are present when the coil current is changing (see Sec. 2.3).

It is important to know the resistance of the coil at 77 K since small increases in resistance indicate decreasing wire cross-section due to the gradual expansion of the inner winding [13,14]. Because of the resulting change in the inside diameter, the coil may have to be recalibrated after repeated use at full power.

The first coil failed after less than 100 shots at 4 kV ($\sim$ 16 T). Arcing had occured in the inner winding close to the axial center. It was found with this coil that the epoxy does not adhere well to the mylar sheets, so these were left out of the second coil in order to improve the effectiveness of the epoxy. The wire insulation is adequate as long as no turns slip into an adjacent layer. The endplates of the former were replaced with 1/16" phenolic board so that the parts of the coil which

are at high voltage do not come close to sharp edges at ground potential. A different type of epoxy was used, Lepage Epoxy, and a thick layer of Eccobond 286 was applied to the outside of the coil. This was then machined down to fit into the mantle. The specifications of the second coil are given in Table 2.1 and the field uniformity is shown in Fig. 2.20. This time the calibration of field and current was done with a current of 2 A which is sufficient and easier to supply.

The second coil performed well with maximum fields up to 22 T (5 kV). So far it has experienced approximately 300 shots with voltages between 2 and 5 kV (35 of these were at 5 kV). The coil will likely withstand repeated firings at maximum fields up to between 25 and 30 T. Beyond this the performance of the coil will be limited by the ability of the epoxy to resist the Lorentz forces on the inner winding.

**Fig. 2.20. Coil Calibration**

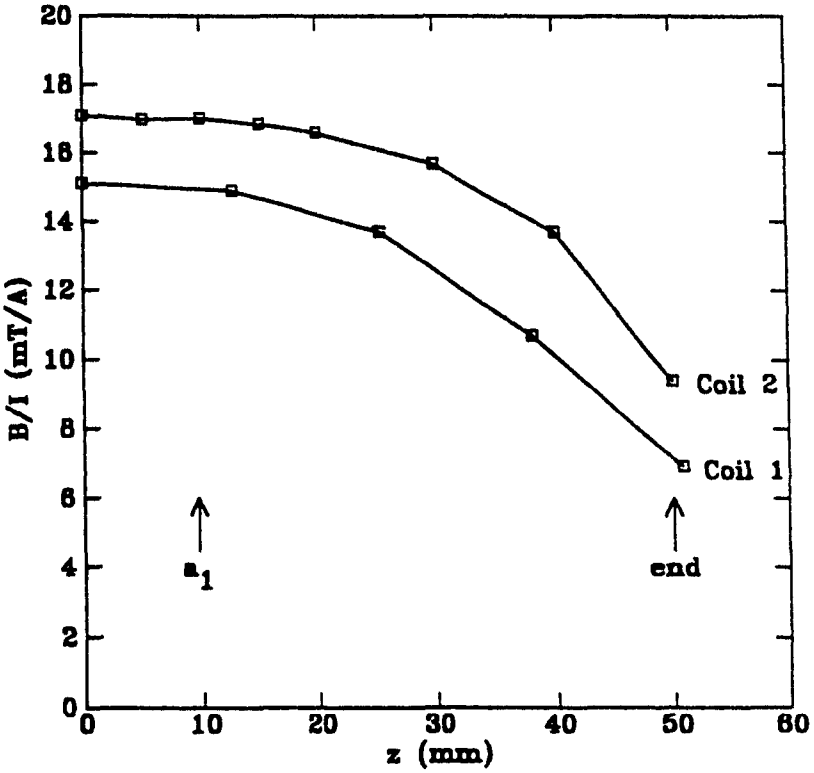

Table 2.1. Coil Specifications

| | Coil #1 | Coil #2 |
|---|---|---|
| I.D. | 19.5 mm | 19.2 mm |
| O D. | 58 mm | 56 mm |
| Length | 100 mm | 100 mm |
| $a_1$ | 9.7 mm | 9.6 mm |
| $\alpha$ | 3.0 | 2.9 |
| $\beta$ | 5 2 | 5.2 |
| N | ≃ 1385 | ≃ 1558 |
| # layers | 16 | 18 |
| $\lambda$ | 0 59 | 0.70 |
| Weight (est.) | 1.25 kg | 1.34 kg |
| R @ 77 K | 0.43 Ω | 0.49 Ω |
| R @ r.t. | 3.5 Ω | 4 0 Ω |
| Calculated parameters: | | |
| L | 17.1 mH | 20.6 mH |
| B/I | 0.0162 | 0.0183 |
| $B_{max}$ @ 4 kV | 19 4 T | 19.9 T |
| $B_{max}$ @ 5 kV | 24.0 T | 24.6 T |
| Mesured parameters: | | |
| | 17.5 mH | 21.8 mH |
| B/I | 0.0151 | 0.0171 |
| $B_{max}$ @ 4 kV | 17.8 T | 18.2 T |
| $B_{max}$ @ 5 kV | ---- | 22.1 T |

Modifications of the design which will improve the reliability of the coil at higher fields are described by Montgomery [32]. This coil uses rectangular copper wire, which is wrapped in fiberglass cloth as it is wound. The coil is then inserted into an epoxy-fiberglass sleeve and vacuum-impregnated with epoxy resin. Different types of epoxy have been used and are described in the literature [13,31]. Van Deursen and de Vroomen [14], in constructing a coil of this type, used epoxy mixed with dolomite powder and then impregnated the coil with transformer oil. The advantage of the rectangular conductors compared with the round wire is mainly the increased space factor, which lessens the stress for a given field. Also, as Knoepfel points out, the rectangular conductors are less apt to slip-over at the ends where the axial forces are strongest [33].

These coils are considered to be reliable for fields up to 25 T [34], at which point the stress limitations for pure copper are exceeded [19,35]. Coils of this type have been built, however, and performed well for fields of 30 to 40 T [13,14].

A further step to strengthen the conductors and so move into a range of higher limiting fields, is to use composite conductors; i.e. copper-clad steel wire. Melville et al. [19] discuss coil design using composite conductors where they claim that a 30% increase in the maximum field is possible over that of coils using pure copper conductors.

In designing any of the above types of uniform-current-density coils, the field homogeneity may be improved by including a notch in the center of the winding next to the bore wall. A method of designing a coil compensated in this way is described by Montgomery [36]. It involves the superposition of the fields from two coils. The field of a solenoid coil with dimensions of the notch is subtracted from the field of the notchless main coil.

The highest fields which still have a useful degree of uniformity are produced by nonuniform-current-density helical coils machined from a solid bar of beryllium-copper alloy. Aside from difficulties in building, the main problem with this type of coil is the small inductance and correspondingly short pulse rise time ($\sim 0.1$ msec). There is much information available on the design and construction of helical coils [10,37-41].

## 2.5 SWITCHING

### 2.5.1 SILICON CONTROLLED RECTIFIERS (SCRs)

Two different systems for switching the capacitor bank to the coil load were installed. A circuit consisting of three series-connected silicon controlled rectifiers (SCRs) fired simultaneously was tried at first. But the SCRs sometimes failed when arcing occured in the coil, so this system had to be abandonned. It was replaced with an ignitron which, although it is more difficult to fire, will withstand coil failures.

The SCR is a three terminal solid state device which controls a high level of power between its anode and cathode terminals by means of a much lower level signal applied between the gate terminal and the cathode. Figure 2.21 shows the SCR circuit. Both the SCRs (#C03-1002) and the gating circuit were supplied by International Rectifiers. Each SCR is rated at 3.5 kV with a maximum surge current of 15,000 A and a maximum di/dt of 800 A/$\mu$s. The snubber network contains resistors for voltage balancing and capacitors to prevent high dv/dt from false-triggering the devices. The oscillator circuit responds to a 12 V step at the input by sending a 40 $V_{pp}$ , 30 kHz square wave to the transformer primary. Separate secondaries of the transformer provide simultaneous signals to the SCR gates and at the same time electrically isolate each gate-cathode circuit. The open circuit gate-cathode voltage is 0.5 $V_p$.

A monostable circuit preceding the oscillator circuit eliminates the possibility of relay bounce which will interrupt the start of the gate pulse train. Stopping the sequence too soon could leave one of the SCRs turned off while the other two are conducting. The voltage on the nonconducting SCR would then rise to a value beyond its rated nonrepetitive forward blocking voltage.

The 30 kHz noise from the gate pulses is significant and was especially noticeable in the voltage signal from the shunt resistor. Most of this was filtered out with a 4-pole low-pass active filter designed with a 10 kHz cut-off. Perhaps a better solution is to raise the frequency of the gating pulses into the megahertz region so that the filtering requirements are not so severe. The modifications to the gating circuit which make this possible are: replacing the transformer driver switches with FETs and replacing the diode bridges on the transformer secondaries with Schottky diode bridges.

On two separate occasions the SCRs failed. In both cases a 1 μF capacitor charged to 4-5 kV, was used in the main ciruit and arcing had taken place in the coil. The low capacitance and loss of inductance during the arcing caused unusually short pulse rise times and large peak currents. The large di/dt through the SCRs probably exceeded their maximum rating, even though the energy transfered was not more than 13 J.

Assuming this was the cause of the SCR failures, one possible solution is to put a saturable reactor (~ 10 A) in series with the coil. This will delay the coil from receiving full voltage until after the SCRs are fully on, at which point a large di/dt is no longer a problem. Whether this is a practicable solution depends on the stored energy in the reactor and on its inductance after saturation compared with the coil inductance.

Another system which was tried was a set of five smaller, less expensive SCRs (GE #B1589142). This SCR has a rated maximum forward blocking voltage of 800 V, although when tested this was found to vary from 750 V to 950 V for different SCRs. The five with the highest blocking voltages were selected and connected to the gating circuit described above. The SCRs were voltage-balanced with 500 kΩ resistance in parallel with each device.

This system worked well at 4 kV and the full 2 mF capacitance despite the relatively low current rating of the SCRs: 150 A continuous, 1500 A surge (estimated). After the failure of the first coil, however, only one of the five SCRs still operated.

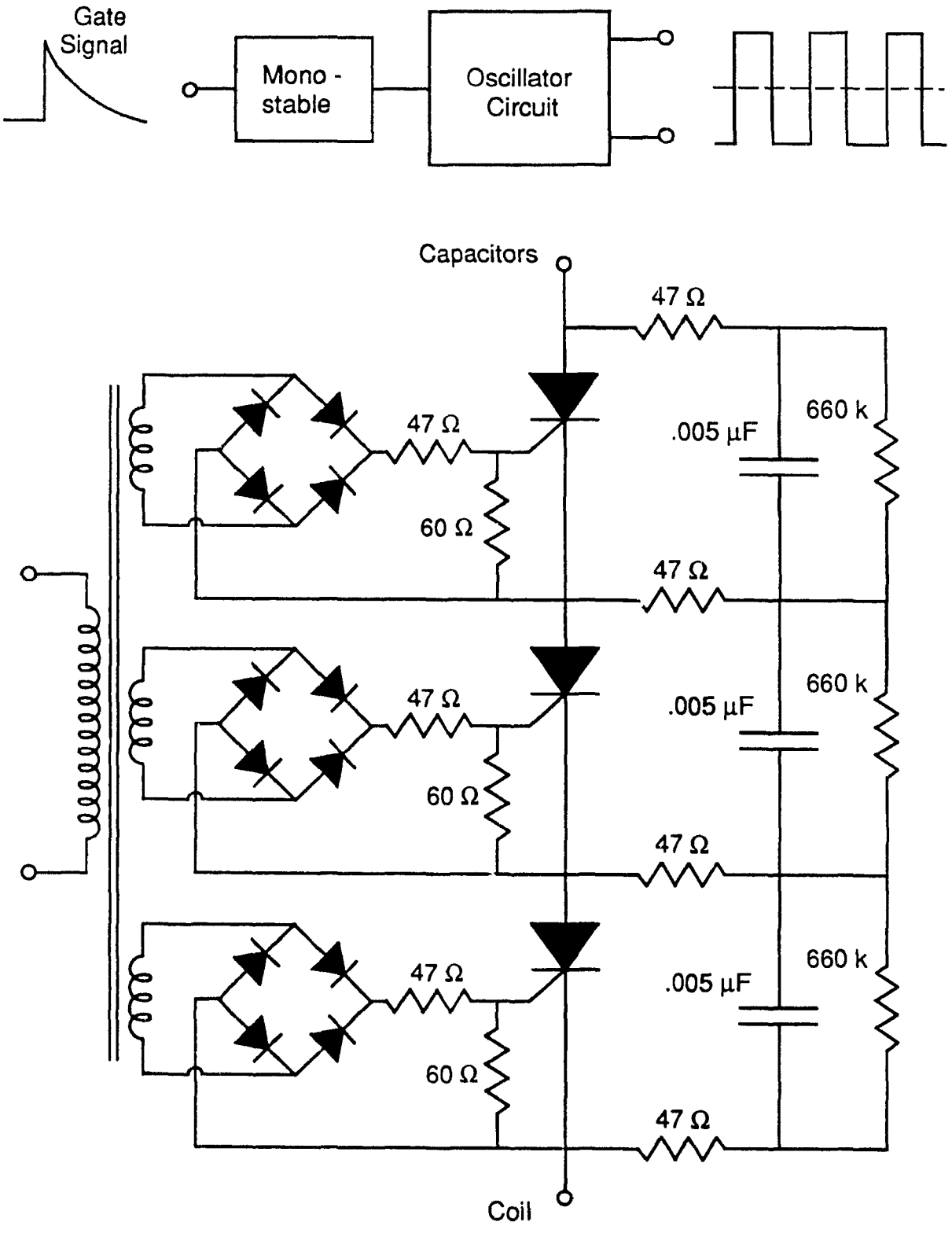


Fig. 2.21. SCR Circuit

## 2.5.2 IGNITRON

The ignitron (National Electronics #NL-1036) is a high voltage mercury-vapour switch. Conduction between the anode and cathode of the ignitron is initiated by a high voltage pulse applied between the ignitor terminal and the mercury-pool cathode. The ignitor current generates ionized mercury vapour which fills the tube and allows conduction to occur. The ignitron is more reliable than the solid state switch although there are several limitations in its use. Figure 2.22 shows the ignitron excitation circuit which is a capacitor discharge circuit switched with a krytron (EG&G #KN6). It is possible to replace the krytron with a set of SCRs, but there are obvious problems with the high voltage. The excitation voltage and the size of the capacitor determine the excitation current pulse shape. It is necessary that the energy of the pulse be large enough to maintain the conduction of the ignitron until the ignitron current has reached its minimum latching value, approximately 5 A. The maximum peak current rating of the krytron, 3000 A for a 50 μsec pulse duration, must not be exceeded when attempting to increase the excitation energy. With the system installed and with the excitation circuit values shown in Fig. 2.22 the ignitron reliably switches anode-cathode voltages as low as 2 kV.

Although the ignitron is rated for 15 kV and 35 kA peak current, repeated firings in the circuit may warm the cathode to the point where

the ignitron loses its voltage hold-off and recovery capabilities. To prevent this the cathode case temperature must be kept below 35°C, using heat sinks or directed air if necessary. The cathode temperature should not exceed the anode temperature.

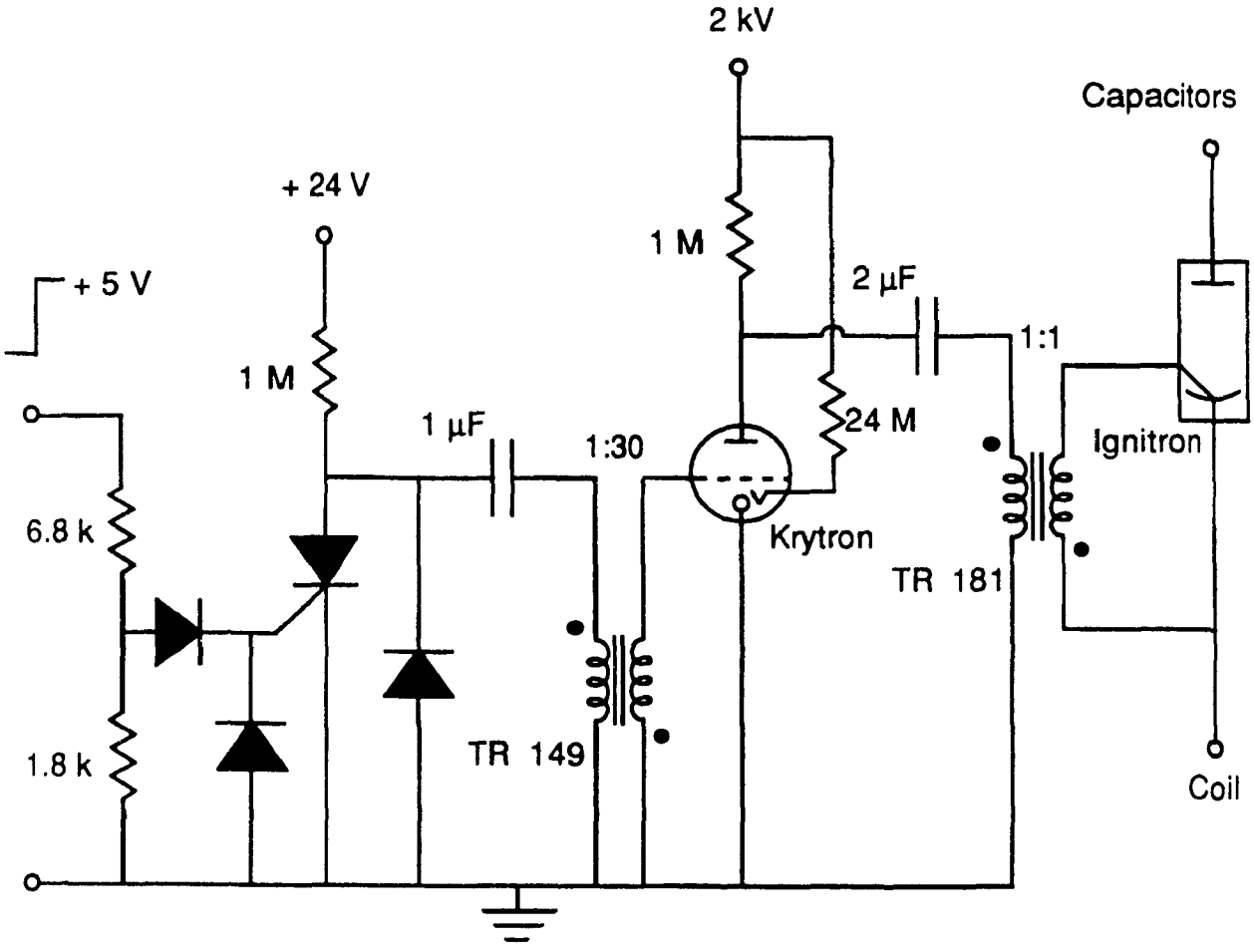


Fig. 2.22. Ignitron Excitation Circuit

## 2.6 FIELD MEASUREMENT

There are several methods of field measurement which are suited for pulsed fields. One of these is the use of a Hall-probe. This was considered but it became clear that, because of pick up on the leads due to the field pulse, there would be difficulties both in keeping the Hall-probe current sufficiently constant and in preventing a signal being induced on the voltage leads. Also, the fact that nonlinear deviations, e.g. magnetoresistance, may show up at high fields, ruled out using the Hall-probe as a practical means of field measurement.

A more common method is to measure the voltage induced on a small pick-up coil inside the solenoid. The integral of this voltage is proportional to the field, and the calibration can be made by using a Hall-probe to measure a small dc field in the center of the solenoid. The pick-up coil must be far enough away from the sample that it does not pick up any of the sample magnetization signal.

As a way of measuring the field directly, the pick-up coil method is the best. In the present system, however, it is possible to determine the field indirectly by measuring the coil current. Since the coil has a uniform current density, the current, neglecting the effects of eddy currents in the mantle, is directly proportional to the field. This is not the case with the helical type coil where current distribution depends on local resistivity of the conductors.

To measure the current a 1 mΩ shunt resistor was used. The choice of resistance value was based on two considerations. First, it must be small compared with coil resistance so that energy diverted from the coil is not significant. For each pulse

$$E_{shunt} = \frac{R_{shunt}}{R_{coil}} E_0 \qquad (2.107)$$

It is also desirable that the temperature of the resistor does not become so high that its resistance changes significantly. The second consideration is that the shunt resistor generate a voltage large enough to be read on the oscilloscope with minimal signal to noise ratio.

Brass and stainless steel were both considered as the resistive material but the temperature coefficients of resistance for these alloys are too large. Inconel was used instead since its resistivity, 1.22 μΩ·m at room temperature, changes by only 0.02% per °C.

The resistor was constructed of a section of inconel (.009" × 1.0" × 6.0") hard-soldered on each side to two copper ends (see Fig. 2.23). The inconel was compressed into an accordian shape for additional strength and compactness. Also shown in the diagram are the voltage leads. The dimensions of each of the sections were chosen not only in order to obtain a particular resistance, but also in consideration of the current paths through the resistor. What must be avoided is a change in current distribution, and therefore a potential drop at the voltage leads, when

the current connector contacts are changed. To solve this problem without making the end sections excessively long, .022" copper was used so that the resistance per unit length through the end sections is much smaller than that through the inconel section. It is also important that there be negligible potential drop between the voltage ground lead and the circuit ground.

The resistance of the shunt resistor was measured as 0.79 mΩ. The measurement was made with the connector configuration shown in the diagram. Play in the connector clamp positions due to the oversize of the bolt holes was found to change the resistance by less than 1%. This may be improved by replacing the copper ends with sections that are much thicker than .022". The inductance of the resistor was measured and found to be $\sim 2$ nH, and so changes in the impedance are not significant for frequencies less than $\sim 1$ kHz. The change in resistance as a result of skin depth effects is not a problem with the present pulse lengths. At 1 kHz the skin depth for inconel is 18 mm where as for copper it is 2.1 mm.

The fairly large loop formed by the voltage leads makes the shunt signal susceptible to pick up from the stray flux caused by the switching of large currents in the circuit, and to noise from the SCR gating circuit, if it is used. Also radio frequency noise is picked up between the resistor and the oscilloscope. For low field measurements the S/N is

worse and shunt resistance should be increased to ~ 10 mΩ. The higher resistance will also reduce the effects of inductance at higher frequencies.

Other types of shunt resistors, such as the double-strip, have lower inductance and are less susceptible to stray flux noise. These are discussed in [42].

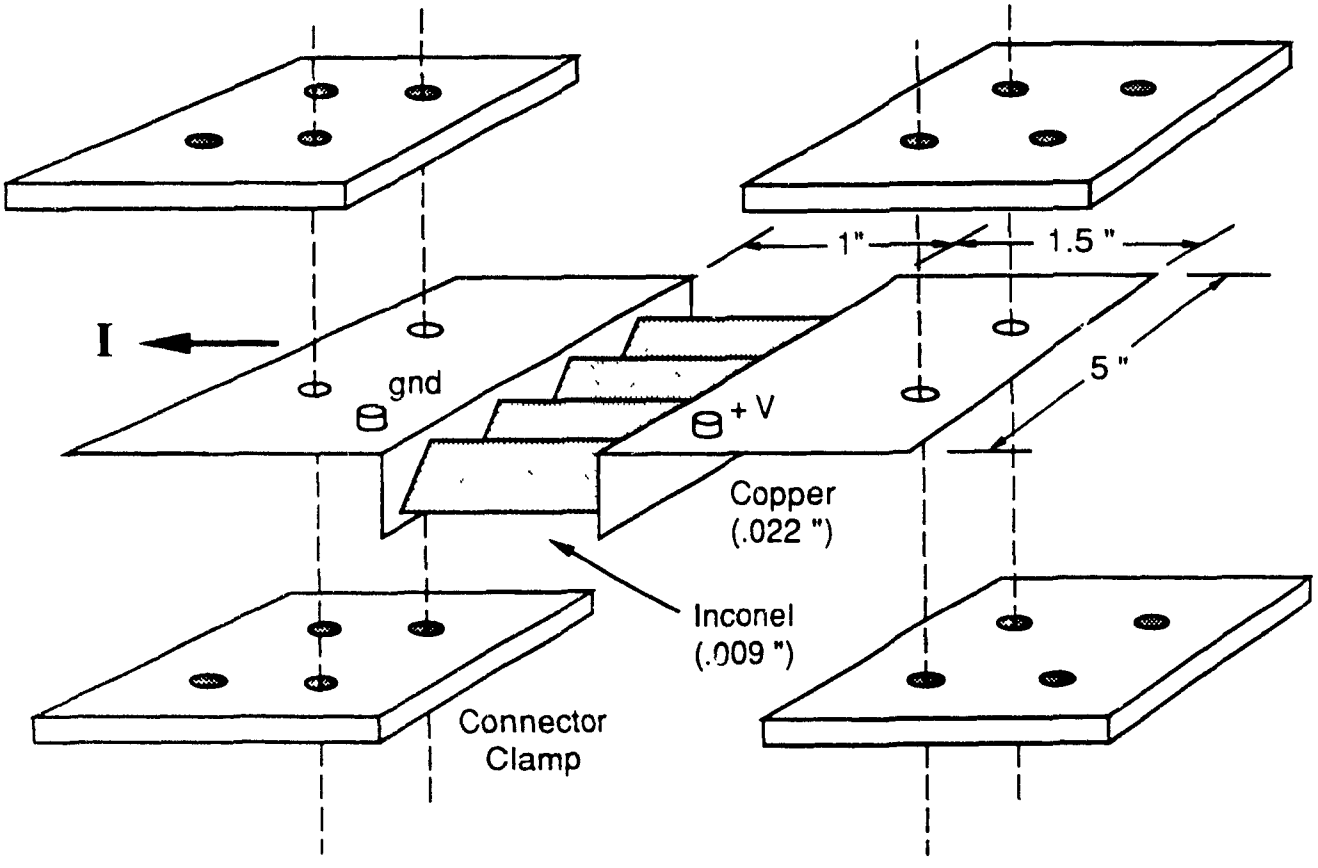


Fig. 2.23. Shunt Resistor

## 2.7 CIRCUIT ASSEMBLY

Figure 4.1 includes the capacitor charging circuit. Power is supplied by a 1.8 kVA transformer (Hammond #131645) which has a 110 V primary and an ungrounded 3500 V rms secondary. The output is full-wave rectified by a diode bridge (I.R. #8HD10J10A) so that a 5 kV peak voltage is available to the capacitors. This voltage can be adjusted to any lower value by a variac at the input to the transformer. The capacitor voltage is read from a voltmeter using a Keithley 1600A high voltage probe.

A ~ 1MΩ (200 W) bleed resistor should be connected between the rectifier output terminals to provide a current path between the capacitor electrodes once the power supply is turned off. This allows the capacitors to discharge within a reasonable time in the event of switching failure, or even to remove residual charge. Much smaller leakage currents also flow through the diode bridge resistors and, if SCRs are used, through the SCR snubber network.

The location of the circuit ground point, as indicated in Fig. 4.1, is necessary if the capacitor casings are to remain at ground potential. The coil mantle is also grounded. Thus during the pulse the potential of the coil lead which is connected to the shunt resistor rises above ground by the value of the drop across the resistor, i.e. several volts.

The conductors connecting the circuit components are 2.5 cm wide copper strips cut from a .022" sheet. The rigidity of these strips is necessary in order to restrain movement during the current pulse. Conductor movement has obvious dangers, and is also a source of noise in the field and magnetization signals. Also, because of the large cross-section of the conductors, negligible resistance, $\sim 1$ m$\Omega$/m , is introduced in the circuit, and the inductance is estimated to be less than 1 $\mu$H/m. This is not significant when compared with the high inductance values of the coils used in this system.

# 3 MAGNETOMETER

## 3.1 PICK-UP COILS

The sample magnetization is detected by two pick-up coils centered within the field-producing coil (see Fig. 3.1). The magnetization signal is the difference between the voltage induced in the coil surrounding the sample, $V_s$, and the voltage induced in the field coil, $V_f$. With no sample, and assuming the coils are identical and the magnetizing field is perfectly uniform,

$$V_s = V_f = -N\frac{d}{dt}\int \vec{B}_{field}\cdot d\vec{s}$$

$$= -\pi N\frac{dB_{field}}{dt}\, b^2 \qquad (3.1)$$

where b is the radius of the coils. But the difference of the voltages will be zero only if the coils are accurately balanced and the coils are exactly centered within the nonuniform yet symmetric field.

An estimate of the strength of the magnetometer signal can be made by assuming the sample is uniformly magnetized with magnetization M in the z-direction. Then the field inside the sample is

$$B_{in} = c\mu_0 M \qquad (3.2)$$

where c is a factor defined in terms of the demagnetizing factor D according to

$$c = 1 - D/\mu_0 \tag{3.3}$$

Therefore c depends only on the sample shape, varying from from 0 for a flat disc to 1 for a thin rod. Typical samples are assumed to be spherical, in which case $c = \frac{2}{3}$ and the field outside the sample is exactly that of a magnetic dipole m, such that

$$m = M \times \text{volume} = M\left(\frac{4}{3}\pi r_0^3\right) \tag{3.4}$$

where $r_0$ is the radius of the sample [43]. The field for $r \geq r_0$ is, in spherical coordinates,

$$B_r = \frac{1}{2\pi}\mu_0 m \frac{\cos\theta}{r^3} \tag{3.5}$$

$$B_\theta = \frac{1}{4\pi}\mu_0 m \frac{\sin\theta}{r^3} \tag{3.6}$$

In cylindrical coordinates the component of the field in the z-direction is

$$\begin{aligned} B_z &= \cos\theta B_r - \sin\theta B_\theta \\ &= \frac{1}{4\pi}\mu_0 m \frac{\left(2z^2 - r^2\right)}{\left(z^2 + r^2\right)^{5/2}} \end{aligned} \tag{3.7}$$

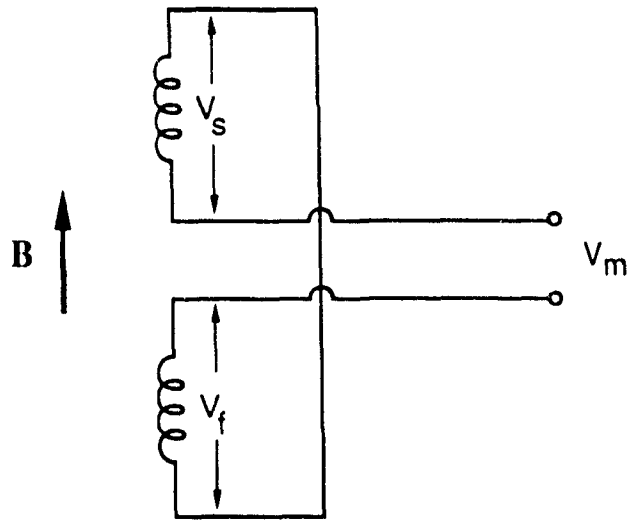


Fig. 3.1. Pick-Up Coil Connections

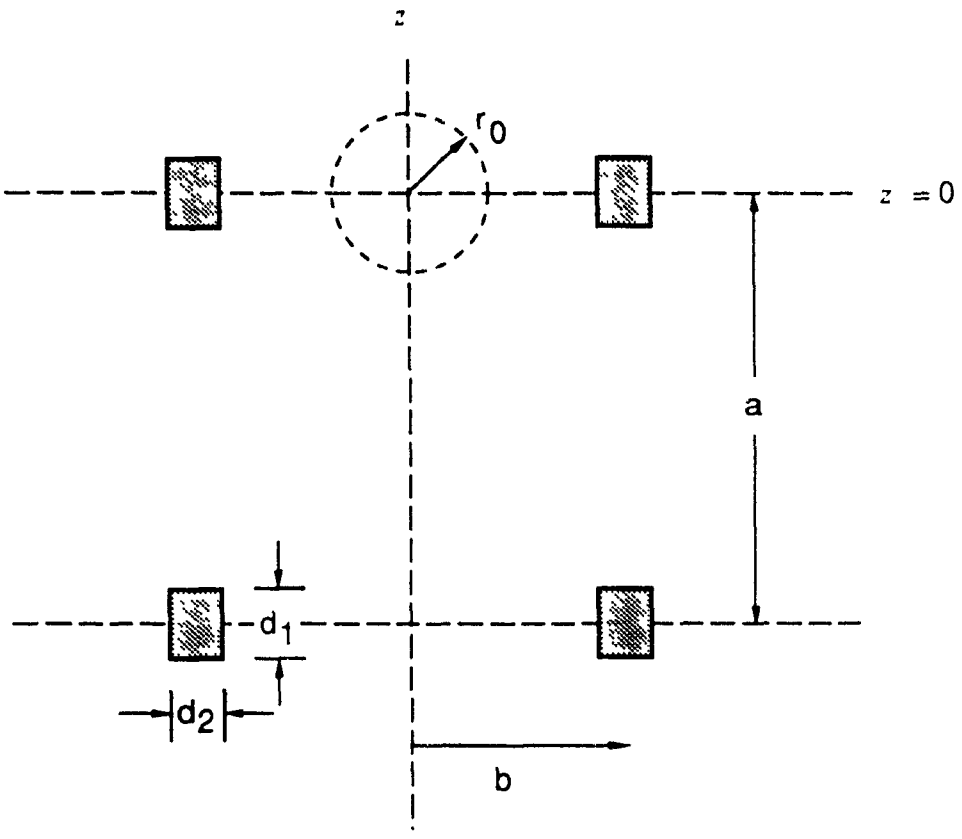


Fig. 3.2. Cross-Section of Pick-Up Coils

Integrating $\frac{dB_z}{dt}$ over the areas bounded by each coil (see Fig. 3.2) gives the induced voltages:

$$V_s = -\frac{1}{2}N\mu_0 \frac{dm}{dt}\frac{1}{b} \tag{3.8}$$

$$V_f = -\frac{1}{2}N\mu_0 \frac{dm}{dt}\frac{b^2}{\left(a^2+b^2\right)^{3/2}} \tag{3.9}$$

where N is the number of turns in each coil. An additional field component $B_{error}$, representing the difference between the magnetizing fields within the two coils, may be included in one of the integrations so that the magnetometer signal $V_m$ is

$$V_m = V_s - V_f - N\frac{d}{dt}\int \vec{B}_{error}\cdot d\vec{s}$$

$$= -\frac{1}{2}N\left\{\mu_0 \frac{dm}{dt}\frac{1}{b}\left[1 - \frac{1}{\left(1+(a/b)^2\right)^{3/2}}\right] + 2\pi \frac{dB_{error}}{dt} b^2\right\} \tag{3.10}$$

Minimizing b will obviously reduce the effects of the error term, but the inside and outside diameters of the coils are already determined by the space available so b is a fixed parameter. To maximize the first term, either the sample size or the distance a may be increased. If a is too large, however, the coils will extend into the regions of the magnetizing field which are significantly nonuniform. The sample is then no longer uniformly magnetized and $B_{error}$ becomes sensitive to small changes in the position of the coils.

The calculation of $V_m$ assumes that the cross-sectional area of the coils is negligible. If the finite dimensions $d_1$ and $d_2$ are taken into account, the effect is to raise the mutual inductance of the two coils [44] so that the difference of the coil signals is actually less than that predicted by Eqn. (3.10). It is therefore desirable to minimize the ratio $d_1/a$.

The overall gain of the magnetometer is proportional to the number of turns on each coil. Increasing N, therefore, increases the signal to noise ratio for noise sources outside the magnetometer. A large number of turns also allows for finer balancing.

Considering the above criteria the pick-up coils were constructed with the following dimensions:

$$a = 13 \text{ mm}$$
$$b = 7.6 \text{ mm}$$
$$d_1 = 3 \text{ mm}$$
$$d_2 = 2.4 \text{ mm}$$

For these values of a and b, according to Eqns. (3.8) and (3.9), 13% of the sample signal will be picked up by the field coil. To maximize N the smallest wire size was chosen, 40 gauge, which was still strong enough to be handled easily without breaking. The number of turns on each coil is approximately 800. As the coils were wound, each layer was coated with GE 7031 varnish. The high potential ( $\sim$ 100V ) between the inside layer of the winding and the grounded dewar wall, eventually resulted in

breakdown of the wire insulation and damage to the sample coil. The coil was then rewound using a sheet of mylar to insulate the coil from the dewar.

In order to balance the coils, a 100 Hz sine wave signal was applied to the field-producing solenoid coil and the pick-up coils were positioned in the center. The induced signal $V_m$ as well as one of the coil voltages, $V_s$, were then read with a lock-in amplifier. The ratio and polarities of these signals indicated the number of turns to be removed from one of the coils, $\Delta N$, according to the formula

$$\Delta N = \frac{V_m}{V_s} N \qquad (3.11)$$

The criterion for balancing was $\Delta N < 1$ corresponding to an error of $< 0.2\%$ . This was met for the range of frequencies 10 Hz to 1 kHz at both liquid nitrogen and room temperature.

Despite accurate balancing, it was still difficult to zero the magnetometer signal because of its sensitivity to the axial position of the pick-up coils inside the solenoid coil. Also, higher order effects due to the asymmetric construction of the pick-up coils or solenoid coil caused $V_m$ to change by as much as a factor of three if the magnetometer was rotated. It is therefore necessary to fix the coils into position in the solenoid coil, using vacuum grease if necessary. With the coils fixed in this way, the magnetometer signal with no sample depends mostly

on $B_{error}$, i.e. on the field, and so, after integration, the signal waveform resembles the field pulse shape. Plotting M vs. B should yield a straight line with a slope that is proportional to $B_{error}$. Actually, because of a small phase displacement between the magnetization and field signals, the curve resembles the shape of an ellipse, Fig. 5.8. This phase displacement is partly due to eddy currents, but may also be the result of mechanical deformations of the coil during the pulse [12].

Allain et al. [12] describe a method for compensating much of this background noise. They have used auxillary coils in the field, which were connected to a phase displacement circuit, to produce both a field compensation voltage and an out-of-phase correction voltage. In the present system the field compensation could just as well be done digitally, after the two signals have been recorded. First the magnetization signal with no sample is integrated. Then the field signal is attenuated so that it resembles the magnetization signal as much as possible. The attenuation factor is then used to compensate subsequent sample magnetization measurements. This does not, however, remove the out-of-phase component of the background noise, or other as yet unexplained distortions to the magnetometer signal.

The background waveform was found to remain mostly unchanged from one pulse to the next as long as the field pulse shapes are identical. This is usually the case if the coil resistance and capacitor voltage are

the same. Then compensation of the magnetization signal is not necessary. The background noise may be removed by first recording a "no sample" magnetometer signal. Then, after the coil has cooled sufficiently, the signal from the magnetometer with a sample is recorded and the background noise is subtracted. A typical background noise signal is shown in Fig. 4.3(c) and in Fig. 5.3.

## 3.2 MAGNETOMETER ASSEMBLY

The sample to be magnetized is contained in a dewar in order to thermally isolate it from the liquid nitrogen bath. The outside and inside walls of the dewar are made from 1/2" and 3/8" stainless steel tubing. A 30 Ω heater to control the sample temperature surrounds the sample region in the vacuum space between the two tubes. The heater is made from cloth-insulated nonmagnetic resistance wire (manganin), which is wound around the inside tube and separated from it by a layer of copper foil. The foil, which is needed to improve the heat conduction to the stainless steel, has a slit along the axis of the tube. This prevents induced currents in the copper. The sample temperature is read by a chromel-constantan (E-type) thermocouple leading down the sample rod to a point just above the sample holder (see Fig. 3.3). A power of 0.5 W is sufficient to keep the sample at room temperature.

The sample holder consists of a threaded nylon tube, in which the sample is placed, and two nylon screws which clamp the sample. The holder screws into the lower nylon section of the sample rod. The screws are of equal length so that regardless of which end of the holder is connected to the rod, the sample is always the same distance from the end of the rod. Ice build-up inside the dewar may impede the movement of the sample rod during operation. For this reason provision was made on the dewar assembly to pump out the space around the sample rod and to

pressurize it with dry helium.

The pick-up coils are wound directly onto the outside tube of the dewar. The inside coil leads are soldered together close to the coils, while the outside leads run up to the top of the dewar as a twisted pair. There they are connected to a BNC connector, one of the leads being grounded. To reduce noise both the coil mantle and dewar are grounded. The pick-up coils are covered with vacuum grease which, in liquid nitrogen, fixes them against the inner stainless steel tube of the solenoid. If the tube itself breaks loose from the inner layer of the solenoid coil, as was the case with coil #2, then vacuum grease must be used there too to keep the whole assembly from moving inside the solenoid. The position of the dewar in relation to the coil is initially adjusted by means of three bolts extending downward from the bottom flange of the dewar. These also provide the grounding for the dewar.

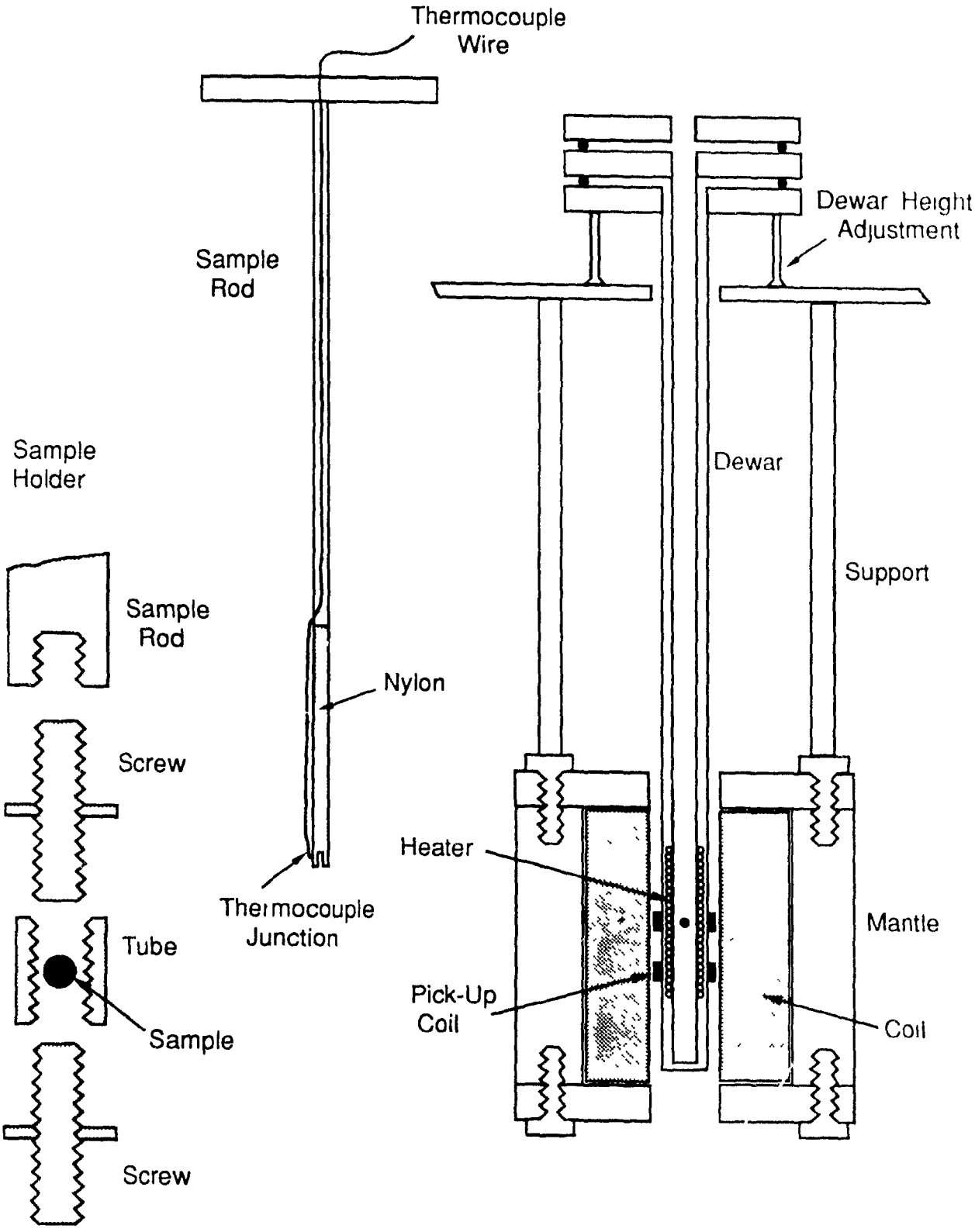


Fig. 3.3. Magnetometer Assembly

# 4 DATA ACQUISITION

## 4.1 SYSTEM

A magnetization measurement with the pulsed field magnet consists of recording and processing two signals:

1) the shunt resistor voltage, $V_{shunt}(t)$, which is assumed to be proportional to the coil field, B(t), and
2) the voltage difference between the two pick-up coils, $V_m(t)$, which is proportional to the sample magnetization signal, dm/dt.

The signals are recorded on the two channels of a digitizing oscilloscope (Tektronix #5223 with a 5B25N time base) and are then transferred to an IBM PC by means of an IEEE interface board. Data transfer as well as signal processing (such as removing the offset level, subtracting reproducible background noise components, and digitally integrating dm/dt) are performed by a set of programs on the PC. Figure 4.1 includes the components of the data acquisition system.

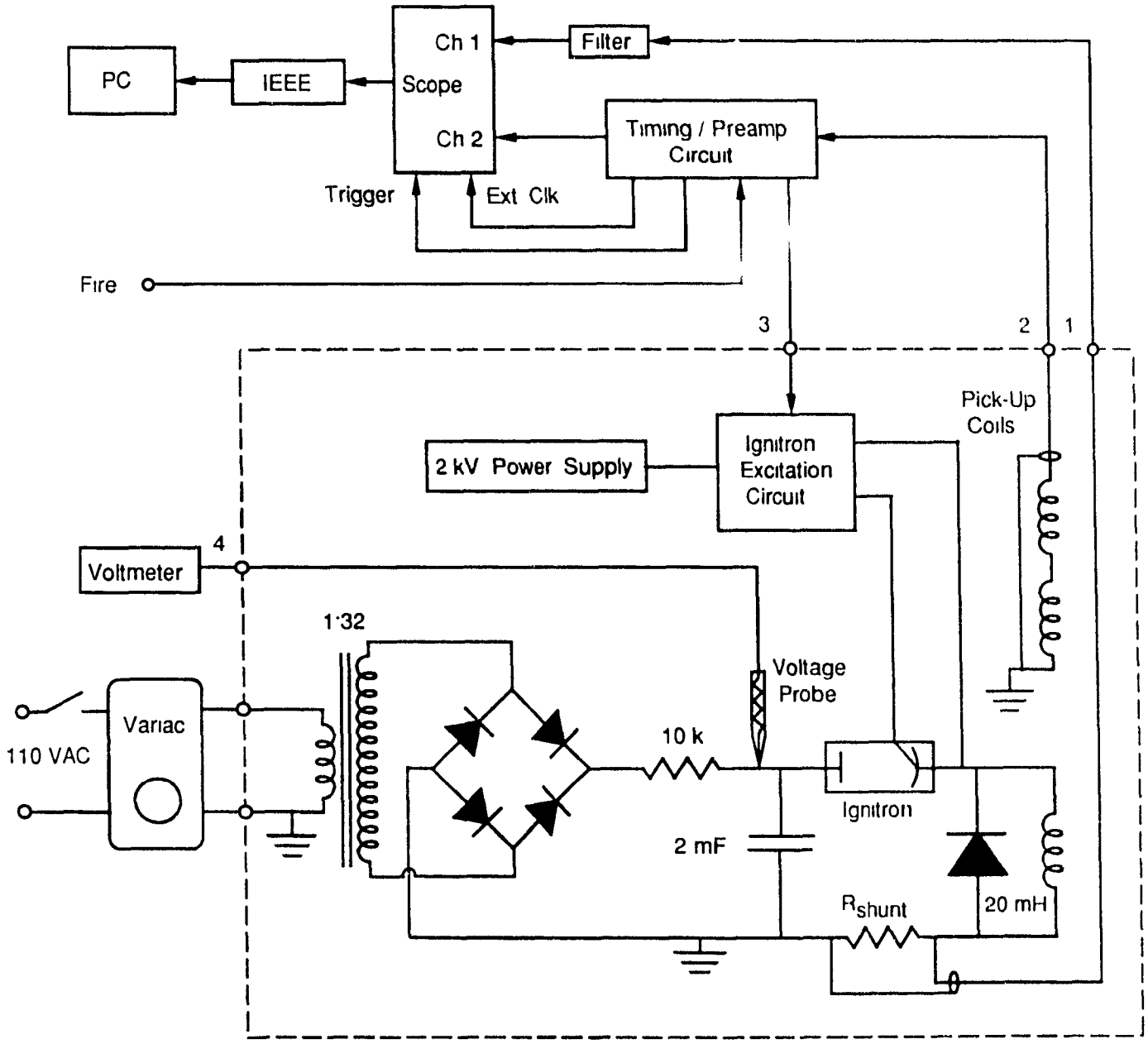


Fig. 4.1. Schematic Diagram of Pulsed Magnet

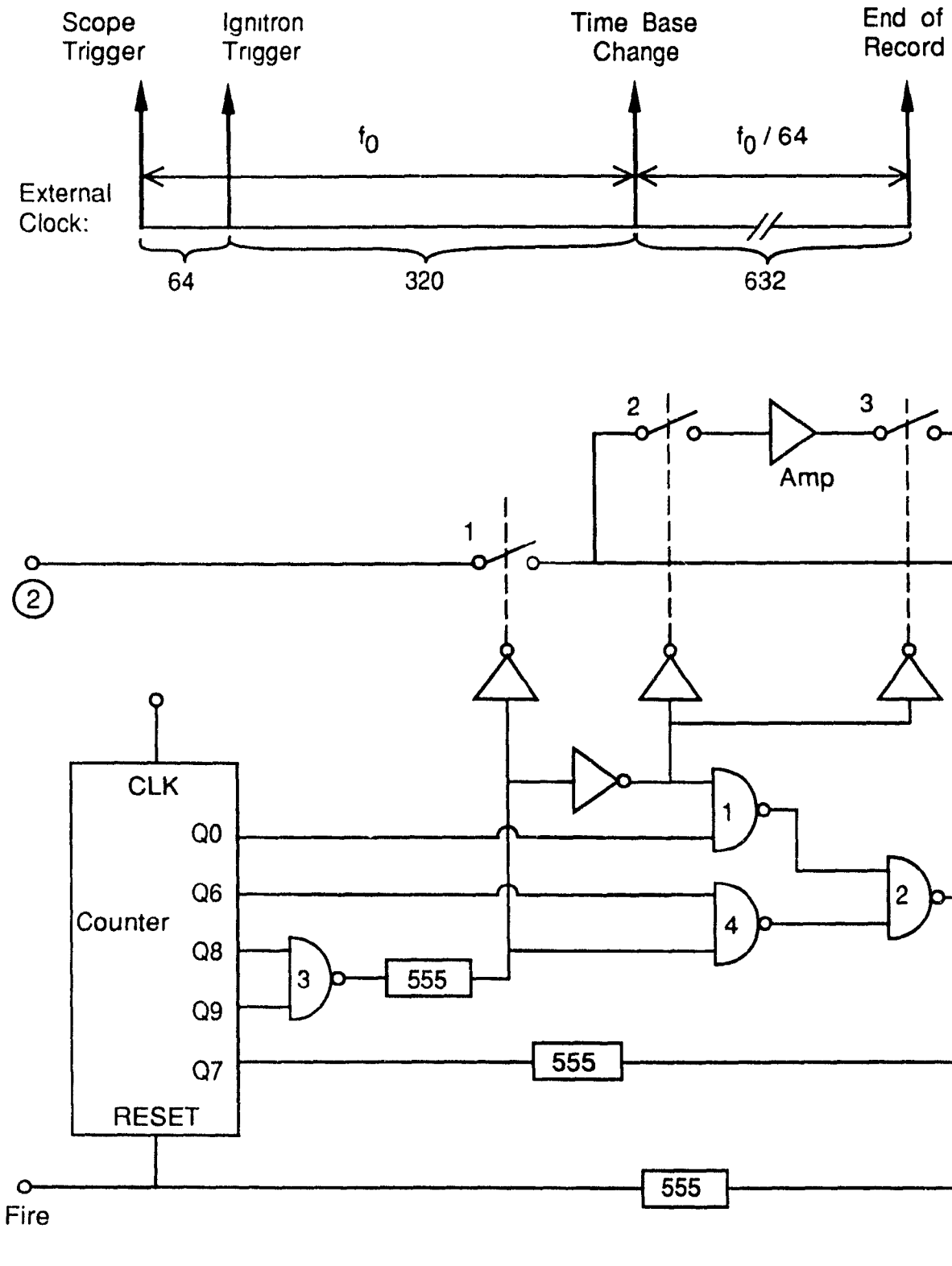


Fig. 4.2. Timing / Preamp Circuit

## 4.2 FIELD AND MAGNETIZATION

The field signal is derived from the shunt resistor voltage through the simple relationship

$$B(t) = \frac{B/I}{R_{shunt}} V_{shunt}(t) \qquad (4.1)$$

where the previously measured calibration constants are

$$B/I = 0.0171 \text{ T/A} \qquad \text{(Coil\#2)}$$
$$R_{shunt} = 0.79 \text{ m}\Omega$$

The ratio B/I is actually frequency dependent, and the above constant, which was measured using direct current, may predict field values at the start of the pulse which have an error of at most 6% of $B_{max}$. This is due to eddy currents circulating in the mantle, as discussed in Sec. 2.3. A typical field pulse measured by the shunt resistor is plotted in Fig. 4.3(a).

Figure 4.3(b) shows the dm/dt signal for a $Nd_2Fe_{14}B$ sample in a 13 T peak field. The magnetization M is clearly nonlinear with the field B, and therefore with time, with most of the change in M occuring in the first part of the signal (i.e. before saturation). The signal may therefore be divided into two regions corresponding to the sample magnetization, and the sample saturation and eventual drop to remanent magnetization. Since the sample saturates at ~ 2 T, the first region

consists of the first 1 or 2 msec of the signal, which is approximately 1% of the signal length. This presents a problem in recording the signal since the digital oscilloscope records only 1016 points and, for accurate integration of the waveform in this region, at least 300 points are needed. By using the oscilloscope in its external clock mode, and varying the sampling rate, it is possible to distribute a large number of points in the first region and at the same time record the entire pulse. Figure 4.2 shows the distribution of points for an initial sampling rate $f_s(\text{region 1}) = f_0$ (typically 130 kHz), and a sampling rate in the second region $f_s(\text{region 2}) = f_0/64$.

On integrating over the second region of the signal it is then necessary to change the weighting of the points to account for the change in time base. The weighting factor is

$$W = \frac{f_s(\text{region 1})}{f_s(\text{region 2})} \tag{4.2}$$

and $W = 64$ for the values of $f_s$ specified above.

In most of the second region of the signal the magnetization is saturated so that dm/dt is essentially zero and only a background signal due to the pick-up coil imbalance is present. Since the number of points in the vertical scale of the oscilloscope is 1024, and the pulse height in the first region is ~ 5 V, most of this background signal has an amplitude which is less than the resolution of the oscilloscope.

Integrating over this region will therefore produce digitization error ot the order of $N^{1/2}$ where N is the number of data points. For a typical sample size (70 mg of NdFeB) this error is only 1% of $M_{sat}$. A weighting factor of 64, however, increases the error to $\sim 64N^{1/2}$, and this is significant.

To reduce this error the magnetometer signal is preamplified with a switch in gain corresponding to the switch in the time base. By adjusting the ratio of the gains such that

$$W = \frac{f_s(\text{region 1})}{f_s(\text{region 2})} \times \frac{\text{gain(region 2)}}{\text{gain(region 1)}} = 1 \qquad (4.3)$$

the digitization error introduced by weighting is eliminated.

The purpose of the timing/preamp circuit shown in Fig. 4.2 is to operate the oscilloscope in its external clock mode, i.e. provide the sampling clock pulses and external trigger, and to amplify dm/dt over the region of low signal.

Application of a 5 V step to the "fire" terminal triggers the oscilloscope and at the same time enables the counter. The oscilloscope is now sampling at the rate of $f_0$ which is the rate of the pulses at the counter output Q0. Analog switch 1 is closed and switches 2 and 3 are open so the magnetometer signal is connected directly to the oscilloscope. After 64 pulses the ignitron excitation circuit is triggered from Q7. The data taken during this delay is used later during

the signal processing to calculate the offset of the signal. The oscilloscope continues to sample at the rate $f_0$ until a time determined by Q8 and Q9, at which point the rate changes to $f_0/64$. This is the pulse rate of Q6. Coincident with the change in external clock rate is the opening of switch 1 and closing of switches 2 and 3. From this point on the oscilloscope is sampling at the rate $f_0/64$ and the magnetometer signal is amplified by the appropriate gain according to Eqn. (4.3). The preamp is an OP07 low voltage offset op amp connected in the standard noninverting configuration.

There are some difficulties in operating the external clock of the oscilloscope when it is in the single sweep mode. For the oscilloscope to acquire data correctly the clock pulses must begin at the same time as the external trigger is pulsed. It is also necessary to position the acquired data onto the oscilloscope storage record by adjusting the time scale setting and calibration knob. The purpose of this adjustment is to have the data acquisition begin as close as possible to the beginning of the clock pulse train. It is usually adequate to have the acquisition begin after 10 or 20 clock pulses. The points of ignitron trigger and time base change must then be found not only after each set-up but after each data acquisition as well, since there is sometimes a variation of several points from one acquisition to the next.

The change in external clock rate of the oscilloscope is accompanied

by a small change in the zero offset so that the later removal of the offset must be done in two parts. The data points prior to the ignitron trigger are used to calculate the offset corresponding to the initial signal. For the rest of the data the offset is calculated from the last 50 to 100 points of the record, depending on the decay of the signal.

**Fig. 4.3 Field and Magnetometer Signals**

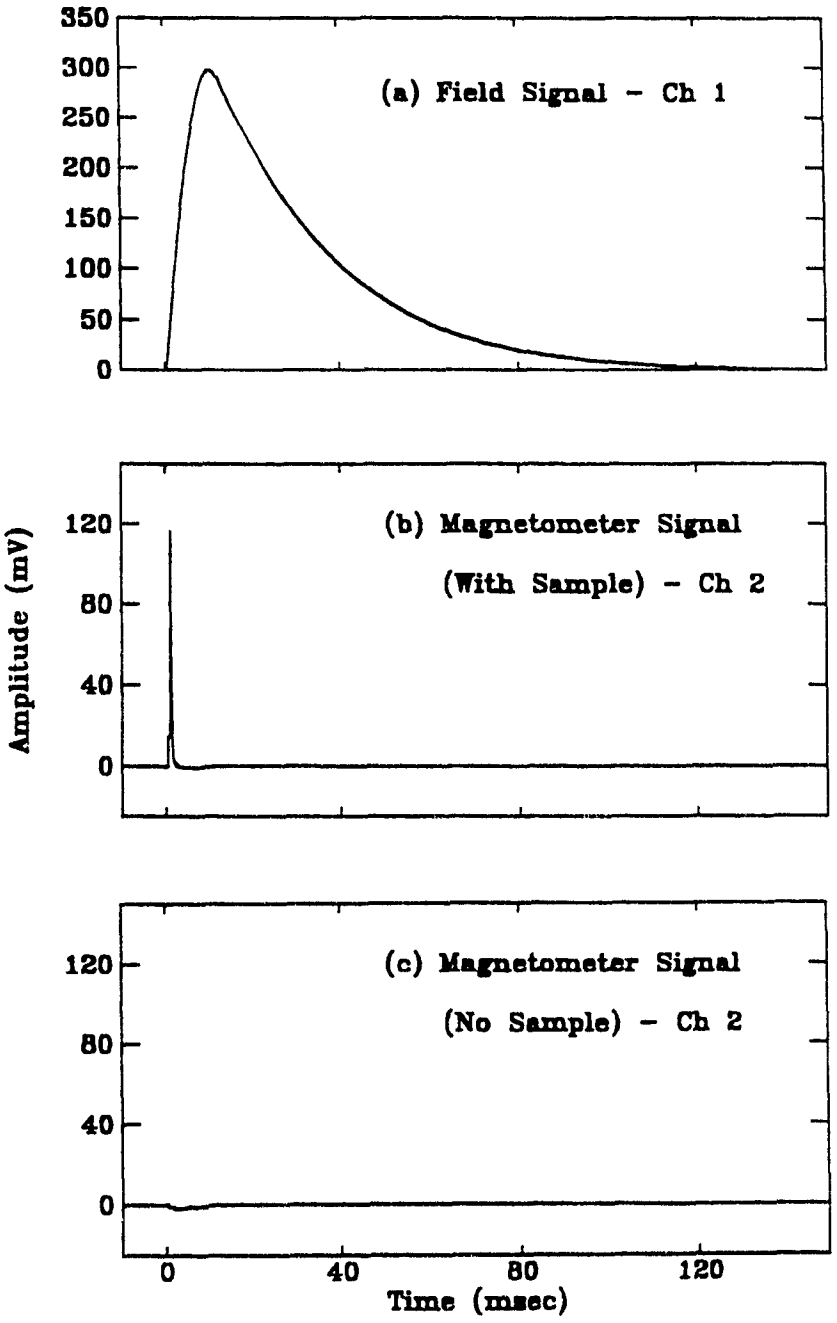

## 4.3 NOISE

The most serious noise on the field and magnetometer signals appears as large voltage spikes in the first millisecond following the start of the pulse. Not only is important information lost in this portion of the magnetization curve but usually the large magnitude of the noise (~ 10 V) is responsible for a significant erroneous contribution to the integral of the dm/dt signal. The cause of the noise is primarily stray flux from the large change in current on the conductors between the capacitors and the coil, and, to a lesser extent, interferance from the ignitron excitation circuit. Also, similar, but much smaller, noise spikes frequently appear at a point on the signals when the peak current is suddenly diverted through the diodes.

There are several ways in which this noise may be reduced. By keeping the current-carrying conductors close to their ground return paths, much of the stray flux can be eliminated. Also, if some of the current flows initially through the capacitors in the diode balancing network, then a leakage current around the ignitron will keep these capacitors charged to a voltage closer to $V_c$, thereby reducing the initial current. Shunting the anode of the ignitron to its cathode with a network of capacitors will have the same effect. That part of the noise which is picked up by the signal cables is best dealt with by transmitting the field and magnetometer signals through double coaxial

cables to differential amplifiers. This technique will eliminate most of the common-mode noise on the signal cables.

Filtering out the noise with a low-pass filter is possible with the field signal. This is not desireable, however, with the magnetometer signal since considerable distortion to the magnetization curve may result depending on the maximum dM/dB of the sample. As a last resort the noise spikes in the magnetometer signal can be removed afterwards, during the signal processing, as long as the correct signal is predictable where the spikes occur. But this becomes increasingly difficult for higher field pulses, since the time at which the peak of the dm/dt signal occurs shifts closer to the start of the field pulse.

Apart from the initial voltage spikes, the signal noise does not seem to greatly affect the magnetization measurement as long as ignitron switching is used. If SCRs provide the switching, then 30 kHz noise from the SCR gating circuit appears on the signals. Techniques for removing this noise are discussed in Sec. 2.5.1. Any reproducible extraneous signal from the magnetometer will, of course, be removed when the reference signal is subtracted from the sample signal.

# 5 MAGNETIZATION MEASUREMENT

## 5.1 OPERATION AND CALIBRATION

The steps involved in setting up the pulsed magnet for magnetization measurements include cooling the coil to liquid nitrogen temperature, positioning the pick-up coils in the center of the field, mounting the sample in the sample holder, and setting the sample temperature. The pick-up coils are balanced by recording a series of no-sample magnetometer signals for various positions of the dewar. The optimum position is the one which minimizes the magnitude of the no-sample magnetometer signal. Once this is found there is no need to change the setting unless the coil assembly is dismantled.

When mounting the sample in the holder, it is important that the sample be symmetric with respect to its center along the axis of the holder, so that if the direction of the holder is reversed, the sample will maintain the same shape and position in relation to the pick-up coils.

Once the initial set-up is completed the pulsed magnet is ready for operation, and for safety reasons, this is done almost entirely from outside the room. It is only necessary to enter the room to remove or reverse the sample holder.

The capacitors are first charged to a voltage $V_c$ roughly corresponding to the desired peak field according to Eqn. (2.98) and the calibration constant B/I. The charging voltage is set by the variac (charging voltage = variac voltage x transformer step-up), and the instantaneous capacitor voltage is read from a voltmeter using the high voltage probe (see Fig. 4.1). When $V_c$ is reached the variac is turned off and the ignitron is triggered. The sample is then reversed, if desired, and after a recooling time of approximately 10 min. (see Sec. 5.2), the procedure is repeated. To obtain the hysteresis loop of an initially unmagnetized sample, the magnet must be fired three times and the sample must be reversed between pulses. The first pulse magnetizes the sample, then two magnetization measurements are made for the two directions of applied field. At the end of the sample measurements the sample holder is removed and a no-sample reference measurement is made. A typical field signal and sample and reference magnetometer signals are plotted in Figs. 5.1 to 5.3. The units are point values from the oscilloscope. A fourth plot, Fig. 5.4, is the difference between the previous two signals.

Fig. 5.1. Field Signal (Ch 1)

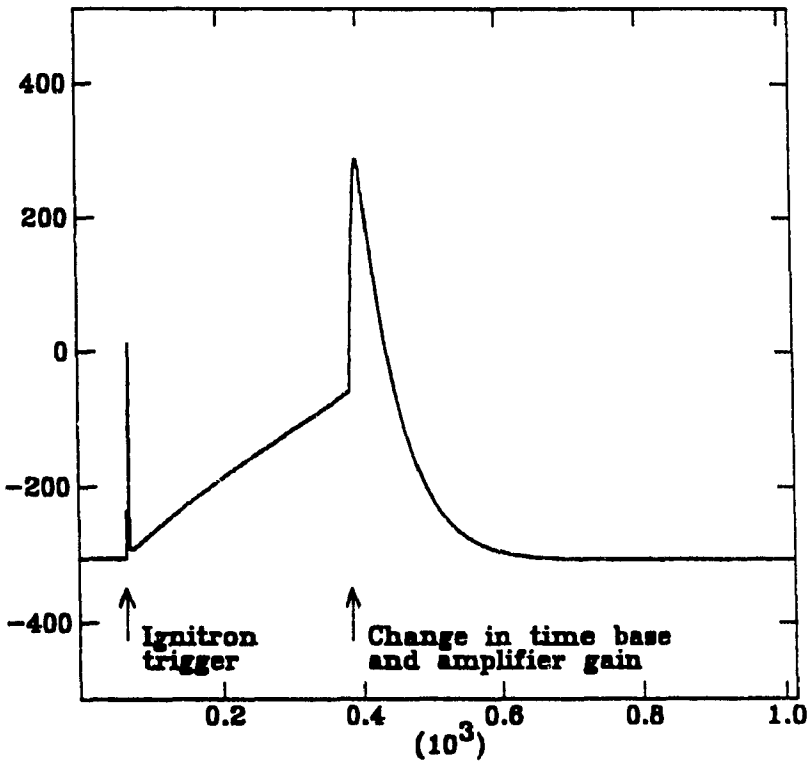


Fig. 5.2. Sample Magnetometer Signal (Ch 2)

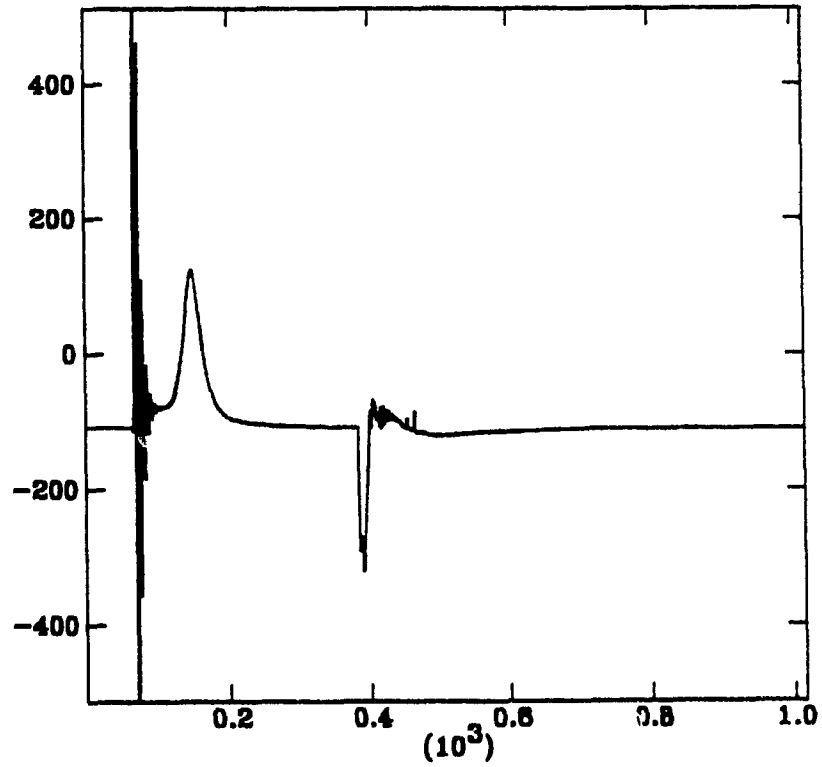

Fig. 5.3. Reference Magnetometer Signal (Ch 2)

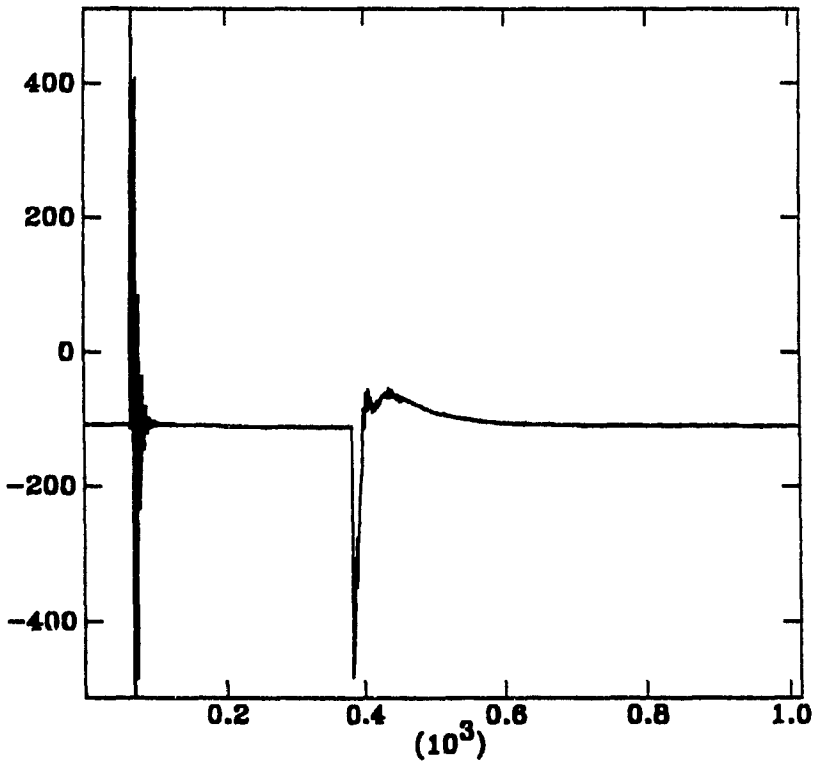


Fig. 5.4. Sample Signal with Reference Subtracted

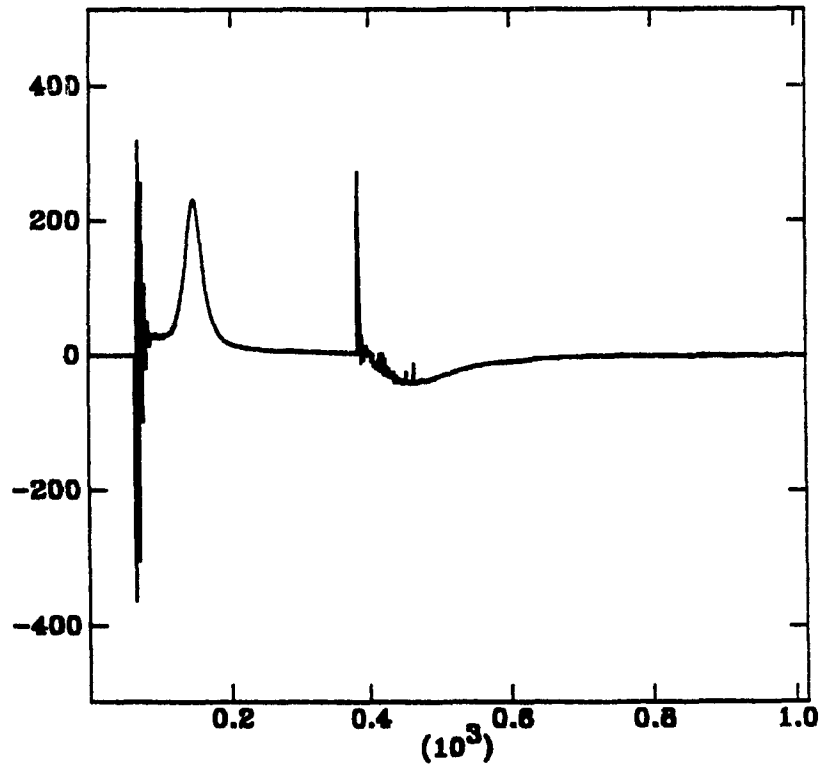

After each pulse of the magnet the data recorded on both channels of the oscilloscope is transferred to the PC. This is done by the program "scope" which runs the IEEE board and sends commands to the oscilloscope. "scope" puts the data into one of two sets of files depending on whether it is a sample measurement or a reference measurement. "col" is a program which arranges the data into columns:

Column 0 - consecutive point numbers representing the time base.

Column 1 - field signal (Ch 1) for the sample measurement.

Column 2 - magnetometer signal (Ch 2) for the sample measurement.

Column 3 - magnetometer signal (Ch 2) for the reference measurement.

The program has an option for shifting the time base of column 3 so that the point of the time base change coincides with that of columns 1 and 2.

The remaining programs perform the signal processing required to produce a magnetization curve. First, any unwanted noise is removed by the program "line" which replaces a specified section of the signal data with a straight line. Next, "off" followed by "sub" remove the signal offsets and subtract the reference signal (column 3) from the sample signal (column 2). "off" calculates two offsets for the two regions on either side of the time base change. The calculation is based on a predetermined number of points at the beginning and end of the data. The data is then passed to the program "int" which integrates the sample signal with reference subtracted. The integration is trapezoidal, i.e.

the area is calculated under lines drawn between points, and takes into account the changes in time base and gain in the signals. Figures 5.5 to 5.8 show the integrated signal, M, plotted against both the time base and the field, B. Also plotted against B are the sample and reference signals integrated separately. After integration, point values of the data are multiplied by scaling factors using the program "scale". This program also calculates B vs. H and B vs. $(BH)_{max}$ curves.

The program listings with more detailed explanations of their operation are given in the appendix.

Fig. 5.5. Sample M vs t with Reference Subtracted

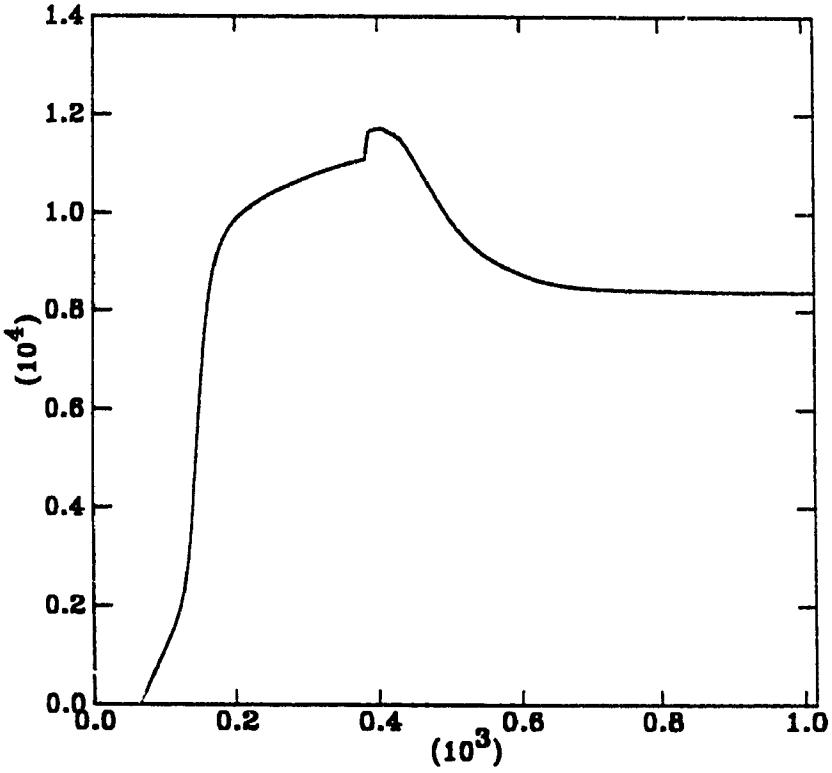


Fig. 5.6. Sample M vs B with Reference Subtracted

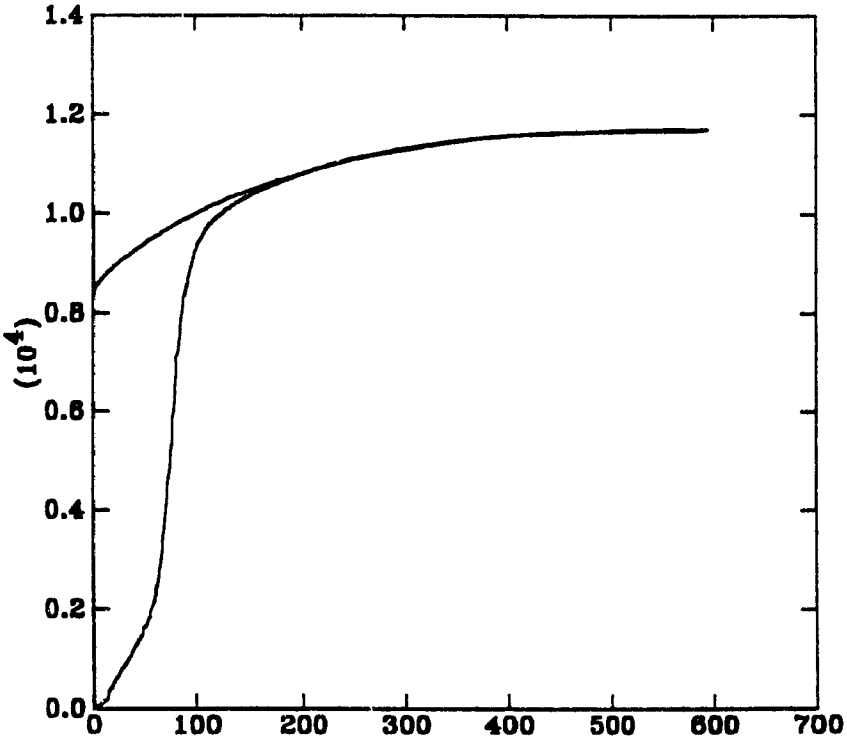

Fig. 5.7. Sample M vs B

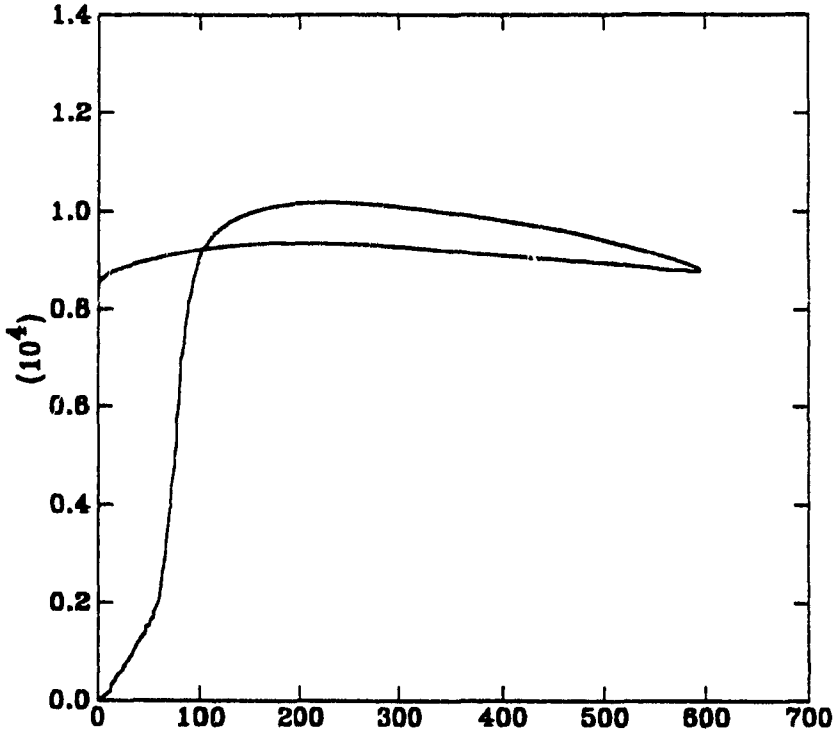


Fig. 5.8. Reference M vs B

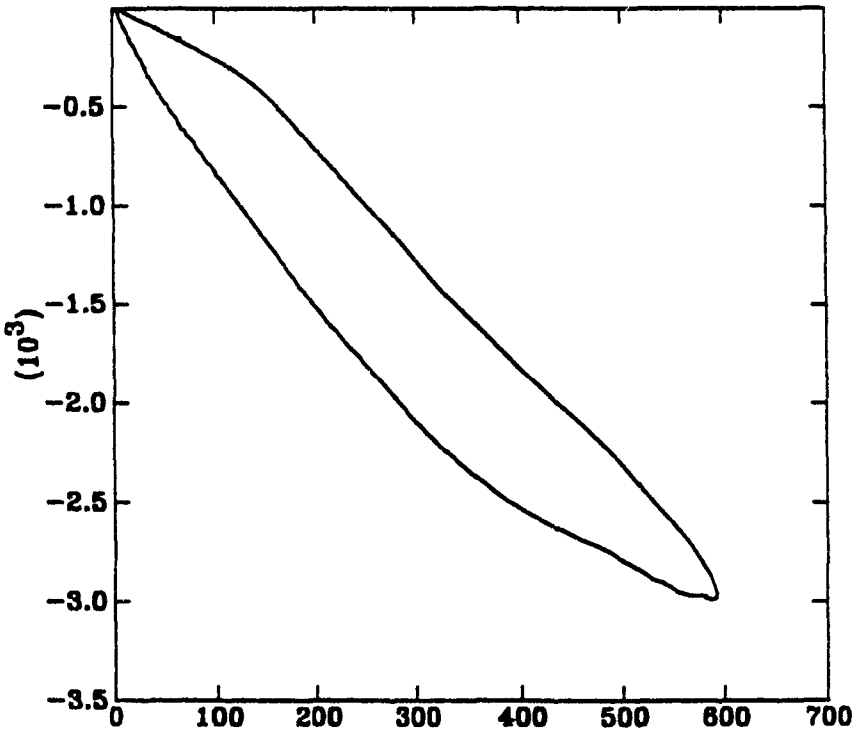

The scaling factors mentioned above convert the point values of the data to values corresponding to physical units. The data transferred from the oscilloscope is converted to voltage by the formula:

$$V = \frac{\left[\text{ amplitde setting (V/div) }\right]}{\left[\text{ \# points/div }\right]} \times \left[\begin{array}{l}\text{point value of}\\ \text{output from "scope"}\end{array}\right] \qquad (5.1)$$

The vertical scale of the oscilloscope contains 100 points per division. With V known for channel 1, the B-axis is found using Eqn. (4.1):

$$B(t) = \frac{(B/I)}{R_{shunt}} V_{shunt}(t) \qquad \text{(in Tesla)}$$

The time base is given by

$$T = \frac{\left[\text{ point value of column 0 }\right]}{\left[\text{ sampling frequency } (\sec^{-1})\right]} \qquad (5.2)$$

where the sampling frequency is $f_0$ before the time base change and $f_0/64$ after.

The formula for determining the scaling of the magnetometer signal after integration is, from Eqn. (3.10),

$$M(t) = \frac{\int V dt}{K \times \left(\frac{\text{sample}}{\text{volume}}\right)}$$

$$= \left[\frac{1}{K \times \frac{\text{sample}}{\text{volume}}}\right] \frac{\left[\text{ amplitude setting (V/div) }\right]}{\left[\text{ \# pts/div }\right]\left[\ f_0(\sec^{-1})\right]}$$

$$\times \left[ \begin{array}{l} \text{point value of output} \\ \text{from "int" (column 2)} \end{array} \right] \qquad (5.3)$$

remembering that gain and change in time base are accounted for in "int". Unless the sample is initially unmagnetized, then the initial magnetization, $M_0$, must be added to the integrated signal. If the previous magnetization of the sample was the same applied field in the opposite direction (i.e. sample reversed), then the final value of M is equal to $-M_0$ and the zero of the M-axis is the midpoint between the initial and final values of M.

The calibration constant K is particular to the sample shape, and according to Eqn. (3.10).

$$K = \frac{1}{2}\mu_0 \frac{N}{b} \left[ 1 - \frac{1}{\left(1 + (a/b)^2\right)^{3/2}} \right] = 0.058 \qquad (5.4)$$

for spherical samples.

For a sample of arbitrary shape there are several ways for scaling the M-axis, which involve determining either K or K × (sample volume). If the coercive field $B_c$ is already known as a function of the maximum applied field $B_{max}$ over some range of $B_{max}$, then K is found by making an initial magnetization measurement such that $B_{max}$ is small enough to correspond to a previously measured $B_c$. If the sample is completely saturated during the pulse and $M_{sat}$ is already known, then the saturated

portion of the curve can be given this value, and the axis scaled accordingly. For a sample of unknown magnetic properties, however, an additional measurement must be made with a sample of the same shape and known magnetic properties. This determines K for any sample with this shape.

An approximate and much simpler calibration can be made by assuming that the measured samples are either spherically shaped or resemble an ellipsoid of revolution, for which the demagnetizing factor can be calculated exactly. Then K is found as in the last method mentioned above. The validity of this approximation depends on the sample size compared with the magnetometer dimensions a and b, and, if a spherical shape is assumed, on the ratio of the sample length to its effective diameter [45]. The magnetometer was calibrated in this way using a 208.2 mg sample of $Gd_2O_3$ which has a susceptibility

$$\frac{\mu_0 M}{B} = 0.0137 \qquad \text{(at } 20^\circ\text{C)}$$

and density 7.407 $gm/cm^3$. The value K = 0.064 was obtained from the slope of the resulting magnetization curve (see Fig. 5.9).

Fig. 5.9. $Gd_2O_3$ Calibration

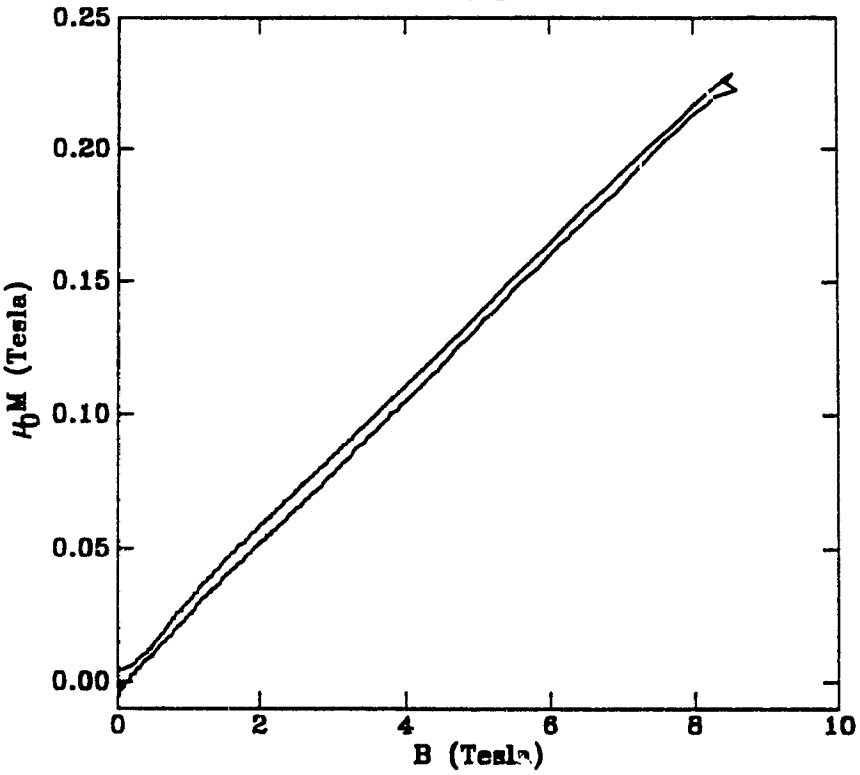

## 5.2 COOLING

Repeated firing of the pulsed magnet results in the gradual increase in coil temperature which affects the coil resistance at the start of each pulse, $R_i$, and therefore the values of $i_{max}$. Since the reproduceability of the background signal depends on identical field pulses, it is important that $R_i$, as well as $V_c$, remain unchanged from one pulse to the next. Figure 2.7 shows the drop in $i_{max}$ for several consecutive firings assuming that the time interval between each is small enough for there to be negligible heat transfer from the coil. Knowing the thermal time constant of the coil and mantle, however, it is possible to calculate the value of coil temperature, T(t), at any time after the pulse. The heat conduction equation is

$$T(t) = (T_f - 77)e^{-t/\tau} + 77 \qquad (5.5)$$

where $T_f$ is the coil temperature at the end of the pulse and $\tau$ is the thermal time constant which has a measured value of 250 sec. This was calculated from measurements of the coil resistance as a function of time after the magnet was pulsed. In terms of coil resistance the equation is

$$R(t) = (R_f - R_{77})e^{-t/\tau} + R_{77} \qquad (5.6)$$

and here $R_f$ is the coil resistance at the end of the pulse.

If the magnet is operated continuously with a duty cycle $1/t_0$ $sec^{-1}$, then a steady state is reached where the values of $R_i$ and $R_f$ stop increasing with successive pulses. An equation, based on Eqn. (5.6), can be written for the steady state:

$$R_i = \left(\frac{1}{e^{t_0/\tau} - 1}\right)\Delta R + R_{77} \tag{5.7}$$

where

$$\Delta R = R_f - R_i$$

A solution for $R_i$ is found iteratively knowing the total energy of each pulse and the coil mass, and referring to the resistance-energy relationship plotted in Fig. 2.6. Then proceeding as in Sec. 2.2, $i_{max}$ is determined. The results of this calculation for a given duty cycle and various values of $V_c$ are shown in Fig. 5.10. Also plotted, in Fig. 5.11, are the values of the maximum instantaneous coil temperature, or $T_f$, as a function of the duty cycle.

Fig. 5.10. Peak Current vs. Duty Cycle

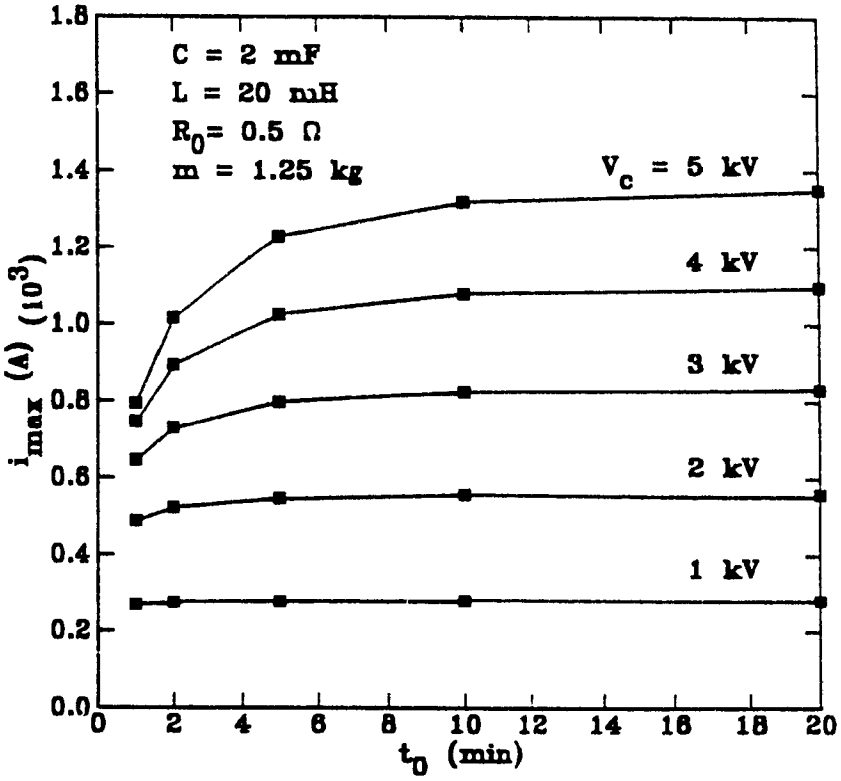


Fig. 5.11. Maximum Coil Temperature vs. Duty Cycle

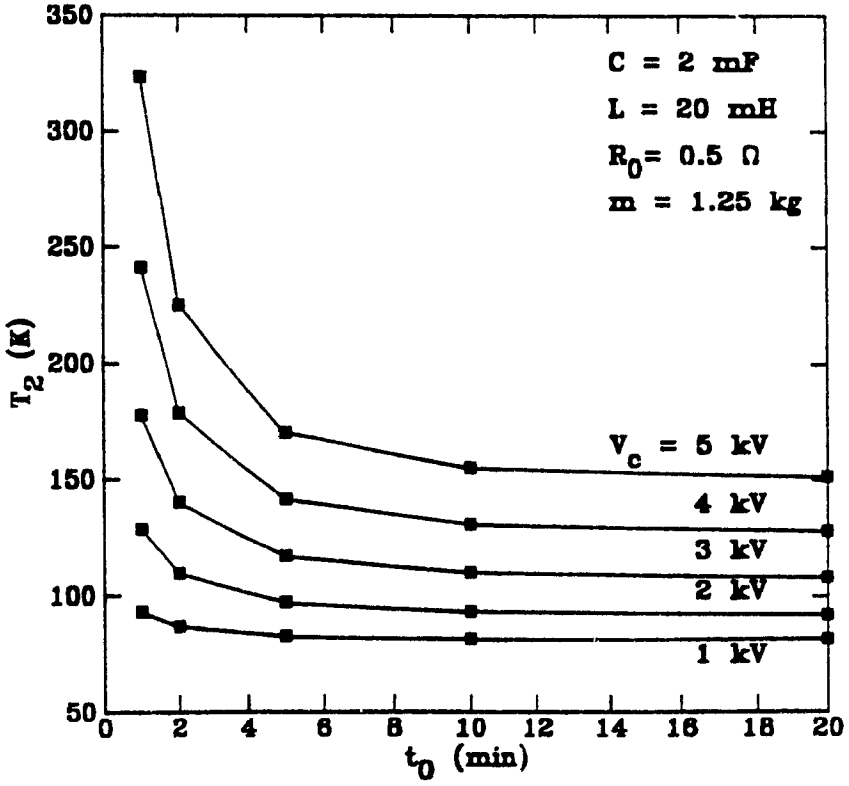

## 5.3 MEASUREMENT OF $Nd_2Fe_{14}B$

The pulsed magnet was used to measure a set of magnetization curves for a sample containing $Nd_2Fe_{14}B$. From these curves the values of remanent magnetization and coercive field were obtained and compared with subsequent measurements of the magnetized sample in an iron-cored electromagnet. In this way the accuracy of the calibration constant K was determined.

The sample was prepared by Dynacast Inc. from $Nd_{14.5}Fe_{80}B_{5.5}$ supplied by General Motors (Magnequench division). The material is rapidly quenched by melt-spinning into a crystalline state with very fine microstructure. This process produces ribbons consisting of small ($\sim$ 500 Å) single domain particles [46]. The material was then consolidated with Nylon-12 and formed by injection molding into a disk 3 mm dia x 2 mm thick. The weight of the isotropic sample is 70.0 mg and its density is 4.64 $gm/cm^3$. The density of the $Nd_2Fe_{14}B$ is 7.55 $gm/cm^3$.

A series of measurements was made with this sample at room temperature and using various peak fields. The sample was positioned in the coil so that its axis of symmetry was oriented perpendicular to the coil field. Using the calibration constant K determined in the previous section, the resulting magnetization curves for $V_c$ = 2,3,4 and 5 kV are plotted in Figs. 5.12 to 5.15 respectively.

An important result of this measurement that is immediately clear is that the remanent magnetization does not change for the different values of maximum applied field, i.e. for $B_{max}$ = 8.6 to 22 T.

Subsequent measurements of the second-quadrant magnetization curve of the sample were made with an iron-cored electromagnet following magnetizations in 8.6 T and 22 T [46]. The curves measured in this way are identical for the two magnetizing fields, giving a remanent field $\mu_0 M_r$ = 0.403 T and coercive field $\mu_{0J} H_c$ = 1.52 T (see Figs. 5.16 and 5.17). The fact that the remanent field value agrees with that measured by the pulsed field confirms the validity of the calibration. The values of the coercive field measured with the pulsed magnet, however, vary considerably (1.5 ± .3 T), and this can be explained by variations in the sample temperature and frequency dependence of $H_c$. At 20 °C the dependence of the coercive field on temperature for this sample is [46]

$$\frac{\Delta \mu_{0J} H_c}{\Delta T} \simeq 0.01 \text{ T/°C}$$

Figure 5.18 shows the full magnetization curve for the 2 kV measurement while Fig. 5.19 is the corresponding B-H loop. This is derived from the magnetization curve through the relations

$$B = B_a + \frac{2}{3}\mu_0 M \tag{5.8}$$

and

$$\mu_0 H = B_a - \frac{1}{3}\mu_0 M \tag{5.9}$$

where the applied field has been renamed $B_a$, and again assuming a demagnetizing factor $c = \frac{2}{3}$. The second-quadrant energy product, BH, as a function of B, was calculated from the B-H curve and this is plotted in Fig. 5.20. The maximum energy product for this measurement is $(BH)_{max} = 35\ kJ/m^3$ (4.4 MGOe).

Fig. 5.12. $Nd_2Fe_{14}B$ Magnetization Curve ($V_c$=2 kV)

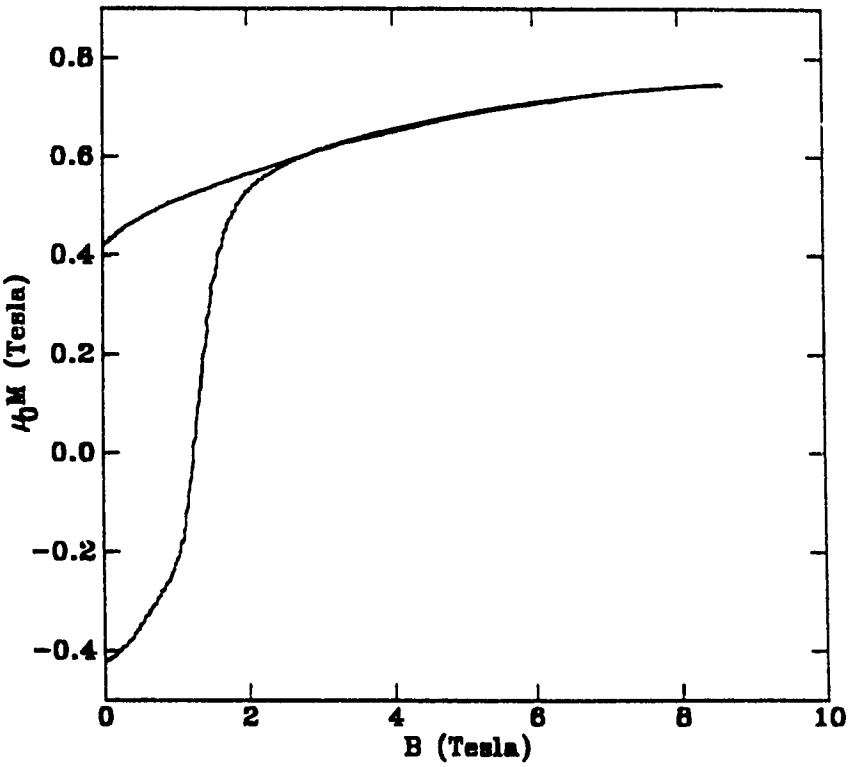


Fig. 5.13. $Nd_2Fe_{14}B$ Magnetization Curve ($V_c$=3 kV)

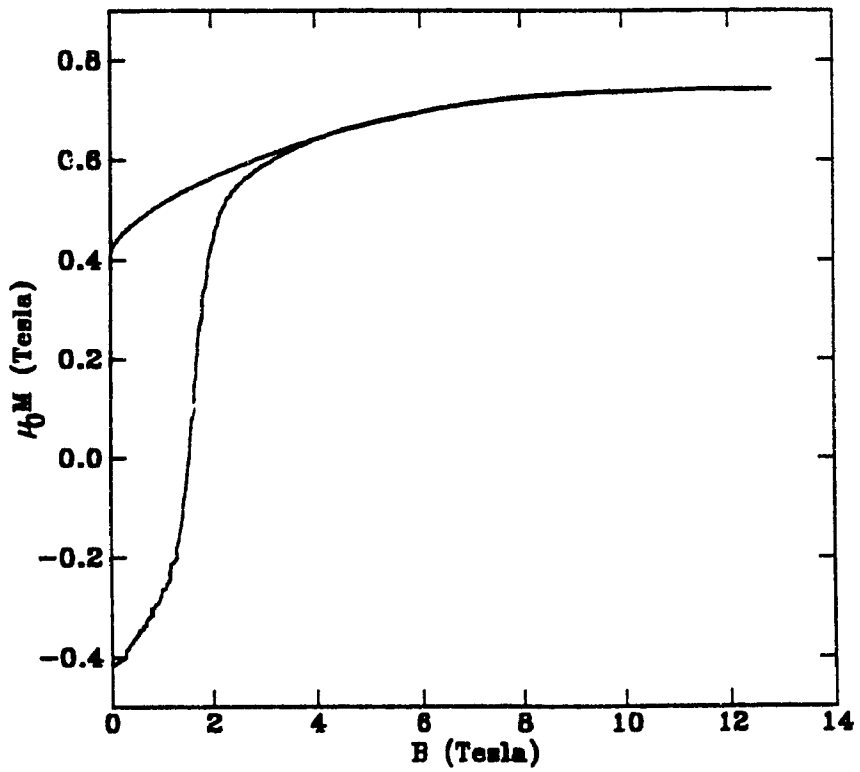

Fig. 5.14. $Nd_2Fe_{14}B$ Magnetization Curve ($V_c$=4 kV)

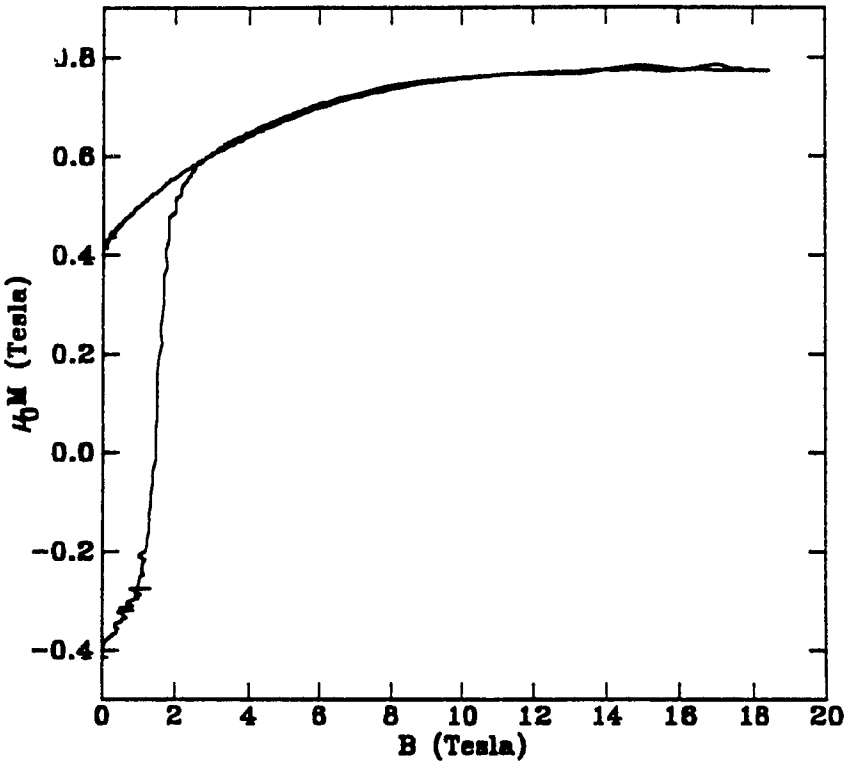


Fig. 5.15. $Nd_2Fe_{14}B$ Magnetization Curve ($V_c$=5 kV)

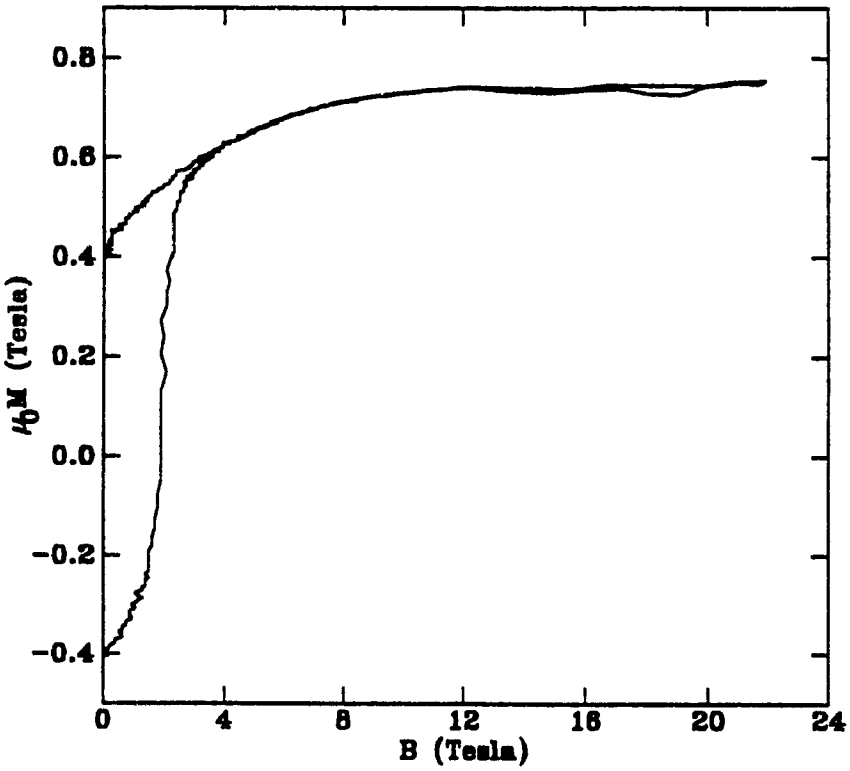

Fig. 5.16. Electromagnet Measurements of $Nd_2Fe_{14}B$

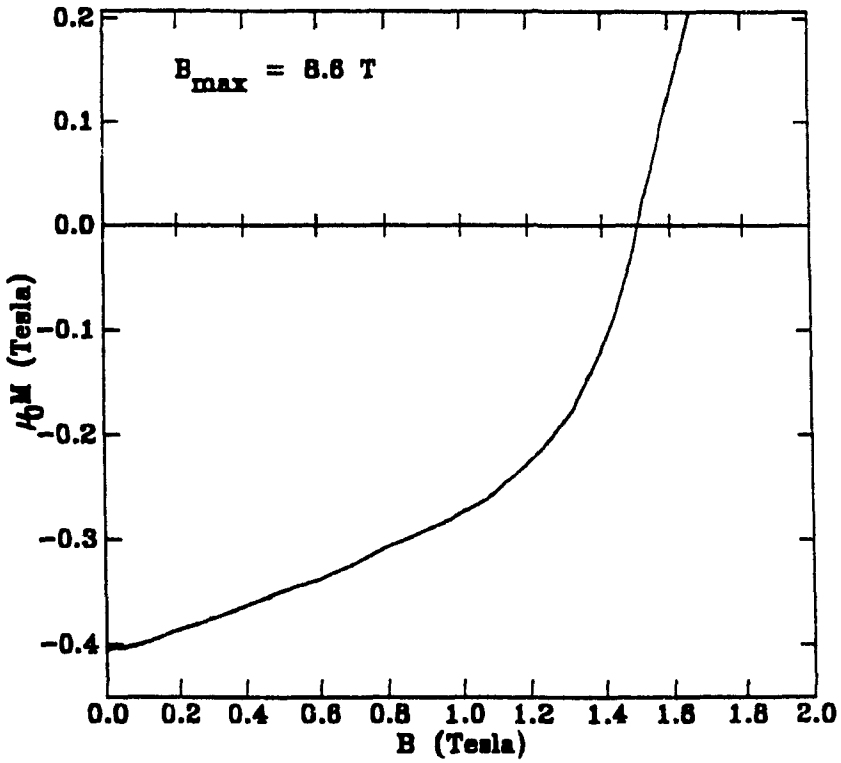


Fig. 5.17. Electromagnet Measurements of $Nd_2Fe_{14}B$

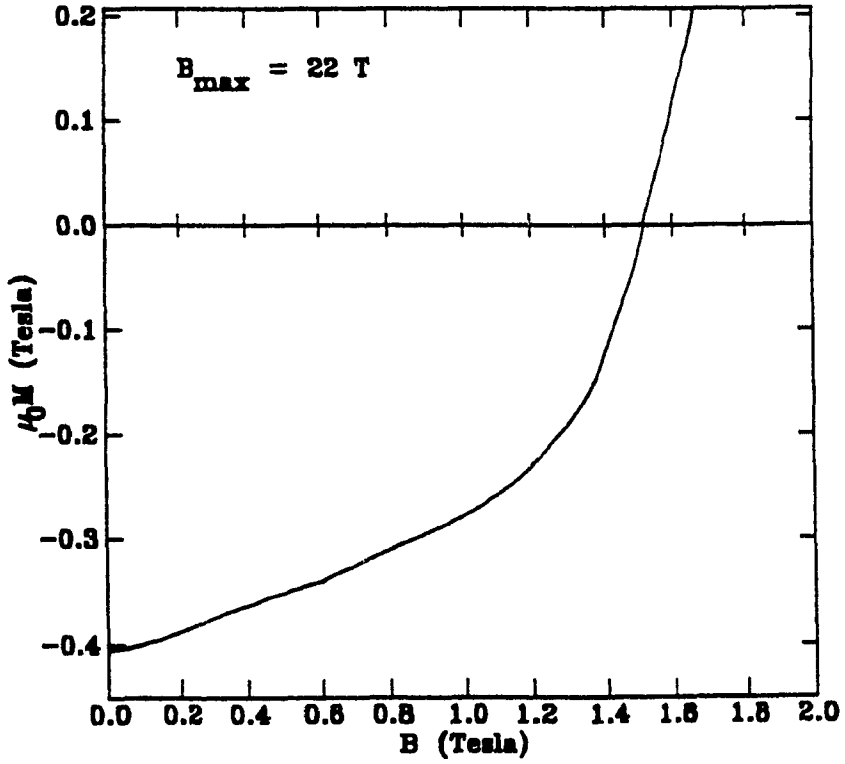

Fig. 5.18. M–$B_a$ Loop For $Nd_2Fe_{14}B$ ($V_c$=2 kV)

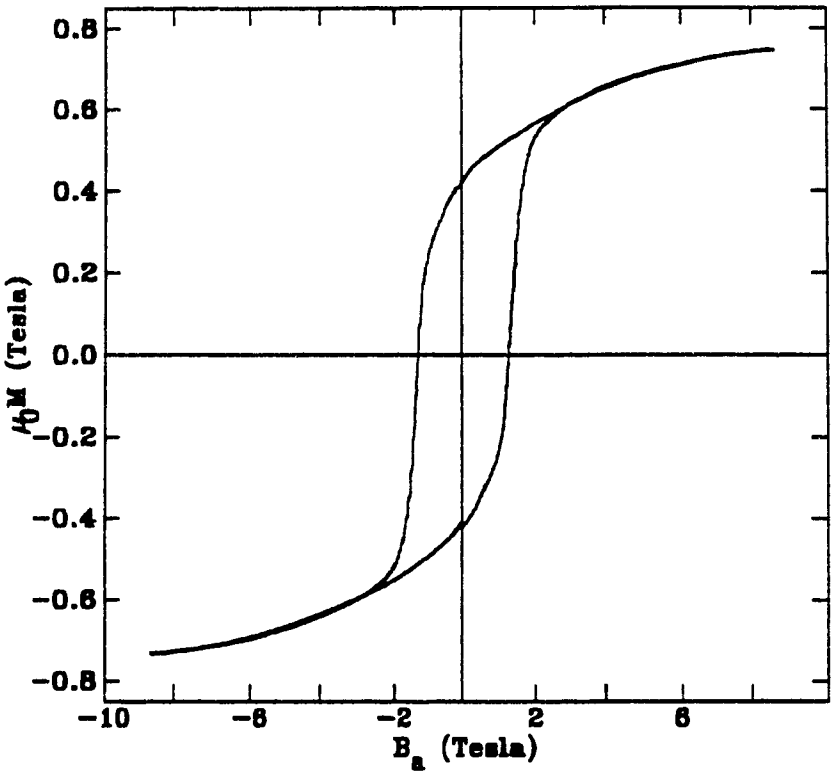


Fig. 5.19. B–H Loop For $Nd_2Fe_{14}B$ ($V_c$=2 kV)

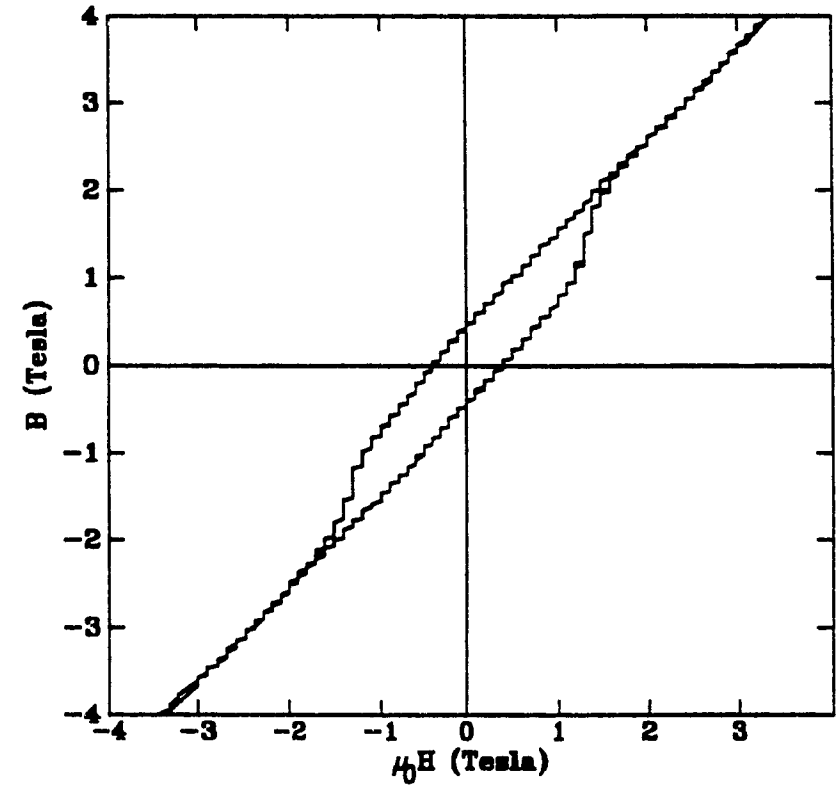

Fig. 5.20. Energy Product For $Nd_2Fe_{14}B$ ($V_c$=2 kV)

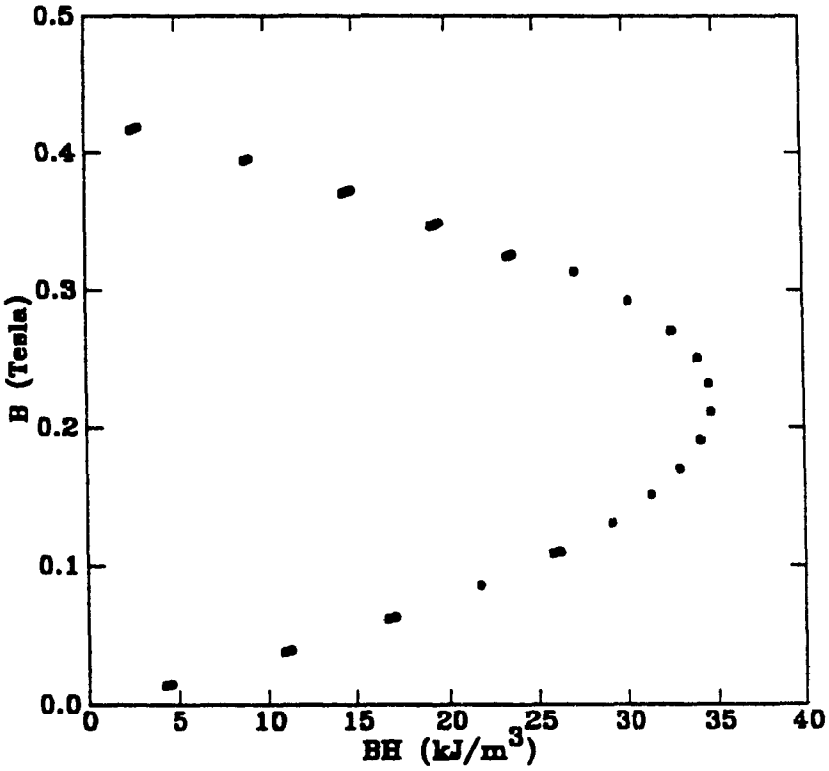

# 6 CONCLUSIONS

A high field pulsed magnet has been designed and constructed. The magnet presently generates fields between 9 and 22 T, and includes a magnetometer and data acquisition system which are capable of routinely measuring magnetization curves at these fields. The system has proven successful in measuring the magnetization of a $Nd_2Fe_{14}B$ sample in fields up to 22 T, and it is therefore believed that the system will be useful for the study of a variety of magnetic materials. This includes determining the critical field of high $T_c$ superconductors as well as measuring the magnetic properties of materials with high anisotropy fields.

A large part of the design of the pulsed magnet involved designing the solenoid coil. This began with an analysis of the circuit which takes into account the changing coil resistance. Then a procedure was developed for optimizing the coil design according to the specific requirements of a capacitor-discharge system. Another major part of the design was dealing with the problem of accurately integrating the magnetometer signal. This was eventually solved by building a data acquisition system which samples the data at a variable sampling rate.

Following the construction of the pulsed magnet two important conclusions were reached concerning the design. First, SCRs are unsuitable for use as a switching device for a capacitor-discharge

system. An ignitron switch is adequate and much more reliable. Second, the effects from eddy currents in the mantle are significant and limit the accuracy of the field measurement as long as a shunt resistor is used.

To improve the quality of the measurements being made with the present system several modifications can be made. Some of these have already been suggested. The most important involves the elimination of the ignitron noise, which is responsible for the loss of the initial part of the magnetization curve. Suggestions for doing this are discussed in Sec. 4.3. The magnetization curve is also affected by the non-reproducible error in the integrated background magnetometer signal. Much of this is due to the failure of the data acquisition system to record the high frequency components of the dm/dt signal. The obvious solution is to reduce the magnitude of this noise as much as possible by optimizing the position of the magnetometer in the coil field. At present, however, this is extremely difficult because of the sensitivity of the pick-up coil signals to position in the coil. A more sophisticated mechanism for fine adjustment of the dewar height with respect to the coil would allow more accurate balancig to be made.

The range of peak fields, $B_{max}$, over which measurements are made presently has a lower limit of approximately 9 T. This range may be extended to include lower values by using a 5 kV power supply for the

ignitron excitation circuit. The minimum value of $V_c$ for which the ignitron fires reliably will then be reduced from 2 kV to ~ 500 V.

Further improvements to the pulsed magnet involving changes in the design are possible. Replacing the oscilloscope with a more suitable large-memory fast analog to digital converter would greatly simplify the data acquisition system as well as eliminate some of the errors mentioned above. Also, the use of a pick-up coil as the means to measure the field is more appropriate for a pulsed magnet, since this will include the field produced by eddy currents in the mantle. Improvements to the system which would make the operation of the magnet more convenient include a higher level of automation than exists now. Using an interface board such as the Lab Tender would allow the charging system and the ignitron firing to be operated by the PC and also allow safety interlocks to be linked to the operating programs. It may be desireable to improve the duty cycle of the magnet. This could be accomplished by modifications of the coil mantle design which would reduce the thermal time constant.

Finally, some conclusions have been reached concerning the methods of upgrading the pulsed magnet to provide higher fields. Designs for various low-inductance coils which produce higher fields for a given amount of stored energy are discussed in Sec. 2.3. With these coils, however, the higher fields are acheived at the expense of a shorter pulse

rise time according to

$$t_p = \frac{\pi}{2}\sqrt{LC}$$

This will worsen the problems associated with a fast rise time, which were encountered and are inherent in the system, such as eddy current effects and data acquisition limitations. Preferable to changing the coil design is increasing the stored energy through the addition of capacitors. The increase in field is proportional to $\sqrt{C}$ so that doubling the number of existing capacitors should increase the field to over 30 T.

**REFERENCES**

[1] Mitcell, I.V., ed., Proceedings of the Workshop on Nd-Fe Permanent Magnets, Brussels, 1984, (Commission of the European Communities, Brussels, 1984).

[2] Buschow, K.H.J., Materials Science Reports 1 (1986) 1-64.

[3] Sweet, W., Physics Today, July, 1988.

[4] Kapitza, P., Proc. Roy. Soc. (London) A105 (1924) 691.

[5] Kapitza, P., Proc. Roy. Soc. (London) A115 (1927) 658.

[6] Wall, T.F., J. Inst. Elec. Engrs. 64 (1926) 745.

[7] Schoenberg, D., Nature 170 (1950) 569.

[8] Olsen, J.L., Helv. Phys. Acta. 26 (1953) 798.

[9] Myers, W.R., J. Sci. Instr. 30 (1953) 237.

[10] Foner, S. and H.H. Kolm, Rev. Sci. Instr. 28 (1957) 799.

[11] Furth, H.P., M.A. Levine and R.W. Waniek, Rev. Sci. Instr. 28 (1957) 949.

[12] Allain, Y., J. de Gunzbourg, J.P. Krebs and A. Miedan-Gros, Rev. Sci. Instr. 39 (1968) 1360.

[13] Jordaan, H.A., R. Wolf and D. de Klerk, Physica 69 (1973) 129.

[14] Van Deursen, A.P.J. and A.R. de Vroomen, J. Phys. E 17 (1984) 155.

[15] Parkinson, D.H. and B.E. Mulhall, The Generation of High Magnetic Fields, (Plenum Press, New York, 1967).

[16] Knoepfel, H., Pulsed High Magnetic Fields, (North Holland, Amsterdam, 1970).

[17] Montgomery, D.B., Solenoid Magnet Design, (Robert E. Krieger, Huntington, New York, 1980).

[18] Kolm, H. et al. (eds.), High Magnetic Fields, (MIT Press, Cambridge, 1962).

[19] Melville, D. et al., J. Phys. E, 14 (1981) 611.

[20] Parkinson, p. 20ff.

[21] Jackson, J.D., Classical Electrodynamics, (Wiley, New York, 1975), p. 192.

[22] Jackson, p. 90.

[23] Parkinson, p. 28.

[24] Parkinson, p.23.

[25] Montgomery, p. 112.

[26] Parkinson, p. 48.

[27] Montgomery, p. 114.

[28] Montgomery, p. 116.

[29] Montgomery, Ch. 6.

[30] Melville, D. and P.G. Mattocks, J. Phys. D., 5 (1972) 1745.

[31] Gersdorf, R., F.A. Muller and L.W. Roeland, Rev. Sci. Instr. 36 (1965) 1100.

[32] Montgomery, p. 219.

[33] Knoepfel, p. 157.

[34] Montgomery, p. 220.

[35] Montgomery, p. 92.

[36] Montgomery, Sec. 8.5.

[37] Foner, S. and W.G. Fisher, Rev. Sci. Instr., 38 (1967) 440.

[38] Kuskowski, R.L., T.B. Novey, and S.D. Warshaw, Rev. Sci. Instr., 32 (1961) 674.

[39] Knoepfel, p. 161.

[40] Montgomery, p. 222.

[41] Parkinson, p. 139ff.

[42] Arnold, A.H.M., Proc. I.E.E., 100, 2 (1953) 319.

[43] Jackson, p. 194.

[44] Grover, F.W., Inductance Calculations, (Van Nostrand, New York, 1947), p. 89.

[45] Crangle, J., The Magnetic Properties of Solids, (Edward Arnold, London, 1977), p. 113.

[46] Altounian, Z., private communication.

**APPENDIX - PC PROGRAMS**

**scope** - reads ch 1 and ch 2 data from Tektronix #5223 oscilloscope and puts data into files **out1** and **out2** or, if the command argument **r** is used, into **ref1** and **ref2**. The address of the oscilloscope is **dev**=16. The functions **i3eopen()**, **i3ewrite(dev,command)**, and **i3eread(dev,data,n)**, which are contained in **ie.c** and **io.s** (written by Mark Sutton), are used to send commands to the oscilloscope and to read **n** characters of data from the oscilloscope.

```
#include <stdio.h>

char data[20000];

main(argc,argv)
int argc;
char *argv[];
{
     FILE *fopen(),*fp1,*fp2;
     if(*argv[1] == 'r') {
          fp1 = fopen("ref1","w");
          fp2 = fopen("ref2","w");
     }
     else {
        fp1 = fopen("out1","w");
        fp2 = fopen("out2","w");
     }
     init_scope(16,"ACCESS L");
     read_scope(16,fp1);
     init_scope(16,"ACCESS R");
     read_scope(16,fp2);
}

init_scope(dev,accessx)
int dev;
char accessx[16];
```

```
{
     static char init_string[50] = "SET DISP.L,DISP.R;ASCII";
     i3eopen();
     i3ewrite(dev,accessx);
     i3ewrite(dev,init_string);
}
read_scope(dev,fp)
int dev;
FILE *fp;
{
     i3ewrite(dev,"CURVE?");
     i3eread(dev,data,20000);
     fprintf(fp,"%s\n",data);
     init_scope(dev,"ACCESS L");
}
```

**col** - Data from the oscilloscope is ASCII characters forming numbers which are separated by commas. The first number corresponds to the first data point of the oscilloscope trace. **col** reads the data from **out1**, **out2**, and **ref2** and arranges the numbers in columns 1,2, and 3 respectively in the file **scpdata**. Column 0 is the time base. An optional positive (or negative) single digit number, **s0**, in the command argument will shift column 3 up (or down) **|s0|** lines with respect to the other columns. The number of data points lost in each column is the number of lines shifted. **last** is the number of data points in each column.

```
#include <stdio.h>

char string1[5],string2[5],string3[5];

main(argc,argv)
int argc;
char *argv[];
{
     FILE *fopen(), *fp1, *fp2, *fp3, *fp4;
```

```
int i,j;
int c1,c2,c3;
char s0,s1;
fp1 = fopen("out1","r");
fp2 = fopen("out2","r");
fp3 = fopen("ref2","r");
fp4 = fopen("scpdata","w");
s0 = (*++argv)[0];
s1 = (*argv)[1];
if ( argc == 1 ) s0 = '0';
if ( s0 == '-' )
{
     j = s1 - '0';
     while (j)
     {
          next(fp1,string1);
          next(fp2,string2);
          --j;
     }
}
else
{
     j = s0 - '0';
     while (j)
     {
          next(fp3,string3);
          --j;
     }
}
i=0;
do
{
     c1 = next(fp1,string1);
     c2 = next(fp2,string2);
```

```
            c3 = next(fp3,string3);
            ++i;
            fprintf(fp4,"%6d %5s %5s %5s\n",i,string1,string2,string3);
        }
        while( c1!=EOF && c2!=EOF && c3!=EOF );
        printf("LAST = %d\n",i);
}

next(fp,string)
FILE *fp;
char string[5];
{
            int j,c;
            do
            {
                j=0;
                c = getc(fp);
                while( c=='-' || ( c>='0' && c<='9' ) )
                {
                    string[j] = c;
                    ++j;
                    c = getc(fp);
                }
                if( c==',' || c==';' || c==EOF || c==10 )
                    string[j]='\0';
                if ( c==10 )  c=EOF;
            }
            while( c!=',' && c!=';' && c!=EOF );
            return(c);
}
```

**line** - substitutes a given section of data points in **scpdata** with a set of points corresponding to a stright line on the oscilloscope trace. Data points in the specified column corresponding to the time base points **x1** and **x2** are replace with **y1** and **y2** respectively. All points inbetween are replaced with points which draw a straight line from (**x1**,**y1**) to (**x2**,**y2**). The command arguments are 1,2, or 3 indicating the column to be modified. All three may be given at the same time and in any order. The points **x1**,**x2**,**y1**, and **y2** for the three columns are taken from three lines in the file **points**. **last** is the number of data points in each column and its value is taken from the file **param**. As each column is modified the new data is placed in **scpdata2** which is then copied back into **scpdata**.

```
#include <stdio.h>

main(argc,argv)
int argc;
char *argv[];
{
     FILE *fopen(),*fp1,*fp2,*fp3,*fp4;
     int i,s,last,x1,x2;
     int out1x1,out1x2,out2x1,out2x2,ref2x1,ref2x2;
     float out1y1,out1y2,out2y1,out2y2,ref2y1,ref2y2;
     float q1,q2,q3,step,y1,y2;
     fp3=fopen("points","r"); fp4=fopen("param","r");
     fscanf(fp3,"%d %d %f %f",&out1x1,&out1x2,&out1y1,&out1y2);
     fscanf(fp3,"%d %d %f %f",&out2x1,&out2x2,&out2y1,&out2y2);
     fscanf(fp3,"%d %d %f %f",&ref2x1,&ref2x2,&ref2y1,&ref2y2);
     fscanf(fp4,"%*d %*d");
     fscanf(fp4,"%*d %d",&last);
     while ( --argc )
     {
          s = (*++argv)[0];
          if ( s=='1' )
          {
               x1 = out1x1; x2 = out1x2; y1 = out1y1; y2 = out1y2;
```

```
}
if ( s=='2' )
{
     x1 = out2x1; x2 = out2x2; y1 = out2y1; y2 = out2y2;
}
if ( s=='3' )
{
     x1 = ref2x1; x2 = ref2x2; y1 = ref2y1; y2 = ref2y2;
}
step=(y2-y1)/(x2-x1);
fp1=fopen("scpdata","r"); fp2=fopen("scpdata2","w");
i=0;
while( i<x1-1 )
{
     fscanf(fp1,"%d %f %f %f",&i,&q1,&q2,&q3);
     fprintf(fp2,"%6d %10.1f %10.1f %10.1f\n",i,q1,q2,q3);
}
if ( s=='1' )
{
     q1=y1;
     do
     {
     fscanf(fp1,"%d %*f %f %f",&i,&q2,&q3);
     fprintf(fp2,"%6d %10.1f %10.1f %10.1f\n",i,q1,q2,q3);
     q1 += step;
     }
     while( i<x2 );
}
if ( s=='2' )
{
     q2=y1;
     do
     {
     fscanf(fp1,"%d %f %*f %f",&i,&q1,&q3);
```

```
                fprintf(fp2,"%6d %10.1f %10.1f %10.1f\n",i,q1,q2,q3);
                q2 += step;
                }
                while( i<x2 );
            }
            if ( s=='3' )
            {
                q3=y1;
                do
                {
                fscanf(fp1,"%d %f %f %*f",&i,&q1,&q2);
                fprintf(fp2,"%6d %10.1f %10.1f %10.1f\n",i,q1,q2,q3);
                q3 += step;
                }
                while( i<x2 );
            }
            do
            {
                fscanf(fp1,"%d %f %f %f",&i,&q1,&q2,&q3);
                fprintf(fp2,"%6d %10.1f %10.1f %10.1f\n",i,q1,q2,q3);
            }
            while( i<last );
            fclose(fp1); fclose(fp2);
            fp1=fopen("scpdata","w"); fp2=fopen("scpdata2","r");
            do
            {
                fscanf(fp2,"%d %f %f %f",&i,&q1,&q2,&q3);
                fprintf(fp1,"%6d %10.1f %10.1f %10.1f\n",i,q1,q2,q3);
            }
            while( i<last );
            fclose(fp1); fclose(fp2);
        }
    }
```

**off** - calculates two offsets corresponding to the two regions of different sampling rates for the data in each column of **scpdata**. **mid** is the first point in the second region. **begin** is the number of points taken from the beginning of the data which are averaged to obtain the offset of the first region. This offset is then subtracted from every data point in this region. Similarly **end** is the number of points taken from the end of each column to calculate the offset for the second region. **begin** and **end** are read from the first line of the file **param** while **mid** and **last** are read from the second line. The offset data is put into the file **data**.

```
#include <stdio.h>

main()
{
     FILE *fopen(),*fp1,*fp2,*fp3,*fp4;
     int i,begin,end,mid,last;
     float division, gain;
     float q1,q2,q3,p1,p2,p3;
     float p1b,p2b,p3b,p1e,p2e,p3e;
     fp1=fopen("scpdata","r");
     fp2=fopen("data","w");
     fp3=fopen("param","r");
     fscanf(fp3,"%d %d", &begin, &end);
     fscanf(fp3,"%d %d", &mid, &last);
     fscanf(fp3,"%f %f", &division, &gain);
     p1=0; p2=0; p3=0;
     do
     {
          fscanf(fp1,"%d %f %f %f",&i,&q1,&q2,&q3);
          p1 += q1; p2 += q2; p3 += q3;
     }
     while( i<begin );
     p1b=p1/begin; p2b=p2/begin; p3b=p3/begin;
     do
     {
```

```
        fscanf(fp1,"%d %*f %*f %*f",&i);
    }
    while( i<last-end );
    p1=0; p2=0; p3=0;
    do
    {
        fscanf(fp1,"%d %f %f %f",&i,&q1,&q2,&q3);
        p1 += q1; p2 += q2; p3 += q3;
    }
    while( i<last );
    p1e=p1/end; p2e=p2/end; p3e=p3/end;
    fclose(fp1);
    fp1=fopen("scpdata","r");
    do
    {
        fscanf(fp1,"%d %f %f %f",&i,&q1,&q2,&q3);
        q1 -= p1b; q2 -= p2b; q3 -= p3b;
        fprintf(fp2,"%6d %10.3f %10.4f %10.4f\n",i,q1,q2,q3);
    }
    while( i<mid-1 );
    do
    {
        fscanf(fp1,"%d %f %f %f",&i,&q1,&q2,&q3);
        q1 -= p1e; q2 -= p2e; q3 -= p3e;
        fprintf(fp2,"%6d %10.3f %10.4f %10.4f\n",i,q1,q2,q3);
    }
    while( i<last ); }
```

**sub** - reads the data from the file **data** and subtracts column 3 (the reference waveform) from column 2. The difference is placed in column 2 of **bv**. Columns 0 and 1 are not changed.

```
#include <stdio.h>

main()
{
     FILE *fopen(), *fp1, *fp2, *fp3;
     int i,last;
     float q1,q2,q3;
     fp1 = fopen("data","r");
     fp2 = fopen("bv","w");
     fp3 = fopen("param","r");
     fscanf(fp3,"%*d %*d");
     fscanf(fp3,"%*d %d", &last);
     do
     {
          fscanf(fp1,"%d %f %f %f",&i,&q1,&q2,&q3);
          q2 -= q3;
          fprintf(fp2,"%6d %10.3f %10.4f\n",i,q1,q2);
     }
     while( i<last );
}
```

**int** - performs a trapezoidal integration of the data in column 2 of **bv** and puts the integrated data into the file **bm**. The integration is weighted for the points from **mid** to **last** to account for the changes in time base and amplifier gain. The weighting factor is **division/gain** and the values **division** and **gain** are read from the third line of **param**.

```
#include <stdio.h>

main()
{
     int i,mid,last;
     float p1,q1,division,gain;
     double p2,q2,q2last;
     FILE *fopen(), *fp1, *fp2, *fp3;
     fp1 = fopen("bv","r");
     fp2 = fopen("bm","w");
     fp3 = fopen("param","r");
     fscanf(fp3,"%*d %*d");
     fscanf(fp3,"%d %d", &mid, &last);
     fscanf(fp3,"%f %f", &division, &gain);
     i = 0;
     p1 = 0;
     p2 = 0;
     q2last = 0;
     do
     {
          fscanf(fp1,"%d %f %lf",&i,&q1,&q2);
          p1 = q1;
          p2 += (q2 + q2last)/2.0;
          q2last = q2;
          fprintf(fp2,"%6d %12.1f %12.1f\n",i,p1,p2);
     }
     while( i<mid-1 );
     do
     {
```

```
        fscanf(fp1,"%d %f %lf",&i,&q1,&q2);
        p1 = q1;
        q2 = q2 / gain;
        p2 += division * (q2 + q2last)/2.0;
        q2last = q2;
        fprintf(fp2,"%6d %12.1f %12.1f\n",i,p1,p2);
    }
    while( i<last );
}
```

**scale** - scales the data in columns 1 and 2 of **bm** for the final magnetization curve. The scaling factors are read from the file **scaling**. The midpoint between the endpoints of the magnetization curve is calculated using the average of the last **end** points of column 2 where **end** is taken from **param**. The BH and energy product curves are determined from the formulas

$$B = B_a + \frac{2}{3}\mu_0 M$$

and

$$\mu_0 = B_a - \frac{1}{3}\mu_0 M$$

The data for the $\mu_0 M$ vs $B_a$, B vs $\mu_0 H$, and B vs BH curves are put in files **BM**, **BH**, and **eprod** respectively.

```
#include <stdio.h>

main()
{
    FILE *fopen(), *fp1, *fp2, *fp3, *fp4, *fp5, *fp6;
    int i,end,last;
    float s1,s2,q1,q2,p1,p2,p2e;
    float ba,um,b,uh,energy;
    fp1 = fopen("bm","r");
    fp2 = fopen("BM","w");
    fp3 = fopen("BH","w");
    fp4 = fopen("eprod","w");
    fp5 = fopen("param","r");
```

```
        fp6 = fopen("scaling","r");
        fscanf(fp5,"%*d %d", &end);
        fscanf(fp5,"%*d %d", &last);
        fscanf(fp6,"%f", &s1);
        fscanf(fp6,"%f", &s2);
        do
        {
             fscanf(fp1,"%d %*f %*f",&i);
        }
        while( i<last-end );
        p2=0;
        do
        {
             fscanf(fp1,"%d %*f %f",&i,&q2);
             p2 += q2;
        }
        while( i<last );
        p2e=p2/end;
        fclose(fp1);
        fp1=fopen("bm","r");
        do
        {
             fscanf(fp1,"%d %f %f",&i,&q1,&q2);
             ba = q1 * s1;
             um = (q2 - (p2e / 2.0)) * s2;
             fprintf(fp2,"%6d %10.4f %10.4f \n",i,ba,um);
             b = ba + ((2.0/3.0) * um);
             uh = ba - ((1.0/3.0) * um);
             fprintf(fp3,"%6d %f %f \n",i,uh,b);
             energy = 795775 * b * uh;
             fprintf(fp4,"%6d %10.1f %10.4f \n",i,energy,b);
        }
        while( i<last );
}
```